EFFECTS OF LOCALIZED GEOMETRIC IMPERFECTIONS ON THE

STRESS BEHAVIOR OF PRESSURIZED CYLINDRICAL SHELLS

A Dissertation

by

ADAM JAMES RINEHART

Submitted to the Office of Graduate Studies of
Texas A&M University
in partial fulfillment of the requirements for the degree of

DOCTOR OF PHILOSOPHY

August 2003

Major Subject: Civil Engineering

EFFECTS OF LOCALIZED GEOMETRIC IMPERFECTIONS ON THE

STRESS BEHAVIOR OF PRESSURIZED CYLINDRICAL SHELLS

A Dissertation

by

ADAM JAMES RINEHART

Submitted to Texas A&M University
in partial fulfillment of the requirements
for the degree of

DOCTOR OF PHILOSOPHY

Approved as to style and content by:

_____
Peter B. Keating
(Chair of Committee)

_____
Jose M. Roesset
(Member)

_____
Norris D. Stubbs
(Member)

_____
Ravinder Chona
(Member)

_____
Paul Roschke
(Interim Head of Department)

August 2003

Major Subject: Civil Engineering

ABSTRACT

Effects of Localized Geometric Imperfections on the

Stress Behavior of Pressurized Cylindrical Shells. (August 2003)

Adam James Rinehart, B.A., Grinnell College;

M.S., Texas A&M University

Chair of Advisory Committee: Dr. Peter B. Keating

The influence of dent imperfections on the elastic stress behavior of cylindrical shells is explored. This problem is of central importance to the prediction of fatigue failure due to dents in petroleum pipelines. Using an approximate technique called the Equivalent Load Method, a semi-analytical model of two-dimensional dent stress behavior is developed. In the three-dimensional situation, decreased dent localization, in particular dent length, and increased dent depth are confirmed to cause dent stress concentration behavior to shift from having a single peak at the dent center to having peaks at the dent periphery. It is demonstrated that the equivalent load method does not predict this shift in stress behavior and cannot be relied upon to analyze relatively small, deep imperfections. The two stress modes of dents are associated with two modes of dent fatigue behavior that have significantly different fatigue lives. A method for distinguishing longer lived Mode P dents from shorter lived Mode C dents based on two measured features of dent geometry is developed and validated. An approach for implementing this analysis in the evaluation of real dents is also suggested.

To my wonderful wife, Sarah

ACKNOWLEDGMENTS

A number of people have contributed directly and indirectly to this dissertation and deserve acknowledgement. Dr. Peter B. Keating, my dissertation advisor, has provided valuable guidance and interesting opportunities, has taught me a great deal about a number of things, and has managed my education and development during the last five years in a responsible and unselfish manner. In particular, he is thanked for giving me a chance to become a civil engineer when others wouldn't. The members of my doctoral committee, Dr. Jose Roesset, Dr. Norris Stubbs, and Dr. Ravinder Chona, have all taught me important things in and out of the classroom and their involvement has been appreciated. Three fellow students have played a significant role. Dr. Ade Oyetunji served as an excellent role model. Dr. Pavlin Entchev provided useful advice about the dissertation process and introduced me to LaTeX. Suraphong Powanusorn promoted technical excellence in my work and provided good company. Richard Gehle is thanked for providing valuable assistance in preparing certain figures.

Both of my parents have provided encouragement, moral support, and great practical advice. My father, Dr. Eric Rinehart, has served as a key role model in my technical career to date and will continue to do so. All members of my immediate and extended family are thanked for their outstanding moral support. Finally, but most importantly, I must thank my wife, Sarah Rinehart, for her enthusiastic support of my efforts, her understanding ear, and her helpful ideas.

TABLE OF CONTENTS

LIST OF TABLES

LIST OF FIGURES

FIGURE   Page

FIGURE   Page

CHAPTER I

INTRODUCTION

Pipelines are relied upon to transport hazardous liquids and gasses over long distances. A significant threat to the integrity of this infrastructure is mechanical damage resulting from what are termed "outside force" events by the U.S. Department of Transportation, Office of Pipeline Safety, the federal regulatory authority for onshore pipelines in the United States [1]. As the name implies, outside force events are events in which an externally applied force acts on a pipeline and causes damage or immediate pipeline failure. Outside force events commonly occur when heavy equipment being operated within the pipeline right-of-way inadvertently comes into contact with the pipe wall. Other sources of onshore outside force damage include pipeline settlement onto rocks [2],construction induced damage, intentional attempts at pipeline damage, and bullets. Outside force events are also a problem in offshore pipelines, which, in most cases, are regulated in the United States by the Minerals Management Service. Outside force damage in an offshore setting can be caused in a variety of ways, including settlement onto rocks, mishandling during construction, ship collisions, mis-located ship anchors, and mis-located jack-up barge legs.

According to statistics made available by the Office of Pipeline Safety, 26% of liquid pipeline failures in 2001 were caused by outside force damage [1]. For gas pipelines, outside force damage caused 80.2% of all failures [1]. In a review of Office of Pipeline Safety statistics, Smith and Gideon note outside force damage as the leading cause of gas pipeline failures [3]. They note sources of outside force incidents. They also note that outside force incidents generally create some combination of a

---

The journal model is ASME Journal of Pressure Vessel Technology.

gouge and a dent in the pipe. A dent is essentially a local flaw in the geometry of the pipe wall. A gouge is a scratch, groove, or other local sharpened flaw that typically coincides with the location of indentor contact. Thus, a leading threat to pipeline integrity is the presence of gouges, gouges and dents, or plain dents. The threat posed by combinations of dents and gouges was noted in early reviews of pipeline failure origins [4, 5, 6]. These early reviews point to local stress concentrations resulting from dent and gouge combinations as the reason this damage class leads to pipeline failure [4, 5, 6].

The problem of dent and gouge failure in pipelines has been studied, to varying degrees, since at least 1983. An overview of much of this work is given by Alexander [7]. There are two primary failure modes for dent gouge combinations. In the first mode, the dent–gouge region bursts when the pipeline is subjected to some static pressure that is below the nominal undamaged pipeline burst pressure. In the second mode, the dent–gouge succumbs to fatigue failure. During operationally induced pressure fluctuations the locally heightened stress fluctuations may be sufficient for the initiation and propagation of fatigue cracks. This process is exacerbated by the presence of a gouge or other localized sharpened flaws.

There have been three major experimental studies that have been published dealing with the problem of pipeline dent fatigue [8, 9, 10]. This work has led to qualitative insights about dent fatigue behavior. In particular, certain parameters have been shown to play significant roles. There is general agreement that dent depth is important. In fact, the conventional understanding of pipeline dent behavior correlates dent severity to dent depth [7, 11, 12, 13] and neglects the influence of other dent parameters, such as length and width.

Other experimental [8] and analytical [14, 8, 15, 16] work has suggested that dent length also plays a role. This role has only been characterized qualitatively. In

essence, relatively long dents develop stress concentration factors in the dent center while smaller dents develop them at the periphery. The longer dents have markedly shorter fatigue lives than to the shorter dents. Thus, there is some indication that a length effect exists in dent stress behavior. However, the current understanding of dent stress behavior and of this length effect is very qualitative.

Shell theory literature does address the problem of dent stress behavior [17, 18, 19, 20]. However, this literature is primarily interested in the application of an approximate method of imperfection analysis called the equivalent load method to the problem. The shell theory literature does not indicate the existence of a size effect.

Finally, some work has been done to develop methods for predicting dent fatigue life [21, 22, 9, 23]. All of this work has pointed to the fact that dent fatigue life can be predicted if dent stress concentration factors can be quantified. Thus, it becomes important to have a more quantitative understanding of dent stress behavior not only for the sake of better understanding the underlying mechanics of dent behavior but also for purposes of predicting the fatigue life of dents found in the field.

Little work exists on the specific problem of quantifying dent stress behavior. At the same time, this problem is both interesting and central to developing safe, accurate pipeline dent acceptance tools. As a result, the present body of work will explore several issues relating to dent stress behavior.

First, a means of solving for stresses in dents is sought. The equivalent load method [17, 20], an approximate method of analyzing imperfections in shells, is used to study the elastic stress concentration behavior of dents. This method is used to develop a semi-analytical model of two-dimensional dent stress behavior that is appropriate for understanding the behavior of relatively long dents. This model contains clear quantitative information about the influence of various features of dent

and pipe geometry on the stress concentration behavior of such dents..

Next, the discrepancy between observations of a dent size effect in the dent fatigue literature and lack of such observations in the equivalent load shell literature is explored. In particular, the applicability of the equivalent load method to three-dimensional imperfections is studied. It is shown that the stress behavior of three-dimensional imperfections undergoes a fundamental change as imperfection localization increases. The fact that the equivalent load method does not predict this shift in behavior is discussed. Finally, fundamental mechanical behavior leading to the size-dependent shift in dent stress behavior is explored.

Having clearly established the existence of a size effect in general dent stress behavior, attention shifts to a practical problem. It will be shown in Chapter II that experiments [8] have demonstrated that shorter dents with peripheral stress behavior have long fatigue lives and that longer dents with center stress behavior have shorter fatigue lives. It would be very useful to be able to determine, based on simple geometry measurements, which stress mode, and thus which fatigue mode, a given dent in a petroleum pipeline falls into. If this categorization could be made, an initial step in accurate dent fatigue assessment could be taken.

Improved understanding of the fundamentals of dent stress behavior is important to advancing the present understanding of pipeline dent failure mechanics. In addition, the problem of shell imperfection behavior appears to have been largely overlooked in general. Thus, the focus taken here on details of the stress behavior of dent imperfections in cylindrical shells is believed to be warranted.

CHAPTER II

EXISTING WORK

In this chapter, important details of the dent fatigue problem will be introduced. Up-to-date approaches for predicting dent fatigue life will be discussed. This discussion will show that in order to develop a better understanding of dent fatigue one must develop a better understanding of dent stress behavior. Several methods that can be used to study dent stress behavior will be introduced.

A.   Current Understanding of Dent Fatigue

Given that dents can threaten pipeline integrity, the practical problem becomes one of determining which dents actually threaten integrity, characterizing the nature of this threat, and responding to the threat. Current methods of understanding and dealing with these problems can be categorized in terms of codified approaches and methods discussed in the developing body of pipeline dent literature.

Liquid pipelines in the United States typically are governed by the code ASME B31.4, *Liquid Transportation Systems for Hydrocarbons, Liquid Petroleum Gas, Anhydrous Ammonia and Alchohols* [11]. Gas pipelines are governed by ASME B31.8, *Gas Transmission and Distribution Piping Systems* [12]. A broad overview of conventional, codified approaches to non-sharpened pipeline flaws, such as dents, is available in [13]. These codes both take a binary, accept/reject approach to dent management, prescribing removal of unacceptable damage. In both liquid and gas pipelines, dents that alter pipe curvature at either seam or girth welds are deemed unacceptable. In addition, for both types of pipelines dents containing sharpened flaws such as scratches, gouges, grooves, or arc burns are not acceptable.

When it comes to assessing the severity of a dent without a gouge, codified ap-

proaches consider the dent depth to pipe diameter ratio, d/D, to be the sole indicator of dent severity [11, 12]. Dents in liquid pipelines where d/D exceeds 6% and the operational hoop stress levels are in excess of 20% of the specified pipe yield stress must be repaired [11]. In gas pipelines, repair is mandated when d/D exceeds 2% and hoop stress exceeds 40% of the specified yield stress [12]. It will be shown shortly that the depth based approach is of limited value, and may even be unsafe, in anticipating dent failure through fatigue for certain types of dents.

The fatigue behavior of dents has been studied by several researchers. Most notably, two published experimental studies have produced a body of full–scale dent fatigue test data. Fowler, *et al.* studied a wide range of pipe diameter and wall thickness combinations, a range of dent depths, and the effect of weld–dent proximity in the laboratory [9]. In addition, Fowler, *et al.* considered various dent–gouge combinations and explored means of gouge repair. Other than variable depth, dent geometry was relatively fixed in this study.

This work clearly demonstrated that dents could fail through fatigue. It found that final, rerounded dent depth is an indicator of dent severity. It pointed to stress concentrations associated with dent damage as a source of dent fatigue failure. These stress concentrations were found to vary with respect to pipe diameter–to–thickness ratio, D/t. In addition, values for dent stress concentration factors (SCF's) found using three-dimensional finite element analyses were tabulated for different d/D values over a range of practical D/t values.

A methodology is presented by Fowler *et al.* for predicting dent fatigue life using the tabulated SCF information. The SCF is used to determine a local stress range from nominal pressure range history. This local stress range history is then related to a predicted fatigue life using a standard /textitS-N curve, the DOE-B curve. A correction factor based on the presence of a gouge or weld is then used to adjust

the fatigue life prediction. An example problem is presented in [9] for the case of a plain dent with final a final d/D depth ratio of 5% in a pipe with a D/t ratio of 50 and uniform pressure fluctuations of 500 psi. The measured fatigue reported in [9] for this case is 118,055. The predicted life, based on the method outlined in [9] is 56,068. Only this one example is given for plain dent analysis. Thus, an overall level of agreement between this predictive approach and the complete experimental data set does not appear to be available.

A second experimental study, conducted by Keating and Hoffmann [8], contributed further to the set of available experimental data. In this study the effects of variable dent depth, dent geometry, pipe D/t ratio, and the presence or absence of dent restraint were studied. Figure 1 illustrates how dent depth, d, dent length, l, and dent width, w, are measured relative to the axis of a pipe of diameter D and thickness t. Pipe diameters ranged from $12''$ to $36''$ and thicknesses were either $1/4''$ or $3/8''$. Steel grades varied among API 5L Gr. B, Gr. X42, and Gr. X60. These grades of steel correspond to nominal yield strengths of 30 ksi, 42 ksi, and, 60 ksi, respectively, and actual, measured yield strengths of 50 ksi, 50 ksi, and 60 ksi, respectively.

Four types of indenters were used in [8], as described in Table I. Indentor orientation described in Table I is with respect to the longitudinal pipe axis. The Type A indentor was a $6''$ long, $1''$ wide block of steel. The ends of this block were rounded to a $1''$ radius and the edges were rounded to a $1/2''$ radius. The Type BH indentors were actual teeth taken from a backhoe excavator bucket. The Type R indentors were relatively round pieces of rock. Artificial damage in the form of scratches or machined grooves were present in the center region of all Type A dents.

Multiple dents of variable depth were formed in a given pipe specimen. Each pipe specimen was then subjected to cyclically applied, variable amplitude pressurization sequences. These pressure sequences consisted of 100 pressure excursions from
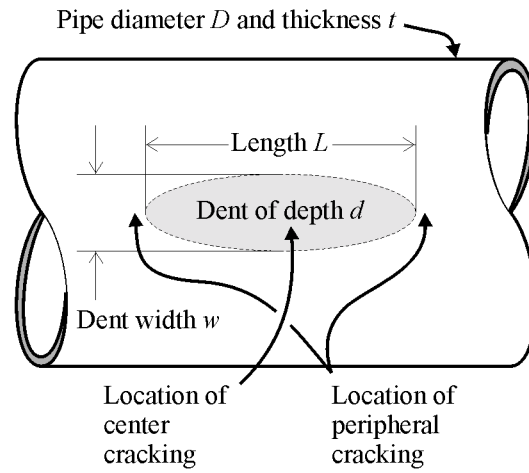
Fig. 1. Schematic diagram showing dent measurements relative to pipe axis and location of center and peripheral cracking.

Table I. Indentor type details.

Indentor	Description	Orientation
A	6″ long x 1″ wide	Longitudinal
BH–L	Single Backhoe Tooth, 2″ long x 0.3″ wide	Longitudinal
BH–T	Single Backhoe Tooth, 2″ long x 0.3″ wide	Transverse
R	Rock	n/a

a low or high base pressure. In general, the maximum nominal pressure value used in each pressure spectrum corresponded to a nominal hoop stress value ranging from 60% to 70% of the nominal yield stress of the material and the minimum hoop stress value corresponded to a nominal hoop stress that was 10% of the yield stress. Discrete pressure excursion values, evenly spaced between the maximum and minimum values, were used. The number of excursions from the base pressure to each excursion value conformed to a normal distribution whose peak was at the mean pressure value. Typical pressure histories with low and high base pressures are shown in Fig. 2. Pressure was cycled until a dent failed due to through–thickness cracking or approximately 100,000 cycles were reached. Pressure history magnitudes were specimen specific. Upon failure of a given dent in a pipe specimen, pressure cycling was stopped so that the failed dent could be repaired. After pressure cycling, all unfailed dents were subjected to a high pressure proof test of 77% of the given pipe's nominal yield pressure [8]. Dent depth was measured at indentation, after elastic rebound following indentor removal, at various stages of rerounding during the initial pressure ramp-up, and at zero pressure following rerounding.

The study by Keating and Hoffmann [8] confirmed the importance of dent depth. It also demonstrated that at least one other aspect of dent geometry, namely dent length, plays a major role in determining dent fatigue life for unrestrained dents. It was seen that relatively long dents created by Type A indenters developed fatigue cracks in the dent center. The relatively short dents, created by Type BH-L and BH-T indenters, developed cracks at the dent periphery. Other researchers have also noted that distinct dent geometry leads to distinct crack location or stress behavior but have not dwelled on this point [24, 25].

More importantly than simply influencing crack location, dent length was seen in [8] to strongly influence dent fatigue life. Long dents had much shorter fatigue lives
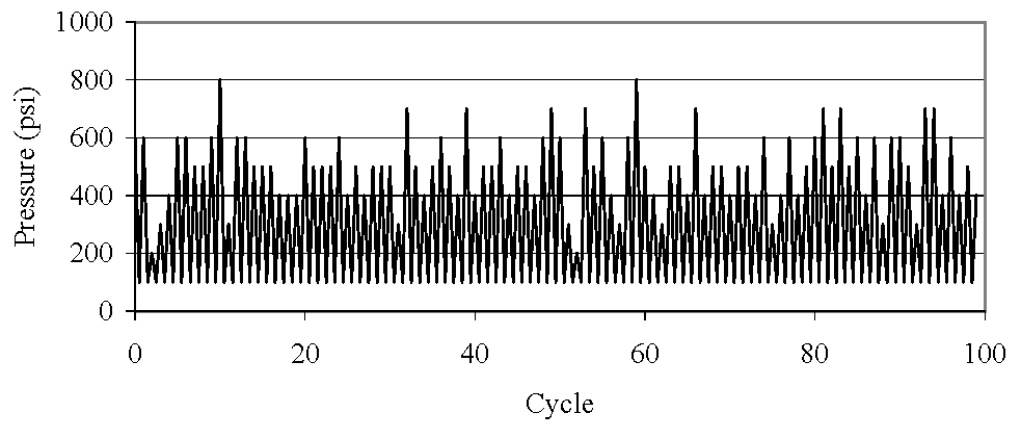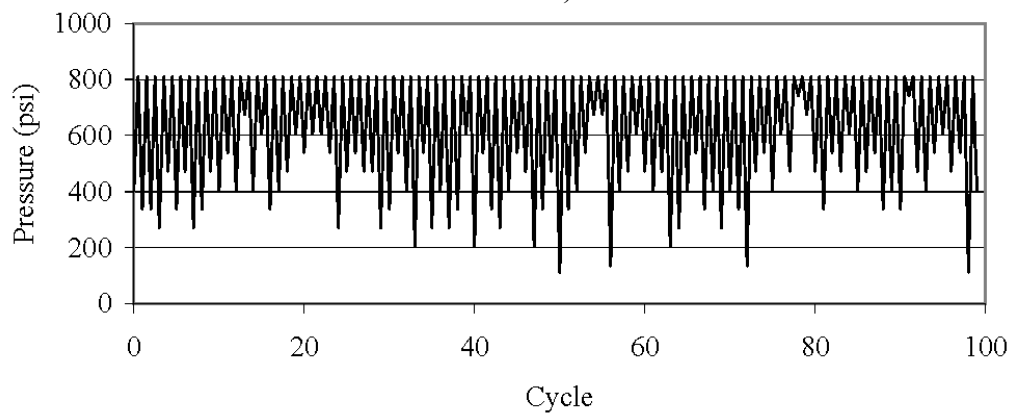
Fig. 2. Representative pressure histories used in experimental study [8], a) low base, high excursion; b) high base, low excursion.

Table II. Comparison of fatigue behavior for long Type A and short Type BH-T dents
in 24″ diameter 1/4″ API 5L X60 pipe seen in data taken from [8].

Indentor Type	Induced Defect	Initial d/D (%)	Failure Mode	Cycles to Failure
A	scratch	5	crack, center of dent	30,108
A	scratch	7.5	crack, center of dent	18,608
A	scratch	10	crack, center of dent	12,711
BH-T	none	5	no cracking	109,332+
BH-T	none	7.5	peripheral crack, post-proof test	109,332+
BH-T	none	10	peripheral crack, post-proof test	109,332+

compared to short dents of similar initial depth. In fact, many short dents did not develop any cracking within 100,000 pressure cycles while most long dents developed failure depth cracks much earlier than 100,000 pressure cycles. This difference is illustrated in Table II. Table II shows measured fatigue lives taken from [8] for Type A and Type BH-T dents of equal initial depth in a 24″x1/4″ X60 pipe. The fact that otherwise similar long and short dents have dramatically different fatigue life raises questions about a purely depth based approach to dent acceptance.

It was noted previously that artificial flaws were introduced in the centers of many dents, especially long dents, in [8]. However, the presence or absence of artificial flaws is not what accounts for the geometry dependence of dent fatigue crack location [16]. The dent is a geometric imperfection in the pipe wall. If no imperfection were present, the pipe wall would develop a uniform tensile membrane hoop stress. However, a dent imperfection alters the fundamental stress flow situation present in the pipe wall and induces nonuniform membrane forces as well as bending moments [17, 20]. Different dent geometries have been shown to produce different pipe wall stress redistributions. Perhaps the earliest to note that short dents and long dent have different hoop stress profiles was Beller [14] who used finite element analysis to demonstrate this difference.

Similar results were seen in more extensive finite element studies done by Keating and Hoffmann [8].

Rinehart and Keating have explored some of the fundamentals and ramifications of the dent length effect on the stress profile [15, 16]. One fundamental is the fact that the effect of dent size is relative to the pipe diameter [16]. For example a dent of a given geometry may have a short dent stress profile in a large diameter pipe but a long dent type stress profile in a small diameter pipe. Second, it has been proposed [15] that the geometry dependent shift in dent stress behavior has to do with the relative stiffness of the dent. Longer dents are fairly broad and may have a stiffness similar to the surrounding pipe wall. Thus, stress flows through the center of these dents and bending develops. Shorter dents may behave in a manner similar to a hole in plate due to their reduced stiffness, producing peripheral stress features. Finally, it has been shown that when long dents are restrained against freely moving in response to pressure they develop peripheral stress features similar to those seen in short dents [16]. This effect accounts for the fact that long dents restrained in the laboratory actually developed long-life, peripheral cracks instead of short-life center cracks [8].

The primary result of dent stress analysis conducted by Beller [14], Keating and Hoffmann [8], and Rinehart and Keating [15, 16] is that features of the hoop stress concentration profile along the longitudinal centerline of the dent vary with dent length. These features can be correlated to fatigue crack location in short and long dents [16]. Figure 3 shows typical short and long dent hoop stress concentration profiles along the centerline of the top of the pipe. These profiles were determined using a finite element analysis model that will be discussed shortly. As shown in Fig. 3, short dents have a single peak in their hoop SCF profile and this peak is located at the dent periphery. Long dents may have a noticeable peripheral stress feature but
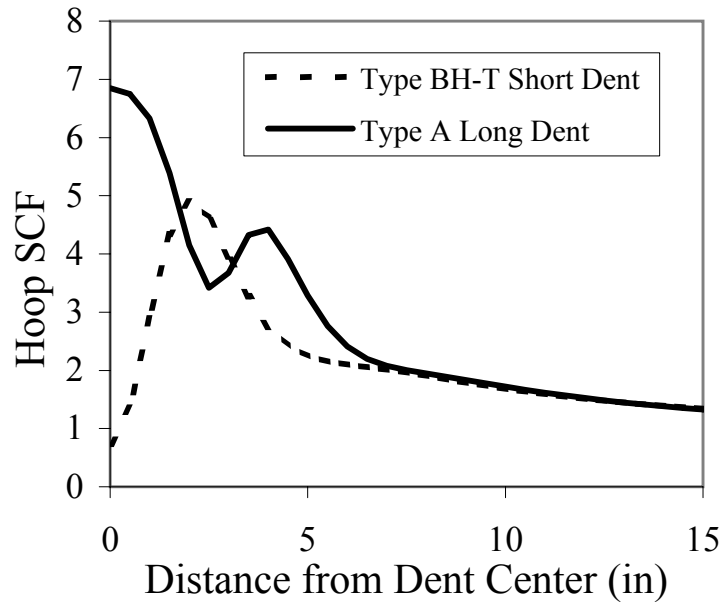
Fig. 3. Hoop stress concentration profiles determined using FEA along the dent centerline and top of pipe for short dent with initial $d/D = 17.5\%$ and long dent with initial $d/D = 7.5\%$ in $18''$x$1/4''$ X60 pipes.

always have a much larger center peak at the dent center. Recalling that short dents suffer from peripheral cracking and long dents experience center cracking, it becomes apparent that the geometry dependent stress profile behavior is what fundamentally drives fatigue crack location [8, 16, 15]. It should also be noted that the profiles shown in Fig. 3 are not for otherwise similar short and long dents. The short dent initial d/D is 17.5% while the long dent initial d/D is only 7.5%. Thus it appears that the long dent stress condition not only has a center peak where sharpened flaws are likely to be present, but that it also has a much higher stress concentration factor relative to an otherwise similar short dent.

It is important to point out that during the dent formation and rerounding process residual stresses develop in the dent region. It will be shown later in this
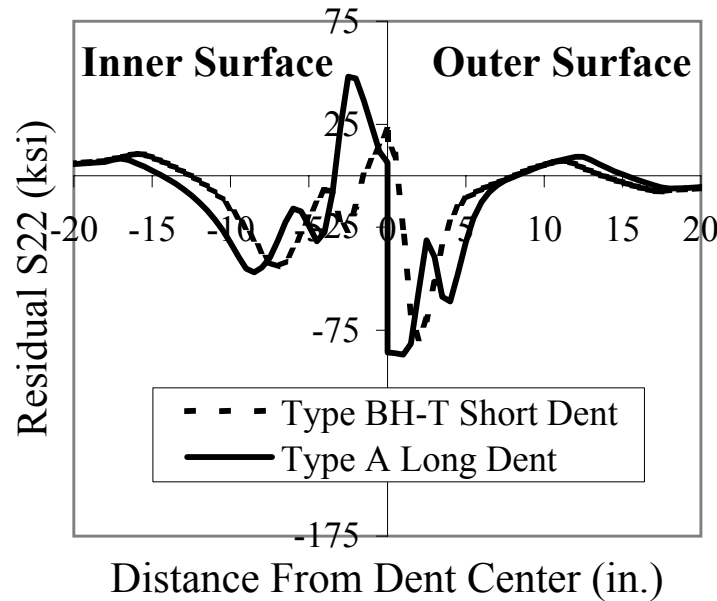
Fig. 4. Post–rerounding residual hoop stress profiles determined using FEA along the dent centerline and top of pipe for short dent with initial $d/D = 17.5\%$ and long dent with initial $d/D = 7.5\%$ in $18''\text{x}1/4''$ X60 pipes.

chapter that these residual stresses play an important role in determining dent fatigue behavior. The residual stress profiles of short and long dents differ, as shown in Fig. 4 which shows the post–rerounding residual hoop stress profiles of the dents with the SCF profiles shown in Fig. 3. Although dent length influences the overall residual stress profile, at the fatigue critical location of the dent where the hoop stress SCF is maximum, the residual stress is typically compressive at the outer surface.

An additional difference between short and long dents is different levels of inelastic rerounding. After an indentor is released a dent may undergo a significant amount of inelastic rerounding, or shallowing out, during early pressure cycles. This behavior has been noted by several sources [8, 7, 24]. Long dents undergo much more rerounding than short dents of equal initial depth. Figures 5 and 6 are photographs

Fig. 5. Photograph of rerounded short dent taken from [8], note concavity in dent interior.

taken from [8] and show rerounded short and long dents, respectively. The short dent in Fig. 5 remains deep and concave while the long dent in Fig. 6 has been forced out in the interior and has become convex. Because of rerounding, dangerous long dents are considerably shallower than less dangerous short dents.

Differences in rerounding have fundamental meaning because they alter dent geometry, which in turn alters dent stress behavior. Rerounding differences also raise serious questions about using a single, depth–based dent acceptance criteria for all dent geometries. In order to reject dangerous, but shallow, long dents, the standard would apparently have to reject a number of possibly benign, but deeper, short dents. Thus, extensive long dent rerounding may push a uniform depth based standard further into overconservatism. However, a second concern exists with the existing depth based standard. As will be shown shortly, long, shallow dents which have short fatigue lives are deemed acceptable under current dent acceptance criteria.

To explore both the conservatism and safety of the existing dent acceptance
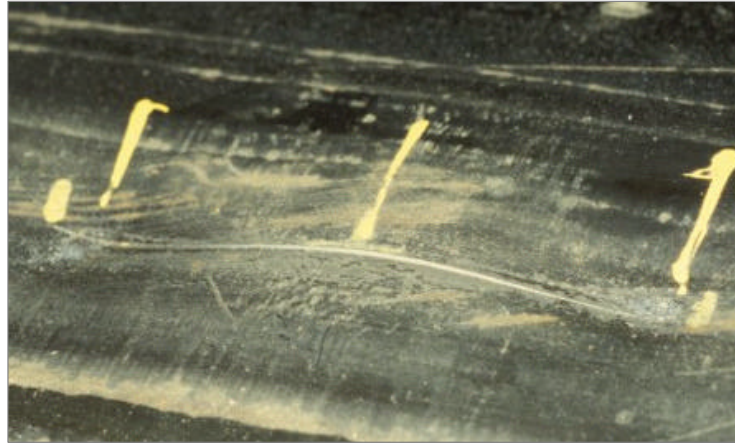
Fig. 6. Photograph of rerounded long dent taken from [8], note convexity in dent interior.

standards [11, 12], Rinehart and Keating [16] applied these standards to the data of Keating and Hoffmann [8]. When measured fatigue life is plotted in terms of rerounded dent depth, as shown in Fig. 7 two important results are evident. First, the depth based standard does not correlate well with measured behavior. While one would expect dent life to decrease with increasing dent depth, the overall data trend in Fig. 7 is the opposite. Within geometry groups the expected inverse relation is present. This group-specific depth dependency is illustrated by the straight lines drawn through limited groups of short and long dent data. While these lines are not based on a rigorous curve fit, they do demonstrate the inverse trend between life and depth within a dent geometry type.

Second, a more serious concern with existing depth–based standards is that they seem to actually accept low–life long dents. For the analysis shown in Fig. 7, dent depth measurements taken from [8] are depths at the center of the dent after rerounding. Because long dents reround the most in the dent center these depth measurements are the shallowest possible. Thus, analysis based on these long dent depth measure-
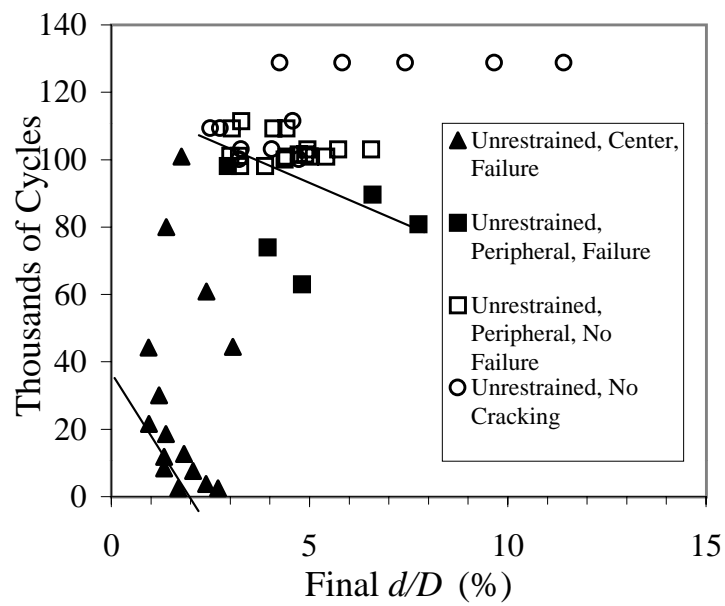
Fig. 7. Measured life of dents in experiments reported by [8] plotted in terms of final rerounded dent depth data given in [8] (taken with permission from [16] courtesy of ASME).

ments will give a worst–case interpretation. In Fig. 7, all long dent d/D values are well below 6% and are marginally less than 2%. Even if Fig. 7 represents a worst–case interpretation, the fact that long dents can be easily deemed acceptable by the 6% liquid pipeline rule leads one to question the safety of the code. At the same time that the code accepts long dents it prescribes the rejection a great number of short dents that either never failed or never even developed visible cracks during 100,000 cycles of testing. Thus, the code actually accepts unsafe long dents and rejects short dents that do not pose a large fatigue threat.

It is true that current standards require removal of any dent with sharpened flaws and that the long dents in Fig. 7 did have sharpened flaws. However, short dents that failed in Fig. 7 did not have sharpened flaws. The stress concentration associated with long dent is typically higher than that associated with short dents. Also, it has been shown that short dent fatigue initiation life only accounts for a relatively small portion of total short dent fatigue life [22]. Thus, long dents without sharpened flaws would still seem likely to pose a significant fatigue threat. At the same time, as indicated in Fig. 7, current acceptance standards do not reject this dangerous class of dent geometries. These facts lead to serious questions about existing depth-based dent acceptance criteria.

Figure 7 raises serious questions about whether existing depth based standards are safe. Indeed, it has been reported that dents in the field occasionally develop leaks when dent d/D is less than 3% [26]. Furthermore, it has been noted that dents in different length categories have order of magnitude differences in fatigue life [8] and have different rerounding characteristics. As a result, even if purely depth based approaches were safe, they would have to be highly overconservative for a common dent configuration. Thus, it appears that a need exists for improved accept/reject dent assessment approaches. In particular, it would be useful to be able to determine

whether to accept or reject a dent based on dent geometry characteristics, including depth and length.

In order to develop an improved geometry-based dent acceptance criterion, two issues must be addressed. First, geometry values must be established that distinguish different dent classes, especially short and long dents. Second, within a given class, geometry values that distinguish safe dents from unsafe dents must be determined. In order to determine improved geometry based assessment criteria without resorting to large amounts of experimental testing it is necessary to develop methods of predicting dent behavior mode and dent fatigue life. These methods could then be used to analyze a range of cases and to make assessment recommendations.

Aside from concerns about safety and/or overconservatism, the depth-based approach to dent acceptance has a second problem. This binary approach does not give any information about probable dent fatigue lifetime. Such information has at least three practical uses. First, multiple dents are present in a given pipeline system, dent life information would permit informed prioritization of repair needs. Second, remaining dent life could be compared to remaining pipeline life or to existing maintenance plans, so an efficient dent maintenance strategy could be adopted. Finally, tools to predict dent fatigue lifetime would permit operators to be able to judge the effects of operational pressure history decisions on dent life. Current industry practice is to cut out any dent encountered in a pipeline. However, more knowledge about dent fatigue behavior might lead to more efficient dent management programs or more efficient repair prioritization. Thus, dent fatigue life prediction methods have practical value.

B.   Dent Fatigue Life Prediction Models

It has been shown qualitatively in the previous section that dent fatigue behavior is driven, in large part, by the influence that dent geometry has on dent stress behavior. In what follow, several approaches to predicting dent fatigue life are discussed and a general approach to predicting fatigue behavior is introduced. This approach is based on a fundamental fracture mechanics based approach to fatigue. It appears to accurately predict dent fatigue life in a wide variety of dent situations. The general stress based nature of this approach reduces the problem of understanding the influence of dent geometry on dent fatigue to one of understanding the influence of dent geometry on dent stress behavior.

An early approach to dent fatigue life life prediction was developed by Fowler, et $al.$ [9]. In this approach tabulated stress concentration values and gouge correction factors are used in conjunction with an $S - N$ type of fatigue life curve to predict fatigue life. It is not clear how generally accurate this approach is as it was only applied to a case study in [9]. It appears to be quite conservative. This approach is also somewhat empirical, as the gouge correction factors are based on full-scale test data and the $S - N$ curve used is a general "code" type of fatigue curve.

One of the main drawbacks of an $S - N$ approach is the material resistance curve that relates stress range, S, to N, the number of cycles to failure. This curve is determined experimentally and is often highly case specific given the expense involved in performing a wide range of tests. Not only is it material specific, but it can be flaw specific, geometry specific, residual stress specific, and load history specific (in particular with regard to the R ratio). A second problem with $S - N$ approaches is that it is not entirely clear how to deal properly with variable amplitude loading. Some sort of cumulative damage law must be used to average individual N_i predictions

for each stress range case, S_i in a load history. A standard approach is to use the rain-flow method to count cycles in a load history and then use the Palmgren-Miner rule to calculate cumulative damage [27]. However, the presence of residual stress induced crack-closure effects in dents complicates damage accumulation by rendering it nonlinear. There is some question as to how to calculate damage accumulation properly for these general circumstances since the Palmgren-Miner approach assumes linear damage accumulation.

Another approach to dent fatigue life prediction has been developed by Hagiwara *et al.* [10, 28]. This approach is empirical and focused on dents with clear mechanical damage in the form of a gouge in the dent center. Based on a study of a number of pipes with different dent depths, gouge depths, pipe diameters, and steel grades an empirical expression relating dent fatigue life to these parameters is developed using linear regression analysis. Dent depth, the only dent geometry factor apparently considered in this study, was shown to have the greatest influence on fatigue life, followed by gouge depth and steel grade. This empirical approach appears to be very successful at predicting the laboratory results it is calibrated against and appears to be simple to apply. However, it does not provide a great deal of insight into the fundamental processes of pipeline dent fatigue. Furthermore, it may be limited to specific circumstances.

A much more general and less empirical approach to fatigue life prediction is the fracture-mechanics based approach. This approach relates remote stress change values to local stress change values present at the crack tip, expressed in terms of the change in the crack tip stress intensity factor, ΔK. Expressions exist for this relationship for a wide variety of crack and specimen geometries. The change in crack tip stress is then related empirically to the amount of incremental crack extension, da through a power law relationship. The number of cycles required to achieve a certain crack depth a is

then determined by integration. While the expression relating ΔK and da is empirical it is specific only to material type and the microstructural mechanism involved in crack formation. Thus, the fracture mechanics approach is more general than the S-N approach in terms of range of application. Furthermore, because crack growth can be calculated on a cycle by cycle basis, variable amplitude situations may be dealt with more directly. The fracture mechanics approach to fatigue is a well-developed and highly successful application of the theory of fracture mechanics [29, 30, 27]

A fracture mechanics based approach to dent fatigue assessment has been proposed by Dinovitzer *et al.* [23, 31]. In this approach, introduced in [23] situational inputs are established, including dent profile, pipe characteristics, pressure history, state of indentor contact, and local issues such as a weld proximity. A finite element model of the dent is created so that dent stress behavior can be determined. Then, these inputs are combined with a power–law fatigue crack propagation model to predict dent fatigue life. This procedure is apparently fairly automated and can evaluate three-dimensional measurements of dent profiles taken from the field using pigs or other pipe inspection tools. The dent geometry is forced into the mesh by deforming the initial pipe geometry to match the geometry found in the field [23]. The stress values of the dent that are associated with pressure cycling are then found using the finite element model.

Work in [31] describes efforts to expand this dent fatigue prediction model to account for effects of residual stress fields associated with welds and corrosion effects. The weld residual stress field is modelled by establishing thermal gradients in the initial pipe mesh. The stress concentration associated with weld geometry is applied to the local dent stress condition that is found using the finite element model. Corrosion effects are also accounted for including both reduction of wall thickness through corrosion and corrosion influences on fatigue processes.

The Dinovitzer model is impressive in scope. However, because it is apparently proprietary many details about implementation are unavailable. In addition, there is only limited published evidence of good agreement between this model and full scale experiments, so that the generality of model success is in question. Also, it is not entirely clear how the model incorporates the rerounding phenomenon. As noted earlier, some dents experience a great deal of rerounding before they achieve the stable configuration in which they spend the majority of their operational life. Dent rerounding influences the final dent residual stress configuration. As a result, there is some concern that the Dinovitzer model doesn't include accurate dent residual stress values. Regardless of these issues, the Dinovitzer approach seems promising. However, its proprietary nature means it is not available for use in a fundamental study of dent fatigue mechanics.

An independent dent fatigue life prediction model has been developed by Rinehart and Keating [22, 21]. Because this model is based on a fracture mechanics approach it appears to be similar to that developed by Dinovitzer *et al.* [23, 31]. This model does not account for the range of situations covered by Dinovitzer *et al.*, especially the influences of welds and corrosion effect discussed in [31]. However, it is based in fundamentals of fracture mechanics and stress analysis and could be extended to consider a wider range of situations, such as the presence of gouges, weld proximity, and corrosion effects. In addition, this approach has some unique features. First, it accounts for crack initiation behavior, an important part of the problem that must be considered when obvious sharpened defects are not present in the dent [22]. In addition, this model takes a fundamental, general approach to accounting for residual stress effects by considering crack closure behavior. Third, the Rinehart–Keating model has been verified against a set of experimental data for a range of cases. Finally details of this model are openly available in the literature.

Because the Rinehart–Keating [22, 21] model is experimentally validated for a range of dent geometries and because it is easily accessible through the literature, it will be used here to demonstrate that a thorough understanding of dent fatigue behavior depends on an understanding of dent stress behavior.

The fracture–mechanics based approach to dent fatigue suggested by Rinehart and Keating [21, 22] is based primarily on the idea that incremental growth, or propagation, of an existing crack can be correlated to changes in the crack tip stress intensity factor through a power-law relationship:

$$\frac{da}{dN} = C(\Delta K_I)^n \tag{2.1}$$

The Eq. 2.1 power-law relationship is a widely accepted model of fatigue crack propagation [29, 30, 27]. In Eq. 2.1, the change in crack length a over a given cycle N is correlated to the change in the crack tip stress intensity factor ΔK_I. The parameters C and n are material specific constants and are taken to be $3.6x10^-6$ and 3.0 respectively. These values are appropriate for analyzing crack growth in ferrite-pearlite steels such as API 5L pipeline steels [30]

The crack tip stress intensity factor K_I is essentially a measure of the load condition present at a crack tip. It is dependent on the mode of crack opening. There are three possible opening modes and Mode I is assumed here [30, 27]. The power law understanding of fatigue, Eq. 2.1, suggests that the larger the change in the crack tip load condition the larger the increase in fatigue crack length. The change in the crack tip stress intensity factor is related to several parameters. As might be expected, load magnitude influences K_I. In addition, the existing crack size and shape as well as the specimen geometry itself all influence K_I.

A crack tip stress intensity model suggested by Isida *et al.* [32] for a semi-elliptical thumbnail type crack in a plate subjected to both bending and axial loads was used

by [22, 21] to study fatigue behavior in pipeline dents:

$$\Delta K_I = \sqrt{\pi a}\left(k_A F_C^A + k_B F_C^B\right)\Delta\sigma_{\text{nominal}} \tag{2.2}$$

In Eq. 2.2, axial and bending stress change components are determined from the nominal stress change $\Delta\sigma$ by axial and bending stress concentration factors k_A and k_B. These stress concentration factors are calculated in [22, 21] from inner and outer surface stress concentration factors, k_{inner} and k_{outer}, found using finite element analysis:

$$k_A = \tfrac{1}{2}\left(k_{\text{outersurface}} + k_{\text{innersurface}}\right)$$

$$\tag{2.3}$$

$$k_B = \tfrac{1}{2}\lvert k_{\text{outersurface}} - k_{\text{innersurface}}\rvert$$

Equations 2.1, 2.2 and 2.3 indicate that the stress concentration behavior of a dent is directly related to the fatigue behavior of the dent.

As noted, crack geometry also plays a role in determining the stress intensity factor. In Eq. 2.2 the terms F_C^A and F_C^B are empirical terms related to crack aspect ratio. Because these terms of are somewhat complicated and because crack aspect ratio effects do not play a significant role in the existing fatigue model [21, 22] the reader is referred to [32, 21, 22] for details.

It was pointed out earlier in this chapter, especially in Fig. 3, that dent stress concentration values can change considerably from dent to dent. The fatigue model describing crack behavior, summarized by Eqs. 2.1 and 2.2, does contain influential parameters other than the stress concentration descriptors k_A and k_B. However, these other parameters, in particular material type and crack aspect ratio, are not assumed to vary significantly from dent to dent. As a result, dent fatigue behavior seems to depend, in large part, on dent stress concentration behavior. Thus a better

understanding of dent stress concentration behavior would appear to be valuable in terms of improved understanding of dent fatigue behavior.

In some cases, dents do not have preexisting sharpened flaws and a fatigue crack must first initiate before propagation behavior described by Eqs. 2.1 and 2.2 begins. A method for estimating the number of cycles required to initiate a crack 0.00984 in. (0.25 mm) deep in a dent is discussed in [22]. This method is based on work discussed by Dowling [33] that relates crack initiation life to the local strain range. A cumulative damage approach is used in [22] to deal with variable amplitude loading. Local strain range is related to nominal strain range in [22] by assuming elastic behavior and using dent specific stress–strain concentration factors. Thus, dent fatigue crack initiation life can also be viewed as being fundamentally influenced by dent stress concentration behavior.

One major finding of Rinehart and Keating's study of dent fatigue behavior in [22, 21] was that dent residual stress behavior also plays a significant role. To check fatigue model validity in [22, 21] case-by-case dent fatigue life predictions were made for situations for which experimentally measured fatigue life and fatigue crack size data were available in [8]. When residual stress effects were ignored, agreement between prediction and experiment was poor, as shown in Fig. 8. This observation illustrates that the effect of dent residual stress on fatigue crack closure behavior needs to be accounted for.

The concept of fatigue crack closure is that a fatigue crack can't grow if the crack tip can't physically open. If some force acts to hold a crack shut, then this force must be overcome before a crack will open and fatigue crack extension can occur at the crack tip. Crack closure effects can stem from crack tip residual streses that act to close the crack, mechanical or chemical adhesion of the fracture surfaces, or the presence of a global residual stress field that acts to keep the crack closed. In Fig. 4
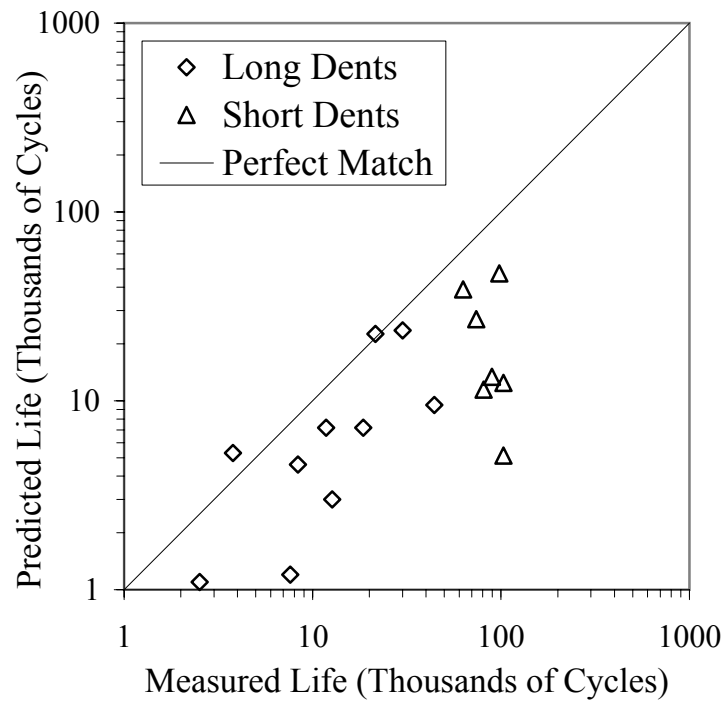
Fig. 8. Plot of predicted versus measured dent fatigue lives generated using approach presented in [21] and [22] with data available in [8] and developed without accounting for the effect of dent residual stress on fatigue crack closure behavior (adapted with permission from [21] courtesy of ASME).

it was shown that a compressive residual stress can exist at the outer surface location where fatigue cracks initiate and propagate in both long and short dents. In [22, 21] it was assumed that these outer surface residual stresses lead to crack closure effects that significantly influence dent fatigue life.

A number of approaches exist for accounting for crack closure effects. A very simple approach proposed by Bloom [34] was used in [22, 21]. Bloom suggests truncating the total stress range experienced by a crack to include only that portion of the stress range spent in tension [34]. This approach does not account for R-ratio effects but it is not clear how significant these effects are compared to global residual stress effects in the case of dent fatigue. Rinehart and Keating further simplify this approach by only considering the outer surface value of residual stress at the location of fatigue crack growth. It would be more accurate to evaluate the residual stress value at the exact crack depth. However, it is assumed that since dent fatigue cracks spend most of their life as relatively small cracks at the outer surface of the pipe wall it is reasonable to assume the residual stress value can be fixed at the outer surface value. Truncating the stress range to include only the tensile portion of the range and then calculating fatigue life using this effective stress range improves overall agreement between dent fatigue life prediction and measurement, as seen in Fig. 9.

Overall root–mean–squared agreement in Fig. 9 is approximately 1.36. For long dents the R.M.S. error in Fig. 9 is approximately 1.38 and for short short dents it is approximately 1.33. There is some question as to whether the power law approach to fracture mechanics is applicable for cases with relatively short lives. If long dent data with lives below 12,000 cycles are neglected, then long dent R.M.S. agreement becomes 1.09. In general, the model used in [22, 21] tends to overestimate life, probably due to limitations of assumptions. Certainly a more refined fatigue model could be developed. However, it seems fairly clear that given an understanding of
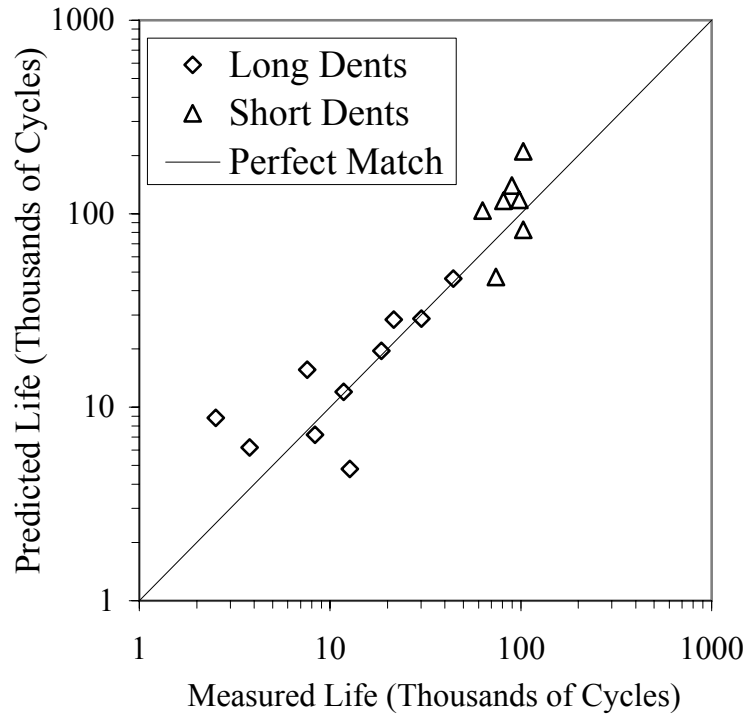
Fig. 9. Plot of predicted versus measured dent fatigue lives generated using approach presented in [21] and [22] with data available in [8] and developed accounting for the effect of dent residual stress on fatigue crack closure behavior through use of an effective stress range (adapted with permission from [21] courtesy of ASME).

dent stress behavior dent fatigue behavior can be predicted.

Several concepts are found in the preceding review of dent fatigue analysis models. First, dent fatigue processes can be modelled in either an empirical or a fracture–mechanics based manner. Second, these models can be calibrated to be accurate for the cases in which experimental data is available. Third, these models, especially the Dinovitzer and Rinehart–Keating models, show that dent fatigue behavior is driven in large part by dent stress behavior. In particular, dent geometry effects on fatigue life are due to dent geometry effects on dent stress. If an improved general understanding of the relationship between dent stress and dent fatigue can be developed then an improved understanding of dent fatigue behavior will result. Finally, while these models provide case-by-case predictive tools that may be accurate they do not provide a great deal of detail as to how dents behave from a mechanical standpoint. The issue of dent mechanics is interesting and not just academic. Recall, Keating and Hoffmann's demonstration that long and short dents have markedly different fatigue lives [8]. A more fundamental and general understanding of dent mechanics could lead to simple, general guidelines that would aid in dent assessment. In particular, two practical questions of dent mechanics would contribute to current understandings of dent fatigue. First, it is important to establish what measurable features of dent geometry distinguish long dents from short dents. Second, the possibility exists that simple, fairly accurate dent fatigue life predictions could be made without constantly needing to resort to finite element analysis if a fairly accurate understanding could be developed of the dependency of important dent stress values on dent geometry features.

C.   Approaches to Dent Stress Analysis

The mechanics of a pipeline dent are quite complicated. To fully model all phases of the dent life cycle one would have to consider contact mechanics and nonlinearities in both material and geometry. However, it has been noted that after a few initial pressure cycles dents achieve a stable rerounded configuration [8, 24]. Dent residual stresses are determined by what happens during the early inelastic cycles. If the early pressure cycles are not exceeded in magnitude by later cycle pressure and if a significant amount of strain hardening does not occur, then the dent residual stress distribution can be assumed to remain relatively fixed throughout the life of the rerounded dent. This result has been shown to be strictly true in the case of a beam cross-section composed of elastic–perfectly plastic material [35]. If one assumes a stable rerounded configuration is achieved early in the dent life, the problem of finding the residual stress distribution becomes separated from the problem of finding the dent stress concentration behavior. Furthermore, if one neglects the fact that dent stress concentration behavior is mildly influenced by geometric nonlinearity, one can treat the dent stress concentration problem as a linear elastic problem of shell mechanics.

It has been proposed here that dent residual stress is developed during early rerounding pressure cycles and is constant throughout the rest of the dent life and that dent stress concentration behavior is linear elastic. These assumptions were used in the fatigue studies carried out by Rinehart and Keating[22, 21]. As noted previously, these studies, and their assumptions, led to good agreement with experimental dent fatigue data. Thus, while special cases will certainly exist in reality, these assumptions appear sound for general application.

Ideally, to understand mechanical relationships it would be best to develop a closed–form analytical model of the situation. However, this approach does not appear

feasible for the case of pipeline dents. Even with the assumptions stated and with regard to the elastic stress concentration part of the problem, the local geometry of the dent is too complicated to readily permit direct analysis. Two other approaches, however, do exist. One may treat the problem with finite element analysis or with approximate semi-analytical approaches.

Finite element analysis has been used widely to study dent mechanics [8, 16, 9, 14, 23, 31, 22, 21, 2, 36]. General-use finite element analysis packages such as ABAQUS [37] are well suited to study all aspects of the dent stress problem. In particular, finite element analysis offers an efficient and accurate means of studying the contact and inelastic phases of the dent life cycle so that dent residual stresses may be fully and accurately characterized. Finite element analysis is a valuable and important tool that should be included in any investigation of dent mechanics.

Finite element analysis does, however, have drawbacks. Mainly, any understanding of a problem developed using this approach will be empirical in nature. Empirical approaches to dent analysis have had limited success. Prime examples are the lack of agreement in the literature over the importance of dent length and the highly qualitative nature of many existing results in dent mechanics. These problems arise because empirical studies are, by nature, bounded. In addition, the large amount of data generated by a finite element analysis of even a simple instance of a complicated feature like a pipeline dent means that it is difficult to gauge important aspects of the problem. A second drawback of finite element analysis of the complete dent problem is that each analysis is computationally intensive. Running the wide range of cases necessary to sufficiently characterize the influence of several dent parameters becomes quite time consuming.

While an analytical solution to the dent stress problem is desirable because it overcomes the shortcomings of the finite element approach, it is not feasible. How-

ever, an approximate approach exists which appears to offer a promising means for studying the elastic stress concentration behavior of dents. This approach, called the Equivalent Load Method, has been used to study the stress behavior of local imperfections in shell structures with apparently reasonable accuracy [17, 20]. It was developed in the late 1970's and early 1980's as a means of studying geometrically imperfect shells with a greater degree of computational efficiency than that which was available using finite element analysis. While the Equivalent Load Method is no longer necessary as a computational tool, it does have certain features that are attractive. It can be implemented in a semi-analytical formulation and so can provide some functional information about the problem it is applied to. The semi-analytical formulation is also easily used to characterize a range of cases. In fact, a combination of finite element analysis and equivalent load analysis appear to offer a way in which an accurate and fairly complete understanding of dent stress behavior can be developed for a range of dent conditions.

As illustrated by the foregoing discussion, a fair amount of work has been done on the problem of dent fatigue. However, a clear, general understanding of the phenomenon does not yet exist. In addition, accurate, simple–to–use dent assessment guidelines do not exist. Previous research has clearly demonstrated that dent geometry features such as depth and length play a major role in determining dent fatigue life. In addition, it has been shown that these features influence fatigue life because they influence dent stress features that drive fatigue crack growth. Models exist that can be used to predict dent fatigue life if dent stress information is available. At the same time, the current understanding of dent stress behavior is poor. However, tools exist that can be used to study dent stress behavior. As a result, a study needs to be performed of the influence dent geometry features have on fatigue inducing dent stress characteristics. Where possible, the results of this study need to be used to address

the dent fatigue problem. In particular, geometry boundaries that distinguish classes of dent stress behavior need to be established for the purposes of dent assessment. Also, accurate models describing dent stress behavior in terms of geometry need to be developed.

CHAPTER III

THE EQUIVALENT LOAD APPROACH

It would be practical to be able to assess dent fatigue life based on dent geometry features. Models of dent fatigue behavior currently exist [22, 21] that can be used to predict dent fatigue behavior given information about the stress concentration factor and the outer surface residual stress value present at the location of fatigue cracking. However, qualitative evidence [8, 16, 14, 15] indicates that these dent stress features are dependent, in large part, on dent geometry. Thus, if the relationship between dent stress geometry and dent stress behavior can be understood, then the relationship between dent geometry and dent fatigue behavior can be calculated directly.

During formation and early pressure cycling, dent behavior is highly inelastic. In particular, once a dent is formed and the indentor removed, early pressure cycles may force the dent to permanently flatten out or reround [8, 24]. This behavior has been investigated experimentally and numerically [8, 24]. If later pressure cycles never exceed the magnitude of the early rerounding pressure cycles, then the dent will achieve a stable rerounded configuration after relatively few cycles and subsequent dent behavior is elastic. A fundamental consideration of multi-cycle inelastic bending has corroborated this result [35].

The assumption of a stable rerounded dent configuration considerably simplifies the analysis of dent fatigue. First, this assumption means that the residual stresses created during early cycle inelastic deformation remain unchanged during later pressure cycling. Second, this assumption permits the problem of the behavior of the stable rerounded dent to be treated as an elastic problem. This assumption was made in case–by–case finite element models used in dent fatigue life predictions [22, 21] that were validated with reasonable accuracy against experimental data. These two

simplifications permit the problem to be split into two simpler problems. The first problem is that of determining the relationship between stable dent geometry and elastic dent stress concentration behavior. The second problem is that of determining the residual stress values associated with a given stable dent geometry.

The determination of the elastic stress concentration behavior may be approached in at least three ways. Ideally, one would like to determine an exact analytical solution. Such a solution directly provides information about the relationship between dent geometry and elastic dent behavior. However, such a solution is either difficult or impossible to find for the general dent situation because the dent has complex local geometry. Another approach is to use Finite Element Analysis. This approach has been demonstrated to provide very accurate results in many situations. However, the finite element approach has drawbacks as well. First, it is empirical, so that information about the relationship between geometry and stress behavior must be inferred. Second, each dent geometry case will require the generation and analysis of a new finite element mesh, which will be time consuming.

A third option does exist. An approximate but fairly accurate approach called the Equivalent Load Method (ELM) has been developed to study the stress behavior of thin–shell structures containing geometric imperfections. In this approach, the effects of complicated geometry are shown to be approximately equivalent to the effects of complicated load patterns. Figure 10 illustrates the equivalent load approach. Essentially, the stress behavior of a geometrically imperfect shell under load is equivalent to the sum of two stress fields. The first stress field is produced by the original load acting on the geometrically perfect version of the shell. The second stress field results from applying to the perfect version of the shell a load pattern that results in perturbation stress behavior equivalent to that which would be induced by the geometric imperfection. It should be emphasized that the equivalent load does not

Imperfect Shell
Under Pressure

≈

+

Perfect Shell
Under Pressure

Perfect Shell Under
1st Order
Equivalent Load
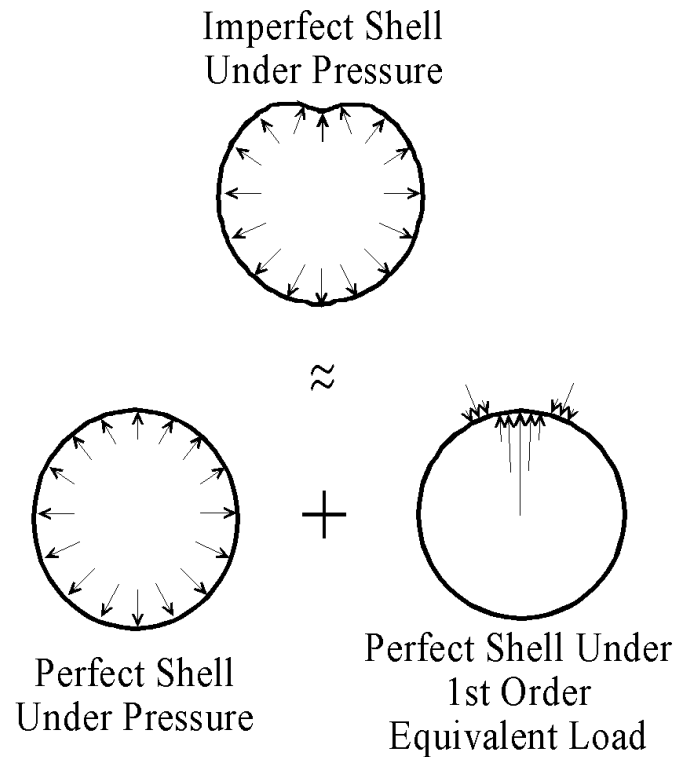
Fig. 10. Schematic illustration of equivalent load analysis of 2–D dented cylinder under internal pressure.

produce the correct dent shape but instead acts to produce a stress effect that is similar to that which would have been produced by the dent.

The Equivalent Load Method can be implemented in a semi–analytical form, as will be shown in Chapter IV. Thus, some functional information about the relationship between dent geometry and dent stress behavior will likely result. This fact means that equivalent load analysis is not purely empirical. Furthermore, the problem of an perfect shell subject to a complicated load pattern can be solved efficiently with a simple numerical routine. As a result, the equivalent load method may provide for examining a wide variety of cases without requiring a new model to be developed for

each one, like in Finite Element Analysis.

The Equivalent Load Method will be explored as a means of developing an understanding of dent stress concentration behavior that is both general and fairly accurate. Where successful, the results of this approximate analysis will then be adjusted for accuracy based on more accurate results taken from a limited number of finite element studies. It will be shown, however, that the equivalent load method has a previously unreported limited range of application.

A.   The Equivalent Load Method

The equivalence between a geometric imperfection in a thin–shell and an externally applied load distribution was first established by Calladine in 1972 [17]. The equivalent load approach was used extensively in the late 1970's and early 1980's to study the implications of geometric imperfections in hyperbolic reinforced concrete cooling towers [38, 39, 18, 40, 19, 41, 42, 43] following the collapse of such a structure in Ardeer, Scotland. It has also been applied to spherical pressure vessels containing imperfections [44] and dented cylindrical shell axial members used in offshore platforms [45, 46]. A book dealing with the subject of imperfections in shell structures [20] also presents this technique. Although the method is approximate, it has been reported to be fairly accurate, especially when second order equivalent load terms are included [47]. In addition, it can be implemented in a semi-analytical manner, so as to give functional information about the role different parameters play in the functional stress behavior of the shell.

The fundamental basis for the Equivalent Load Method has been shown in three ways. Calladine wrote the governing equations for a thin-shell of revolution and considered the influence of small deviations in radius through the application of a

variational operator [17]. In the formulation that results, the situation of an imperfect shell under loading is shown to be approximately equivalent to that of a perfect shell under the same loading with an appropriate additional load distribution acting on it. In a slightly different approach, the imperfection is represented as a displacement from an initially perfect geometry [20, 40]. The total displacement value used in the shell strain-displacement relations is then replaced with the sum of the displacements due to the loading acting on the perfect shell and the imperfection's displacement profile. The formulation that results also demonstrates the equivalence shown by Calladine. A final approach is to use equilibrium to relate geometric deviations to membrane and bending forces in a differential shell element and show these forces to be equivalent to those resulting from an appropriate equivalent load distribution [42]. Although all of these arguments suggest the Equivalent Load Method could be used in a variety of structural mechanics problems, application of the technique has been confined primarily to problems of shell analysis.

In his paper [17], Calladine considered the effect of a geometric imperfection in a thin–shell of revolution. The geometry, as considered by Calladine, is shown is Fig. 11. As shown in Fig. 11, a point on the shell surface is given in terms of the meridional angle, ϕ, and the circumferential angle, θ and two of several important radii. The term r_0 is the perpendicular distance of a point on the shell surface from the axis of revolution, r_1 is the meridional radius of curvature, r_2 is the circumferential radius of curvature, and r_3 is the distance along the meridional tangent from the point on the surface to the axis of revolution. Using this definition of shell geometry, the membrane equation of equilibrium that relates the meridional and circumferential membrane forces N_ϕ^* and N_θ^* to the applied pressure p is:

$$\frac{N_\phi^*}{r_1} + \frac{N_\theta^*}{r_2} = p \tag{3.1}$$
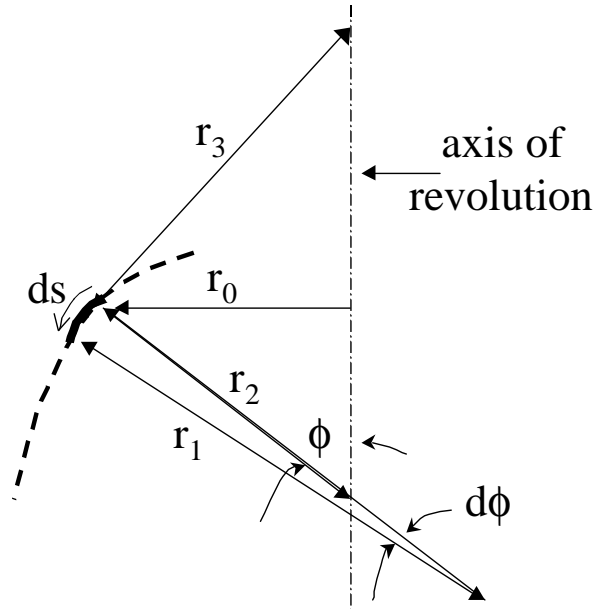
Fig. 11. Geometry of meridian of shell of revolution considered by Calladine.

Calladine's definitions of shell geometry also lead to bending equilibrium equations. However, to derive the standard expression for the equivalent load Calladine considers only the shell membrane equation. Thus, the resulting equivalent load expression is only approximate.

Calladine considers the effect of a deviation in geometry by examining the effect of such a deviation on membrane equilibrium:

$$\frac{\Delta N_\phi{}^*}{r_1} + N_\phi{}^* \Delta \left(\frac{1}{r_1}\right) + \frac{\Delta N_\theta{}^*}{r_2} + N_\theta{}^* \Delta \left(\frac{1}{r_2}\right) = p \qquad (3.2)$$

The imperfection is described by the function $\xi(s)$, which gives the magnitude of the imperfection in terms of location, s, on the meridian. Using geometric arguments

Calladine approximates two of the terms in Eq. 3.2 in terms of the function ξ:

$$\Delta\left(\frac{1}{r_1}\right) \approx \frac{d^2\xi}{ds^2} \tag{3.3}$$

$$\Delta\left(\frac{1}{r_2}\right) \approx -\frac{d\xi/ds}{r_3} - \frac{\xi}{r_2^2} \tag{3.4}$$

Calladine then shows that for typical imperfections:

$$\Delta\left(\frac{1}{r_2}\right) \ll \Delta\left(\frac{1}{r_1}\right) \tag{3.5}$$

Thus, the fourth term in Eq. 3.2 is neglected. Next, the membrane equilibrium of the shell "cap" is considered. The cap is the rounded top portion of the shell of revolution where the meridional angle θ approaches zero. This consideration shows that $\Delta N_\phi{}^*$ is approximately zero. As a result of this condition and Eqs. 3.2 and 3.3, the changes in membrane forces due to a meridional imperfection ξ are:

$$\Delta N_\phi{}^* \approx 0 \tag{3.6}$$

and

$$\Delta N_\theta{}^* \approx r_2 N_\phi{}^* \frac{d^2\xi}{ds^2} \tag{3.7}$$

As a result, the membrane forces present in a shell with an imperfection can be approximated as:

$$N_\theta{}^* \approx N_\theta{}^p + r_2 N_\phi{}^* \frac{d^2\xi}{ds^2} \tag{3.8}$$

$$N_\phi{}^* \approx N_\phi{}^p \tag{3.9}$$

In Eqs 3.8 and 3.9, the terms $N_\theta{}^p$ and $N_\phi{}^p$ represent the membrane forces that would be present in the shell if no imperfection existed. Substitution of Eqs 3.8 and 3.9 into Eq. 3.1 leads to the idea of an equivalent load describing the effect on shell forces of

a geometric imperfection. This equivalent load has the form:

$$p \approx N_\phi{}^* \frac{d^2\xi}{ds^2} \tag{3.10}$$

Calladine's equivalent load term only describes the effect of an axially symmetric meridional imperfection. Croll *et al.* appear to be the first to have adapted Calladine's expression to consider a general, localized three-dimensional imperfection [38]. In this case, the equivalent load is given as:

$$p^* \approx N_1\chi_1^* + 2N_{12}\chi_{12}^* + N_2\chi_2^* \tag{3.11}$$

In Eq. 3.11, χ^*_1 and χ_2^* are the changes in curvature in the two principal directions and χ_{12}^* is the change in twist. The terms N_1, N_{12}, and N_2 refer to the membrane forces present in the equivalent perfect shell due to the actual loading acting on the imperfect shell. Eq. 3.11 is the standard form of the equivalent load that has been used by most researchers studying the stress behavior of shells with imperfections [20, 38, 40, 46]. Godoy [47] has emphasized that imperfections that are deeper than the shell thickness should be modelled in an iterative nonlinear scheme using an equivalent load expression that takes into account higher order terms. He shows that such an approach considerably improves accuracy for deep imperfections.

The first order equivalent load representation of Eq. 3.11 will be used in the present study. While it is not as accurate as the scheme proposed by Godoy [47], its simple form will permit semi–analytical expression to be developed that give direct information about the relationship between dent geometry and stress behavior in the dent region. Finally, because finite element analysis will be used to validate results, a correction factor can be applied to account for inaccuracies that may exist.

B.   Implementation of Equivalent Load Method for Dents in Pipes

1.   Analytical Approach

Pipelines are cylindrical shells. The equations describing the linear–elastic small–deformation behavior of this class of shells are widely available. Flügge's notation for cylindrical shells will be used here and are taken from [48]. While Flügge's discussion of shell mechanics is clear it has a practical orientation. A more fundamental discussion of the origins of classical shell equations is given by Novozhilov [49].

Because they will become useful, the complete set of cylindrical shell equations will be given here. The coordinate system used here is presented in Fig. 12. Because the cylinder has constant radius R, every point on the shell surface can be described in terms of its longitudinal distance x from a reference circumference, its angular location ϕ relative to a reference meridian, and its distance z from the shell middle surface. The assumptions of classical shell theory are used. Specifically, shell thickness is small compared to shell radius, perpendiculars to the shell middle surface remain perpendicular after deformation, deflections are small, and deformations across the shell thickness vary linearly. These assumptions reduce the problem of shell analysis to a consideration of the behavior of the middle surface, since all thru-thickness variations in mechanical quantities can be related to middle surface behavior.

The strains in the shell wall ϵ_x, ϵ_ϕ, and $\gamma_{x\phi}$ can be found in terms of the middle surface displacements u, v, and w:

$$\epsilon_x = \frac{u'}{R} - z\frac{w''}{R^2} \tag{3.12}$$

$$\epsilon_\phi = \frac{v^{\cdot}}{R} - \frac{z}{R}\frac{w^{\cdot\cdot}}{R+z} + \frac{w}{R+z} \tag{3.13}$$

$$\gamma_{x\phi} = \frac{u^{\cdot}}{R+z} + \frac{R+z}{R^2}v' - \frac{w'^{\cdot}}{R}\left(\frac{z}{R} + \frac{z}{R+z}\right) \tag{3.14}$$
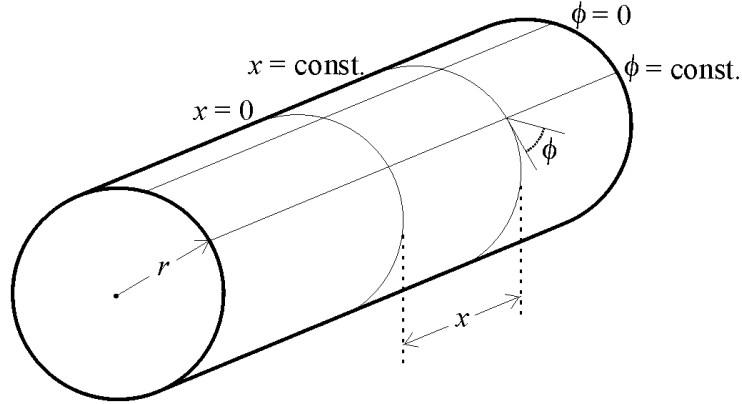
Fig. 12. Coordinate system of cylindrical shell.

where the operators $()^\cdot$ and $()'$ are defined as:

$$()' = R\frac{\partial\,()}{\partial x} \tag{3.15}$$

$$()^\cdot = \frac{\partial\,()}{\partial \phi} \tag{3.16}$$

The constituitive relations between the strains, ϵ_x, ϵ_ϕ, and $\gamma_{x\phi}$, and the stresses, σ_x, σ_ϕ, and $\tau_{x\phi}$, are those of a linear elastic material:

$$\sigma_x = \frac{E}{1-\nu^2}\left(\epsilon_x + \nu\epsilon_\phi\right) \tag{3.17}$$

$$\sigma_\phi = \frac{E}{1-\nu^2}\left(\epsilon_\phi + \nu\epsilon_x\right) \tag{3.18}$$

$$\tau_{x\phi} = \frac{E}{2\left(1+\nu\right)}\gamma_{x\phi} \tag{3.19}$$

In these expressions, E is Young's Modulus and ν is the Poisson Ratio. From the stresses the resultant forces, N_x, N_ϕ, $N_{x\phi}$, and $N_{\phi x}$, and resultant bending moments, M_x, M_ϕ, $M_{x\phi}$, and $M_{\phi x}$ can be determined. The meaning of these forces and moments in terms of shell geometry is shown in Fig. 13. The resultant–stress

relations consist of simple integrals performed over the shell thru-thickness:

$$N_x = \int_{-t/2}^{+t/2} \sigma_x \left(1 + \frac{z}{R}\right) dz \qquad N_\phi = \int_{-t/2}^{+t/2} \sigma_\phi dz$$

$$N_{x\phi} = \int_{-t/2}^{+t/2} \tau_{x\phi} \left(1 + \frac{z}{R}\right) dz \qquad N_{\phi x} = \int_{-t/2}^{+t/2} \tau_{\phi x} dz \tag{3.20}$$

$$-M_x = \int_{-t/2}^{+t/2} \sigma_x \left(1 + \frac{z}{R}\right) z dz \qquad M_\phi = -\int_{-t/2}^{+t/2} \sigma_\phi z dz$$

$$M_{x\phi} = -\int_{-t/2}^{+t/2} \tau_{x\phi} \left(1 + \frac{z}{R}\right) z dz \qquad M_{\phi x} = -\int_{-t/2}^{+t/2} \tau_{\phi x} z dz \tag{3.21}$$

In Eqs. 3.20 and 3.21, t is the shell thickness. The forces and moments shown in Fig. 13 and applied tractions or pressures, p_x, p_ϕ, and p_r can be related by equilibrium:

$$N_x' + N_{\phi x}^{\cdot} + p_x R = 0 \tag{3.22}$$

$$R N_\phi^{\cdot} + R N_{x\phi}' - M_\phi^{\cdot} - M_{x\phi}' + p_\phi R^2 = 0 \tag{3.23}$$

$$M_\phi^{\cdot\cdot} + M_{x\phi}'^{\cdot} + M_{\phi x}^{\cdot} + M_x'' + R N_\phi - p_r R^2 = 0 \tag{3.24}$$

$$R N_{x\phi} - R N_{\phi x}^{\cdot} + M_{\phi x} = 0 \tag{3.25}$$

Knowing the equilibrium relations and the other preceding relations it is possible to express equilibrium in terms of the displacements. It is found that the fourth equilibrium condition, Eq. 3.25, is satisfied identically so that the shell problem is reduced to set of three differential equations:

$$u'' + \frac{1-\nu}{2} u^{\cdot\cdot} + \frac{1+\nu}{2} v'^{\cdot} + \nu w' + k \left(\frac{1-\nu}{2} u^{\cdot\cdot} - w''' + \frac{1-\nu}{2} w'^{\cdot\cdot}\right) + \frac{p_x R^2}{\bar{D}} = 0 \tag{3.26}$$

$$\frac{1+\nu}{2} u'^{\cdot} + v^{\cdot\cdot} + \frac{1-\nu}{2} v'' + w^{\cdot} + k \left(\frac{3}{2}(1-\nu) v'' - \frac{3-\nu}{2} w''^{\cdot}\right) + \frac{p_\phi R^2}{\bar{D}} = 0 \tag{3.27}$$

$$\nu u' + v^{\cdot} + w + k \left(\frac{1-\nu}{2} u'^{\cdot\cdot} - u''' - \frac{3-\nu}{2} v''^{\cdot} + w'''' + 2w''^{\cdot\cdot} + w^{\cdot\cdot\cdot\cdot} + 2w^{\cdot\cdot} + w\right) + \frac{p_r R^2}{\bar{D}} = 0 \tag{3.28}$$

In Eqs. 3.26 through 3.28 the terms $\bar{D}$ and k are:

$$\bar{D} = \frac{Et}{1-\nu^2} \tag{3.29}$$
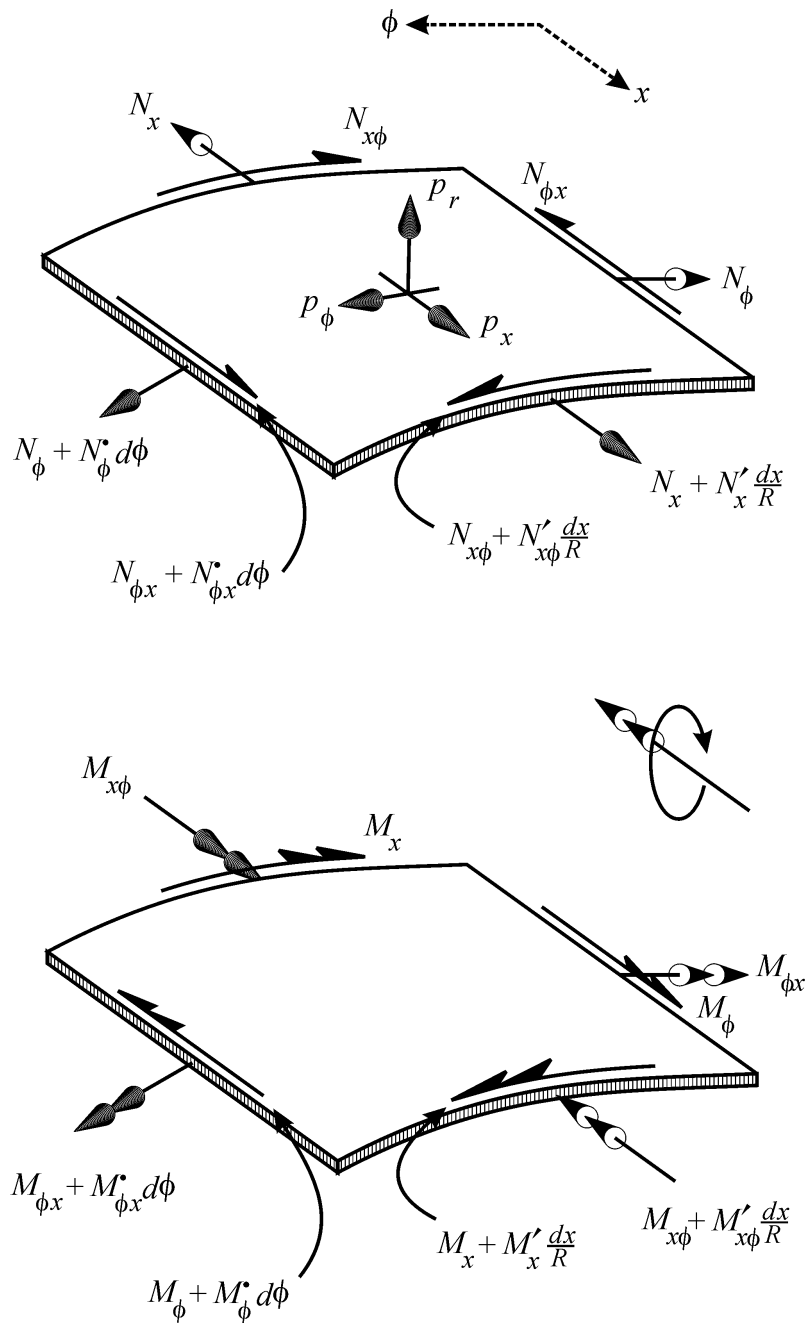
Fig. 13. Illustration of cylindrical shell membrane forces and bending moments.

$$k = \frac{t^2}{12R^2} \tag{3.30}$$

Alternatively,

$$k = \frac{K}{\bar{D}R^2} \tag{3.31}$$

where:

$$K = \frac{Et^3}{12\left(1 - \nu^2\right)} \tag{3.32}$$

It can be shown that the displacement equilibrium equations, Eqs. 3.26 to 3.28, are satisfied if the load terms and displacement terms can be written in the form of a Fourier Series [48]. Thus, if the pressure loading applied to the shell can be expressed as a Fourier Series, the form of the displacement solution is known and the problem of finding the particular solution reduces to one of solving for the Fourier Coefficients of the displacement Fourier Series. Once the displacement functions are known other useful information, such as the stress functions, can be determined. In the present situation, the pipe is assumed to be infinitely long, so that the particular solution is the solution of interest.

Most dents have a smooth profile. In addition, although dents are localized, unique features in a real pipeline, the idealized dent profile might be modelled as a periodic function if an adequate spacing is maintained so as to prevent interaction between dents. Thus, the geometric imperfections of many pipeline dents can be modelled as smooth, periodic functions. Equation 3.11 relates the equivalent load function to the imperfection geometry. The curvature terms χ_1, χ_2, and χ_{12} in Eq. 3.11 are simply second partial derivatives of the function which describes the imperfection profile. Because the imperfection profile can be expressed as a Fourier Series, the equivalent load function can also be expressed as a Fourier Series. Thus, the problem of the perfect cylinder subjected to the equivalent load can be solved with a Fourier Series Approach and an approximate solution for the elastic stresses present in the

dented pipe may be found.

Many dents essentially have double symmetry about some reference circumference and reference meridian pair. Assuming double symmetry and taking the intersection of the meridian and circumference of symmetry as the origin of the shell coordinate system, the pressure loads in Eqs. 3.26 to 3.28 may be given as Fourier Series:

$$
\begin{aligned}
p_x &= p_{x,mn} cos\left(m\phi\right) sin\left(\tfrac{\lambda x}{R}\right) \\
p_\phi &= p_{\phi,mn} sin\left(m\phi\right) cos\left(\tfrac{\lambda x}{R}\right) \\
p_r &= p_{r,mn} cos\left(m\phi\right) cos\left(\tfrac{\lambda x}{R}\right)
\end{aligned}
\tag{3.33}
$$

The λ term conveniently represents the longitudinal Fourier Series index n and period l:

$$
\lambda = n\frac{\pi R}{l}
\tag{3.34}
$$

While it was noted that the load has even symmetry, there are sine terms in Eq. 3.33. These sines are a result of sign convention requirements at the coordinate system origin. The three shell differential equations Eqs. 3.26 to 3.28 are satisfied if the loads are of the form given in Eq. 3.33 and the displacement are of a similar form:

$$
\begin{aligned}
u &= u_{mn} cos\left(m\phi\right) sin\left(\tfrac{\lambda x}{R}\right) \\
v &= v_{mn} sin\left(m\phi\right) cos\left(\tfrac{\lambda x}{R}\right) \\
w &= w_{mn} cos\left(m\phi\right) cos\left(\tfrac{\lambda x}{R}\right)
\end{aligned}
\tag{3.35}
$$

As noted, when loads and displacements are written as Fourier Series in the forms of Eqs. 3.33 and 3.35, the three equilibrium equations, Eqs. 3.26 to 3.28, are satisfied. In particular, one is left with a set of three coupled linear equations that

must be solved for each m, n combination:

$$\begin{bmatrix} k_{11} & k_{12} & k_{13} \\ k_{21} & k_{22} & k_{23} \\ k_{31} & k_{32} & k_{33} \end{bmatrix} \begin{pmatrix} u_{mn} \\ v_{mn} \\ w_{mn} \end{pmatrix} = \begin{pmatrix} \frac{R^2 p_{x,mn}}{D} \\ \frac{R^2 p_{\phi,mn}}{D} \\ \frac{R^2 p_{r,mn}}{D} \end{pmatrix} \tag{3.36}$$

The k_{ij} coefficients of the matrix are given in terms of m and $\lambda = (n\pi R)/l$:

$$k_{11} = \lambda^2 + \left(\frac{1-\nu}{2}\right)(1+k)m^2 \tag{3.37}$$

$$k_{12} = k_{21} = \frac{1+\nu}{2}m\lambda \tag{3.38}$$

$$k_{13} = k_{31} = \nu\lambda + k\left(\lambda^2 - \left(\frac{1-\nu}{2}\right)\lambda m^2\right) \tag{3.39}$$

$$k_{22} = m^2 + \frac{(1-\nu)(3k+1)}{2}\lambda^2 \tag{3.40}$$

$$k_{23} = k_{32} = m + k\left(\frac{3-\nu}{2}\right)\lambda^2 m \tag{3.41}$$

$$k_{33} = 1 + k(\lambda^4 + 2m^2\lambda^2 + m^4 + 2m^2 + 1) \tag{3.42}$$

Equation 3.36 and Eqs. 3.37 through 3.42 may be used to determine the Fourier components of the displacement functions from the Fourier components of the load terms. The displacement functions may be reassembled from these coefficients, as in Eq. 3.35, and the resulting membrane and moment results may be determined based on equations given in [48]:

$$N_\phi = \frac{\bar{D}}{R}(v^{\cdot} + w + \nu u') + \frac{K}{R^3}(w + w^{\cdot\cdot}) \tag{3.43}$$

$$N_x = \frac{\bar{D}}{R}(u' + \nu v^{\cdot} w + \nu w) - \frac{K}{R^3}(w'') \tag{3.44}$$

$$N_{\phi x} = \frac{\bar{D}}{R}\left(\frac{1-\nu}{2}\right)(u^{\cdot} + v') + \frac{K}{R^3}\frac{1-\nu}{2}(u^{\cdot} + w'^{\cdot}) \tag{3.45}$$

$$N_{x\phi} = \frac{D}{R}\left(\frac{1-\nu}{2}\right)(u^{\cdot} + v') + \frac{K}{R^3}\frac{1-\nu}{2}(v' - w'^{\cdot}) \tag{3.46}$$

$$M_\phi = \frac{K}{R^2} \left(w + w^{..} + \nu w'' \right) \tag{3.47}$$

$$M_x = \frac{K}{R^2} \left(w'' + \nu w^{..} - u' - \nu v^{.} \right) \tag{3.48}$$

$$M_{\phi x} = \frac{K}{R^2} \left(1 - \nu \right) \left(w'^{.} + \frac{1}{2} u^{.} - \frac{1}{2} v' \right) \tag{3.49}$$

$$M_{x\phi} = \frac{K}{R^2} \left(1 - \nu \right) \left(w'^{.} - v' \right) \tag{3.50}$$

Substituting for u, v, and w in Eqs. 3.43 through 3.50 with the Fourier Series version of the displacements, Eq. 3.35, leads to a set of equations for Fourier Series components of membrane and bending resultants. For example, the N_ϕ resultant can be written as:

$$N_\phi = N_{\phi,mn} \cos\left(m\phi \right) \cos\left(\frac{n\pi x}{L} \right) =$$
$$\sum_{m=0}^{M} \sum_{n=0}^{N} \left[\frac{\bar{D}}{R} \left(m v_{mn} + w_{mn} + \frac{\nu R n \pi}{L} u_{mn} \right) + \frac{K}{R^3} \left(1 - m^2 \right) w_{mn} \right] \cos\left(m\phi \right) \cos\left(\frac{n\pi x}{L} \right) \tag{3.51}$$

Equation 3.51, demonstrates that relationships exist between resultant coefficients and displacement coefficients. For $N_{\phi,mn}$ and $M_{\phi,mn}$ These relationships take the form:

$$N_{\phi,mn} = \frac{\bar{D}}{R} \left(m v_{mn} + w_{mn} + \frac{\nu R n \pi}{L} u_{mn} \right) + \frac{K}{R^3} \left(1 - m^2 \right) w_{mn} \tag{3.52}$$

$$M_{\phi,mn} = \frac{K}{a^2} \left(1 - m^2 - \nu \frac{a^2 n^2 \pi^2}{l^2} \right) w_{mn} \tag{3.53}$$

Thus, coefficients for Fourier Series representing resultants can be determined directly from the displacement coefficients.

Stress terms can be written in terms of membrane and moment resultants. Flugge[48] gives these relationships as:

$$\sigma_x = \frac{N_x}{t} - \frac{12 M_x}{t^3} z \tag{3.54}$$

$$\sigma_\phi = \frac{N_\phi}{t} - \frac{12 M_\phi}{t^3} z \tag{3.55}$$

$$\tau_{x\phi} = \frac{N_{x\phi}}{t} - \frac{12M_{x\phi}}{t^3}z \tag{3.56}$$

$$\tau_{\phi x} = \frac{N_{\phi x}}{t} - \frac{12M_{\phi x}}{t^3}z \tag{3.57}$$

Equations 3.54 through 3.57 represent stress components over the through-thickness variable z. Outer and inner surface stress values can be obtained by substituting $z = \pm t/2$. The stress function can be written as double Fourier Series in terms of the force and moment resultant Fourier Series coefficients. As noted in Eq. 3.52 these coefficients can then, in turn, be written in terms of the displacement coefficients u_{mn}, v_{mn}, and w_{mn}. As a result, the stress functions can be written directly in terms of the displacement coefficients. The resulting expressions for the inner and outer surface values of σ_x and σ_ϕ are:

$$
\begin{aligned}
\sigma_x = {}& \frac{\bar{D}}{tR} \sum_{m=0}^{M} \sum_{n=0}^{N} \\
& \left(\frac{Rn\pi}{L}\right)\left(1 \pm \frac{t}{2R}\right) u_{mn} \\
& + \nu m \left(1 \pm \frac{t}{2R}\right) v_{mn} \\
& + \nu \left(1 \pm \frac{t}{2R}m^2\right) w_{mn} + \frac{R^2 n^2 \pi^2}{L^2}\left(\frac{t^2}{12R^2} \pm \frac{t}{2R}\right) w_{mn} \\
& \cos(m\phi)\cos\left(\frac{n\pi x}{L}\right)
\end{aligned}
\tag{3.58}
$$

and

$$
\begin{aligned}
\sigma_\phi = {}& \frac{\bar{D}}{tR} \sum_{m=0}^{M} \sum_{n=0}^{N} \\
& \left(\frac{\nu Rn\pi}{L}\right) u_{mn} \\
& + m v_{mn} \\
& + \left(1 + \frac{t^2}{12R^2}(1 - m^2) \mp \left(1 - m^2 - \frac{\nu R^2 n^2 \pi^2}{L^2}\right)\right) w_{mn} \\
& \cos(m\phi)\cos\left(\frac{n\pi x}{L}\right)
\end{aligned}
\tag{3.59}
$$

Using the preceding equations one can solve for stress in a pipe produced by the application of an equivalent load, and thus can solve approximately in a semi-analytical manner for the stresses produced by imperfections in the pipe. First, the equivalent load distribution is calculated based on knowledge of the imperfection

geometry and the membrane forces present in the perfect structure. The double Fourier Series coefficients of this equivalent load distribution are then found. This approach has been taken by Godoy to study spherical shells with imperfections [44]. Using Eq. 3.36 the displacement coefficients resulting from the load coefficients may be calculated in a term by term manner. Then, the hoop and longitudinal stress distributions may be determined directly using Eqs. 3.58 and 3.59. This process can be implemented through a computer program.

2.   Computational Approach

It is believed that the equivalent load approach was developed as a computation approach for studying imperfect shells at a time when limited computation resources were available. Computational speed has increased tremendously in the last few decades, mitigating the need for efficient computational approaches to imperfections. The primary value of the equivalent load approach appears to be that it can provide analytical information not offered by a completely numerical approach. However, it is important to be able to validate that the equivalent load approach is capable of accurately studying a problem before time is invested in seeking analytical insight.

Much of the effort in the analytical approach to applying the equivalent load method is expended in taking an equivalent load distribution and solving for the resulting stress behavior. As a means of checking the veracity of the equivalent load method itself a simpler approach to solving the actual shell problem would be useful. In fact, a general finite element software package can serve as a solver which can be used to check the accuracy of the equivalent load method. Once reasonable accuracy has been confirmed, the possibility of the equivalent load method providing useful functional information can be pursued with classical approaches like the one outlined in the previous section.

There are two main numerical approaches to shell analysis other than the semi-analytical approach outlined in the previous section. The first is finite differences and the second is finite elements. The finite difference method is well suited for shell analysis, however it is a geometry specific approach. As a result, it is not well-suited to provide both a solution platform and an independent evaluation of the stresses produced by a geometric imperfection in a shell.

Finite element analysis is capable of much more general application from a geometry standpoint. All that is needed to study the elastic stress behavior of an imperfect shell is a mesh of the shell geometry. In addition, finite element analysis can be used to check the accuracy of the equivalent load method.

Figure 14 illustrates the approach that can be taken to use finite element analysis as the solver engine for equivalent load analysis. A computer code or spreadsheet can be used to calculate the equivalent load distribution. The value of the equivalent load is determined at each nodal location. This value is converted into a nodal load by multiplying by the tributary area, typically the element surface area. The nodal load is decomposed into x- and y-components and list of nodal loads is prepared. This list is imported into an input file that sets up the problem of a perfect cylinder subject to the imported nodal loads. The analysis is then conducted. Finite element analysis results are processed to determine the stress predicted in the imperfect shell by adding the analysis result produced by the equivalent load to the stresses present in the perfect shell due to the original loading. Some authors [38, 42] have implied that iteration of the equivalent load analysis may improve the analysis accuracy. Further manipulation of results can be carried out and a second iteration list of nodal equivalent loads can be prepared and incorporated into another finite element model.

Using this computational approach the suitability and accuracy of the equivalent
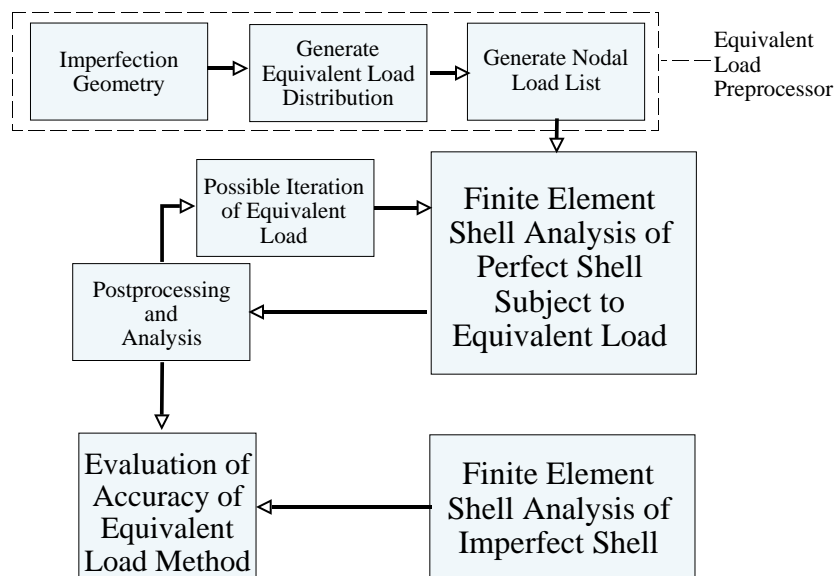
Fig. 14. Schematic representation of process in which equivalent load method calcula-
tion can be carried out using existing finite element solver routines for pur-
poses of confirming accuracy of equivalent load method.

load method itself can be judged in a simple and direct manner. Where the equivalent load method is judged to be accurate the analytical approach can be used to seek functional information about the behavior of imperfections in shells. The next chapter explores some of these issues for dents in pipes.

CHAPTER IV

APPLICATION OF EQUIVALENT LOAD ANALYSIS TO PIPELINE DENTS

In the preceding chapter an analytical framework was established for studying geometric imperfections in cylindrical shells using the equivalent load method. In this chapter two main applications of this approach are carried out. First, the simplified situation of a two-dimensional dent is considered. A simple, semi-analytical solution is found that describes behavior in this situation. Second, the application of the equivalent load method to the case of three-dimensional imperfections in shells is studied. In particular, localized, dent–like imperfections are emphasized as opposed to more broad ranging and shallow structural imperfections. Interestingly, a size effect is shown to exist in the behavior of localized three-dimensional damage. The equivalent load method is shown not to predict either this size effect or the correct behavior of highly local imperfections.

A. A Two-Dimensional Dent Model

The simplest geometric imperfections in shells are those that exist only in one coordinate direction. Indeed, in deriving the equivalent load method Calladine only considered a one-dimensional imperfection and only derived a one-dimensional version of the equivalent load distribution [17]. The early applications of the equivalent load method to analysis of cooling tower shells also restricted their attention to imperfections either in the circumferential or meridional directions [19, 38, 18].

For the case of a cylinder, the one-dimensional imperfection that makes most sense to analyze is an imperfection in the circumferential direction. This imperfection direction results in a two-dimensional dent model, where the same dented cross-section exists uniformly throughout the length of the cylinder. Figures 15 and 16
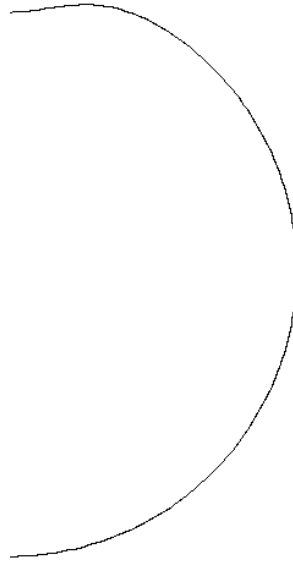
Fig. 15. Front view of half of a pipe with a two-dimensional longitudinal dent generated using a finite element mesh of a two-dimensional dent and ABAQUS VIEWER.

show profile and three-dimensional views generated in ABAQUS VIEWER of halves of a two-dimensional dent mesh. The simplified two-dimensional dent model does have some practical meaning. Presumably, the center of a long three-dimensional dent will behave in a manner similar to that of a two-dimensional longitudinal dent. In addition, a two-dimensional model might be adapted to consider the effects of weld misalignment, another important class of pipe imperfection.

1. Problem Solution

The first issue needing to be addressed in applying the equivalent load method is the matter of the imperfection geometry. Early work with hyperbolic cooling towers took direct measurements of structural imperfections from the structures themselves. In
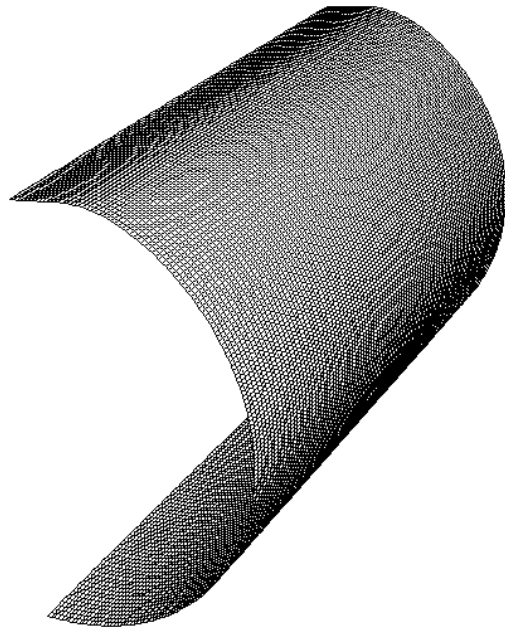
Fig. 16. Three-dimensional view of half of a pipe with a two-dimensional longitudinal dent generated using a finite element mesh of a two-dimensional dent and ABAQUS VIEWER.

the present case, measurements of real dents could be used. However, it would be difficult to study the influence of dent parameter variations with such an approach. A functional description of dent geometry would be helpful.

Some authors have used a portion of a cosine function to describe the deviation from the undamaged shell profile [20, 50, 51]. This defect description must be written with a conditional statement:

$$r(\phi) = \begin{cases} R & |\phi| > \phi_0 \\ R - \frac{\xi}{2}\left(1 + cos\left(2\pi\frac{\phi}{\phi_0}\right)\right) & |\phi| \leq \phi_0 \end{cases} \tag{4.1}$$

In Eq. 4.1, the circumferential profile $r(\phi)$ is given as a deviation from the pipe radius R. The magnitude of the deviation is controlled by the ξ term and the circumferential extent is controlled by the ϕ_0 term. The fact that Eq. 4.1 is a conditional statement means that this approach to modelling the dent profile requires some care in handling with closed-form analysis. Because the present interest is to use the equivalent load method to seek functional information about the influence of dent imperfections it would seem that Eq. 4.1 may not be the best choice.

One readily available, smooth function appears to offer an alternative to the half cosine dent model for modelling two-dimensional dents. The normal distribution is simple to implement, decays and is smooth. As a result, the normal function can be subtracted from the pipe radius to give a description of dent profile:

$$r(\phi) = R - \xi exp\left(-\frac{1}{2}\left(\phi/\phi_0\right)^2\right) \tag{4.2}$$

In Eq. 4.2 the normal distribution is subtracted from the radius R to give the profile $r(\phi)$ around the circumference of the pipe of a dent centered at $\phi = 0$. The dent depth is controlled by the magnitude of ξ and the spatial extent, or width, of the dent is controlled by the angular "decay" term ϕ_0. Figure 17 shows normalized dent

cross-sections generated using Eq. 4.2 and a relative d/D of 5%, or $\xi = 0.05$. To demonstrate the flexibility of the normal distribution dent model, four ϕ_0 values were used to generate the cross-sections in Fig. 17 and are indicated in the figure. The normal distribution dent model appears capable of producing a range of dent geometries from narrow and deep to broad and flat.

The normal and cosine dent models actually result in similar two-dimensional dent geometries, as shown in Fig. 18. In the two methods the decay coefficient ϕ_0 influences dent width differently. As a result, the profiles generated in Fig. 18 are based on model specific ϕ_0 values given in the caption. The cosine model of the dent tapers off more abruptly than the normal dent model. Since both approaches are both idealized models such small differences are considered unimportant. The present study will use the the normal distribution dent model since it is more straightforward to implement. Other functions, such as Student's t distribution, are available that could also probably be used to develop successful dent models.

Assuming a normal distribution dent geometry model, e.g. Eq. 4.2, it is possible to determine an expression for the equivalent load distribution. The traditional equivalent load distribution, discussed in Chapter III, is written for a cylinder as:

$$p^* = N_{xx}\chi_{xx} + 2N_{x\phi}\chi_{x\phi} + N_{\phi\phi}\chi_{\phi\phi} \tag{4.3}$$

In the case of a two–dimensional dent, the change-in-curvature χ_{xx} and $\chi_{x\phi}$ terms are zero and:

$$\chi_{\phi\phi} = \frac{1}{R^2}\frac{\partial^2 r(\phi)}{\partial \phi^2} = \frac{\xi}{R^2\phi_0^2}\left[1 - \left(\frac{\phi}{\phi_0}\right)^2\right]exp\left(-\frac{1}{2}\left(\frac{\phi}{\phi_0}\right)^2\right) \tag{4.4}$$

Because there is no χ_{xx} term in the two-dimensional problem, longitudinal membrane forces do not play a role in the equivalent load, Eq. 4.3. In addtion, in two-dimensions there is no ϕx cross–term because both the change–in–curvature and membrane force
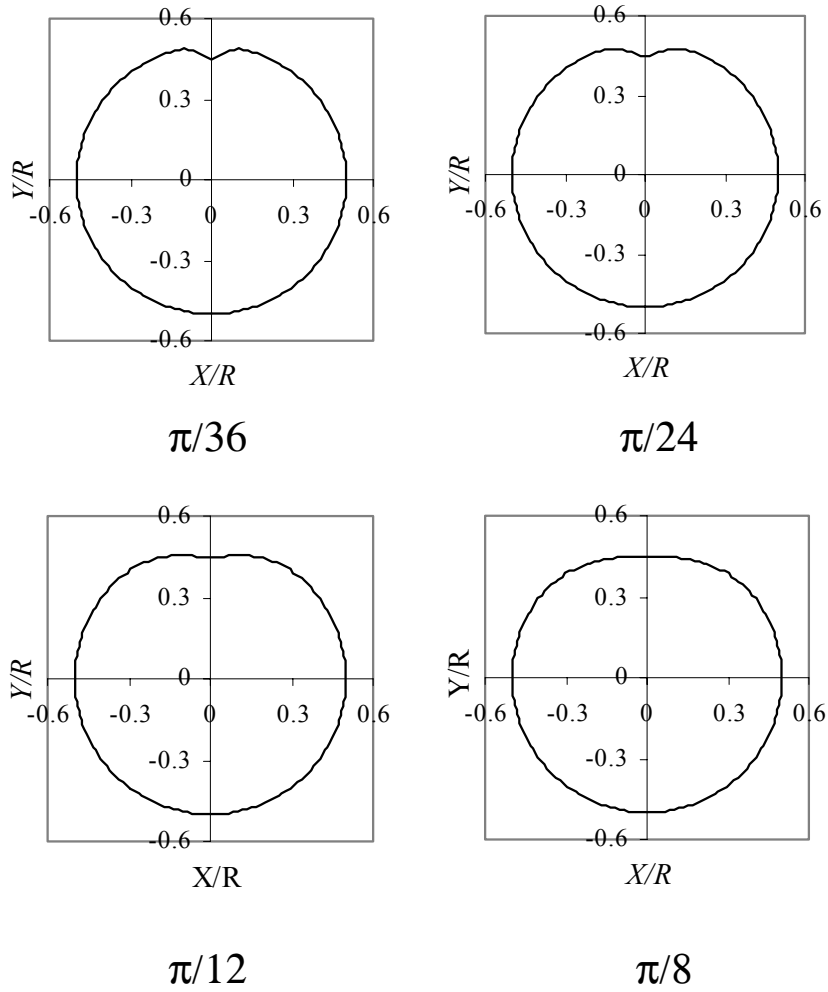
Fig. 17. Normalized two-dimensional dent cross-sections generated using Eq. 4.2 with $\xi = 0.05$, equivalent to $d/D = 5\%$ and four values of ϕ_0, $\phi_0 = \pi/36, \pi/24, \pi/12$, and $\pi/8$.
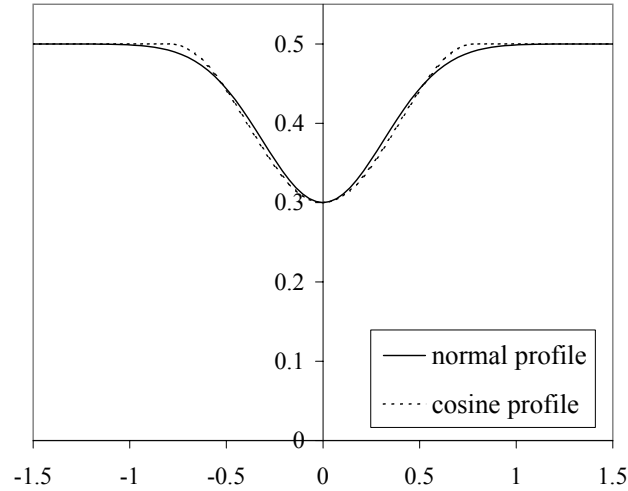
Fig. 18. Normalized two-dimensional dent cross-sections generated comparing profiles generated with Eqs. 4.1 and 4.2 with $R = 0.5$ and $\xi = 0.03$, equivalent to $d/D = 30\%$. The ϕ_0 values for the normal distribution and cosine models are $\pi/10$ and $\pi/4$ respectively.

components are zero. Thus, the equivalent load expression follows from Eq. 4.4:

$$p^* (\phi) = \frac{N_\phi \xi}{R^2 \phi_0^2} \left[1 - \left(\frac{\phi}{\phi_0} \right)^2 \right] exp \left(-\frac{1}{2} \left(\frac{\phi}{\phi_0} \right)^2 \right) \tag{4.5}$$

This equivalent load distribution is a radial pressure with a magnitude varying with ϕ.

A fourier cosine series can be found for Eq. 4.5 such that:

$$p^* = p_0^* + \sum_{m=1}^{\infty} p_m^* cos \left(m\phi \right) \tag{4.6}$$

The Fourier coefficients are found through the integrals:

$$p_0^* = \frac{1}{\pi} \int_{-\pi}^{\pi} \frac{N_\phi \xi}{R^2 \phi_0^2} \left[1 - \left(\frac{\phi}{\phi_0} \right)^2 \right] exp \left(-\frac{1}{2} \left(\frac{\phi}{\phi_0} \right)^2 \right) d\phi \tag{4.7}$$

$$p_m^* = \frac{1}{\pi} \int_{-\pi}^{\pi} \frac{N_\phi \xi}{R^2 \phi_0^2} \left[1 - \left(\frac{\phi}{\phi_0} \right)^2 \right] exp \left(-\frac{1}{2} \left(\frac{\phi}{\phi_0} \right)^2 \right) cos \left(m\phi \right) d\phi \tag{4.8}$$

A drawback of the normal distribution dent model is that the integrals in Eqs. 4.7 and 4.8 are not easily solved in closed-form. However, for a given harmonic m the integral is a constant that can be evaluated numerically, so that the equivalent load coefficients are simply:

$$p_0^* = \frac{N_\phi \xi}{R^2 \phi_0^2} I_0 \tag{4.9}$$

$$p_m^* = \frac{N_\phi \xi}{R^2 \phi_0^2} I_m \tag{4.10}$$

The I_0 term and I_m terms are constant for a given m and ϕ_0 and represent the solution to the integrals:

$$I_0 = \frac{1}{\pi} \int_{-\pi}^{\pi} \left[1 - \left(\frac{\phi}{\phi_0} \right)^2 \right] exp \left(-\frac{1}{2} \left(\frac{\phi}{\phi_0} \right)^2 \right) d\phi \tag{4.11}$$

$$I_m = \frac{1}{\pi} \int_{-\pi}^{\pi} \left[1 - \left(\frac{\phi}{\phi_0} \right)^2 \right] exp \left(-\frac{1}{2} \left(\frac{\phi}{\phi_0} \right)^2 \right) cos \left(m\phi \right) d\phi \tag{4.12}$$

The coefficients represented by Eqs. 4.11 and 4.12 depend only on ϕ_0 and can be determined using numerical integration.

In Chapter III, Eq. 3.36 established that the Fourier coefficients for the displacements are related to the Fourier coefficients of the loads. In the two-dimensional case only one harmonic is present, the other being zero. This situation considerably simplifies Eq. 3.36. The resulting relationship between load and displacement coefficients for the the two-dimensional case is considerably simplified:

$$\begin{bmatrix} 0 & 0 & 0 \\ 0 & m^2 & m \\ 0 & m & 1 + k \left(m^4 + 2m^2 + 1 \right) \end{bmatrix} \begin{pmatrix} u_m \\ v_m \\ w_m \end{pmatrix} = \begin{pmatrix} 0 \\ 0 \\ \frac{R^2 p_{r,m}}{D} \end{pmatrix} \tag{4.13}$$

The k and $\bar{D}$ terms in Eq. 4.13 are given in Eqs. 3.29 and either 3.30 or 3.31. The zeros appear on the load side of Eq. 4.13 because equivalent load analysis involves

only the analysis of radial pressure coefficients, $p_{r,m} = p_m^*$. For the special case $m = 0$, Eq. 4.13 reduces to:

$$w_0 = \frac{R^2 p_{r,0}}{\bar{D}(1+k)} \tag{4.14}$$

For situations in which m is nonzero, Eq. 4.13 can be solved for the displacement coefficients:

$$v_m = -\frac{a^4 p_{r,m}}{K(m^5 + 2m^3 + m)} \tag{4.15}$$

$$w_m = \frac{a^4 p_{r,m}}{K(m^4 + 2m^2 + 1)} \tag{4.16}$$

The K parameter in Eqs. 4.15 and 4.16 is given by Eq. 3.32. Equations 4.14, 4.15 and 4.16 provide a simple means of determining displacement Fourier coefficient directly from load Fourier coefficients for two-dimensional circumstances.

Since the two–dimensional situation involves no geometric deviations in the x direction, the equivalent load will not result in longitudinal force or moment resultants. Thus, attention will be restricted to N_ϕ, M_ϕ, and σ_ϕ. Equations 3.52 and 3.53 in Chapter III gave the Fourier coefficients of N_ϕ and M_ϕ in terms of the displacement coefficients. These general relationships simplify somewhat for the two-dimensional case. Using these relationships, the force and moment resultants can be constructed from the displacement coefficients as follows:

$$N_\phi = \frac{D}{a}\left(w_0 + \sum_{m=1}^{M}(mv_m + w_m)\cos(m\phi)\right) + \frac{K}{R^3}\left(w_0 + \sum_{m=1}^{M}\left(1 - m^2\right)w_m\cos(m\phi)\right) \tag{4.17}$$

$$M_\phi = \frac{K}{R^2}\left(w_0 + \sum_{m=1}^{M}\left(1 - m^2\right)w_m\cos(m\phi)\right) \tag{4.18}$$

Expressions were found in Eqs. 4.9 and 4.10 for the load coefficients associated with the normal distribution dent model equivalent load. With solutions for the two–dimensional cylindrical shell problem available in Eqs. 4.14 through 4.18 the resultant forces and moments produced by the equivalent load can be determined.

The deflection coefficients are found by substituting Eqs. 4.9 and 4.10 into Eqs. 4.14 and 4.15:

$$v_m^* = -\frac{R^2 N_0 \xi}{K \phi_0^2 \left(m^5 + 2m^3 + m\right)} I_m \tag{4.19}$$

$$w_0^* = \frac{N_0 \xi}{\bar{D} \left(1 + k\right) \phi_0^2} I_0 \tag{4.20}$$

$$w_m^* = \frac{R^2 N_0 \xi}{K \phi_0^2 \left(m^4 + 2m^2 + 1\right)} I_m \tag{4.21}$$

The displacement coefficients, Eqs. 4.19 through 4.21, resulting from the equivalent load can be substituted into Eqs. 4.17 and 4.18 and the resultant force and resultant moment functions associated with the equivalent load can be found. These may be added to the resultants that would exist in a version of the original shell that does not contain the imperfection and that is subjected to the original loading. There would be no "perfect" version of the resultant moment since only membrane action is assumed present. The total predicted resultant force and moment expressions are:

$$N_{\phi,total} = N_0 + N_\phi^* = N_0 + \frac{N_0 \left(\xi/R\right)}{\phi_0^2} \left[I_0 + \sum_{m=1}^{M} I_m \left(\frac{1 - m^2}{m^4 + 2m^2 + 1}\right) \cos\left(m\phi\right)\right] \tag{4.22}$$

$$M_{\phi,total} = M_\phi^* = R\frac{N_0 \left(\xi/R\right)}{\phi_0^2} \left[\frac{k}{1 + k} I_0 + \sum_{m=1}^{M} I_m \left(\frac{1 - m^2}{m^4 + 2m^2 + 1}\right) \cos\left(m\phi\right)\right] \tag{4.23}$$

These expressions describe the resultant hoop force and bending moment present around the circumference of a pressurized cylinder that contains an imperfection that can be described using the normal distribution. Recall that Eq. 3.55 in Chapter III can be used to relate these resultants to the function describing the hoop stress distribution:

$$\sigma_\phi = \frac{N_\phi}{t} - \frac{12 M_\phi}{t^3} z \tag{4.24}$$

To consider the outer and inner hoop stress situations, $z = \pm t/2$ is substituted into

Eq. 4.24:

$$\sigma_{phi,outer} = \frac{N_\phi}{t} - \frac{6M_\phi}{t^2}$$
$$\sigma_{phi,outer} = \frac{N_\phi}{t} + \frac{6M_\phi}{t^2}$$

(4.25)

It is now possible to write expressions for the hoop stress distributions present at the outer and inner surfaces of a cylinder containing a two-dimensional dent. Substituting the total resultant force and moment expressions, Eqs. 4.22 and 4.23, into the outer and inner hoop stress formulas in Eq. 4.25 the stress expressions are found. Dividing these expression by the nominal hoop stress σ_{nom} that would be present in an undamaged cylinder of the same radius R and thickness t, expressions for outer and inner surface stress concentration factors result:

$$k_{outer} = \frac{\sigma_{\phi,outer}}{\sigma_{\phi,nom}} = 1 + \frac{\xi/R}{\phi_0^2}\left(1 - 6\frac{R}{t}\right)\left[\frac{1+2k}{1+k}I_0 + \sum_{m=1}^{M} I_m \frac{1-m^2}{m^4 + 2m^2 + 1}cos\left(m\phi\right)\right]$$

(4.26)

$$k_{inner} = \frac{\sigma_{\phi,outer}}{\sigma_{\phi,nom}} = 1 + \frac{\xi/R}{\phi_0^2}\left(1 + 6\frac{R}{t}\right)\left[\frac{1+2k}{1+k}I_0 + \sum_{m=1}^{M} I_m \frac{1-m^2}{m^4 + 2m^2 + 1}cos\left(m\phi\right)\right]$$

(4.27)

In these expressions the term I_0 and the sequence of terms I_m are constants and are found from the integrals:

$$I_0 = \frac{1}{\pi}\int_{-\pi}^{\pi}\left[1 - \left(\frac{\phi}{\phi_0}\right)^2\right]exp\left(-\frac{1}{2}\left(\frac{\phi}{\phi_0}\right)^2\right)d\phi$$

(4.28)

$$I_m = \frac{1}{\pi}\int_{-\pi}^{\pi}\left[1 - \left(\frac{\phi}{\phi_0}\right)^2\right]exp\left(-\frac{1}{2}\left(\frac{\phi}{\phi_0}\right)^2\right)cos\left(m\phi\right)d\phi$$

(4.29)

The surface hoop stresses present in a pressurized cylinder containing a two-dimensional dent described by a normal distribution dent profile are readily obtained from these semi-analytical expressions. This solution can be implemented in a code that solves numerically for I_0 and the I_m coefficients and carries out the summations in Eqs. 4.26 and 4.27. An example of such a code is given in Appendix A.

2. Solution Accuracy

The accuracy and implications of Eqs. 4.26 and 4.27 now need to be addressed. In terms of accuracy, two issues must be addressed. The first issue is whether enough Fourier Series modes are included in the analysis. Enough modes must be included in the analysis to insure that the solutions found through Eqs. 4.26 and 4.27 have converged. The number of necessary modes is dependent on the width of the dent, or, in terms of parameters, the value of ϕ_0. The situation where $\phi_0 = \pi/24$ will be used here. This situation represents a fairly narrow dent, as seen in Fig. 17. Figure 19 shows the convergence of the outer surface SCF value predicted by Eq. 4.26 and indicates that twenty to thirty Fourier cosine series modes are apparently adequate to represent Eq. 4.26 for $\phi_0 = \pi/24$. This convergence occurs over the entire ϕ range modelled by Eq. 4.26, as shown in Fig. 20. In this figure, the five and ten mode situations deviate substantially from the profiles predicted using twenty and thirty modes. The twenty and thirty mode profiles are well converged enough to be almost indistinguishable. If a certain number of modes leads to convergence for $\phi_0 = \pi/24$ it should lead to convergence for larger ϕ_0 values since these values are associated with "wider" dents that do not require higher frequency cosine terms to model. Although thirty modes appears to be adequate, fifty modes will be used as there are no significant increases in computation time.

Having demonstrated that the Equivalent Load based solution for the two–dimensional dent converges to an answer, the next question is whether the answer obtained is a realistic model of two–dimensional dent stress behavior. The accuracy of the equivalent load based solution can be judged by comparing it to the solution obtained by an independent method. Finite element analysis of a two-dimensional cylinder containing a normal distribution dent offers a means of independent verifi-
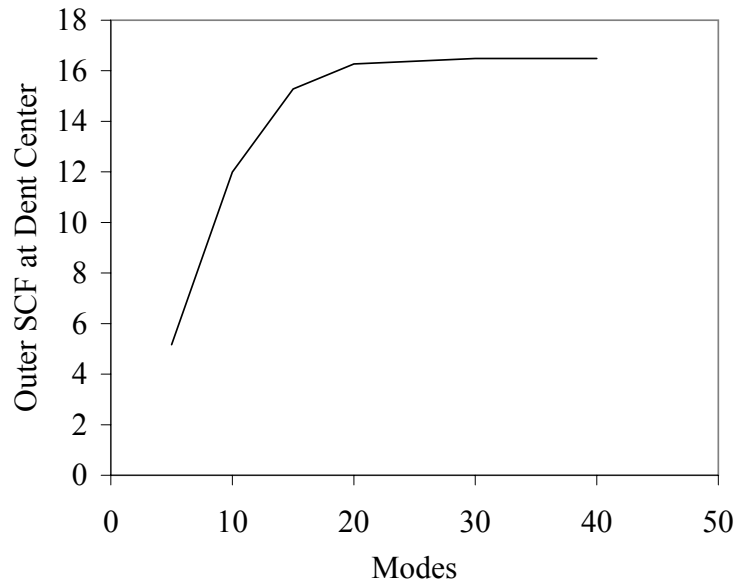
Fig. 19. Values predicted using Eq. 4.26 for the outer surface SCF at $\phi = 0$ using increasing numbers of modes.
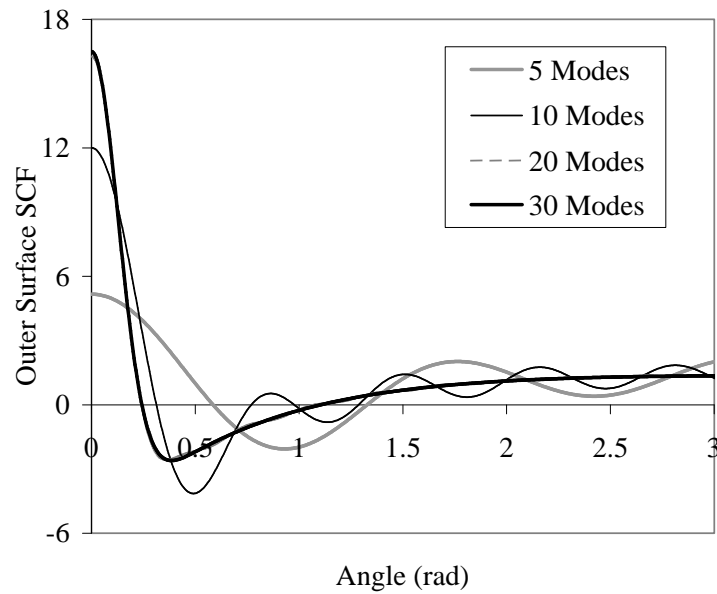
Fig. 20. Profiles of outer surface SCF over angle ϕ predicted by Eq. 4.26 using increasing numbers of Fourier modes.

cation of accuracy.

For comparison purposes, a finite element model of a two–dimensional dent was set up using ABAQUS software [37]. Figure 21 is an image of the overall mesh produced using ABAQUS VIEWER and Fig. 22 is a detail view. The mesh was comprised of linear S4R elements and assumes the pipe cross-section to be symmetric. There were 720 elements distributed around the half–pipe cross-section. This number of elements is assumed to be adequate as a more complex model discussed elsewhere [8, 16, 21, 22] converges reasonably well with only 90 elements around the half–pipe cross-section. The two–dimensional pipe model is elastic and the nonlinear geometry analysis option is invoked. The mesh geometry is generated using the two–dimensional normal distribution dented pipe profile given in Eq. 4.2. The FEM model is subjected to uniform pressure distribution. The boundary conditions, illustrated in Fig. 23 are selected to enforce symmetry and two–dimensional behavior. Both the FEM model and the ELM model assume an $18''$ diameter $1/4''$ thick pipe for the purposes of validating model accuracy. With each element having an angular extent of $\pi/720$ or an arclength of $0.039''$, the longitudinal element length is taken to be $0.01''$ so as to maintain a reasonable element aspect ratio.

Before proceeding to assess accuracy, it should be pointed out that the FEM solution is itself only a numerical model of actual physical circumstances. It is assumed that FEM solutions are more accurate because they are based on a less approximate method. Experimentally measured dent strain behavior would be the ideal benchmark for assessing solution accuracy. Because this information is unavailable, finite element solutions are used.

In comparing accuracy between the equivalent load based solutions of Eqs. 4.26 and 4.27 and the finite element solution for the same situation two issues need to be addressed. Accuracy in terms of predicted profile shape and in terms of magnitude
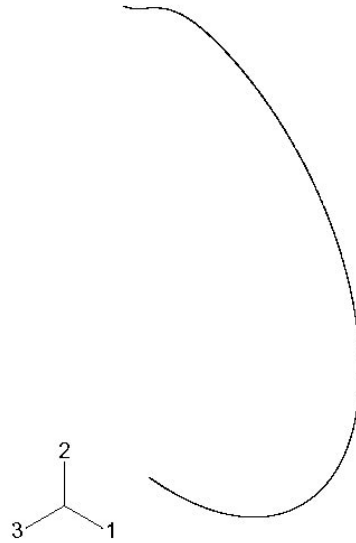
Fig. 21. View generated in ABAQUS VIEWER of finite element mesh used to check accuracy of two-dimensional equivalent load model.
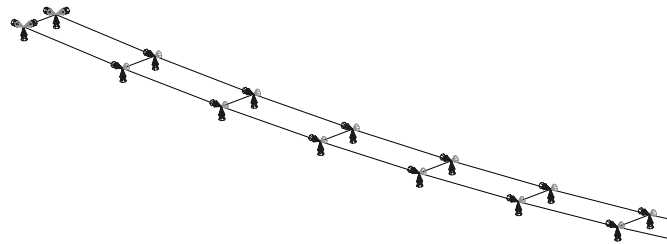
Fig. 22. Close-up view generated in ABAQUS VIEWER showing mesh structure and boundary conditions of finite element mesh used to check accuracy of two-dimensional equivalent load model.
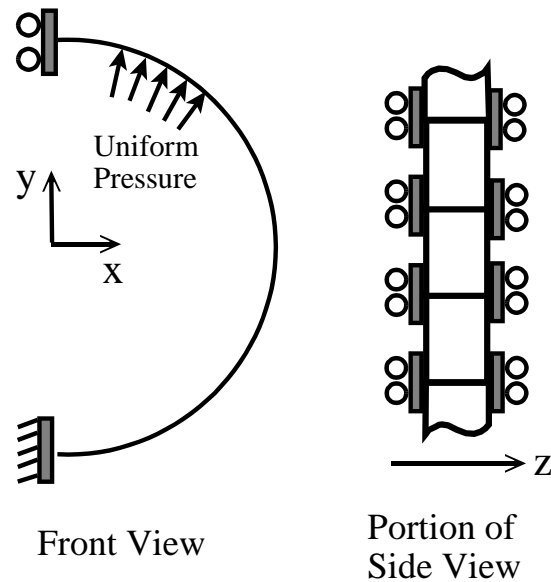
Fig. 23. Schematic diagram showing boundary conditions of two–dimensional finite element model used to investigate accuracy of equivalent load dent model.

prediction must both be investigated. If the semi-analytical solution predicts profile shape reasonably accurately but fails to predict magnitude, it can probably be corrected and at a minimum will provide insight into the functional behavior of the two-dimensional dent stress profile. If profile shape cannot be accurately predicted then one begins to suspect the validity of the semi-analytical solution.

Figures 24 and 25 show comparisons between the finite element and the semi-analytical, equivalent load based solutions for the outer surface SCF profiles of two-dimensional dents with $\phi_0 = \pi/12$ and $\phi_0 = \pi/24$ respectively. Remembering that the semi-analytical solution is based on an approximate approach to analyzing geometric imperfections agreement seems fairly reasonable. Both approaches predict a large central outer surface SCF and a smaller, off-center stress peak. It would appear that the semi-analytical SCF solutions of Eqs. 4.26 and 4.27 provide a fairly accurate

Fig. 24. Comparison of finite element and semi-analytical, equivalent load based, solutions for the outer surface SCF profile of a $\phi_0 = \pi/12$, $\xi = 0.9$ dent in and 18″ diameter, 1/4″ thick cylinder.

understanding of the SCF profile developed by a two-dimensional normal distribution dent model. The semi-analytical solution can be used to easily develop a parametric understanding of the stress behavior of two-dimensional dents.

The next issue is that of accuracy at the location of main interest, $\phi = 0$ or the dent center. Figure 26 plots peak values predicted for the inner and outer SCF's at $\phi = 0$ found using both Eqs. 4.26 and 4.27 and finite element analysis. Calculations were made at a range of d/D or ξ values between 0.25% and 5%. In this case, a $\phi_0 = \pi/8$ dent is considered. Figure 26 shows that the linear relationship between SCF magnitude and ξ, or dent depth d/D, predicted by Eqs. 4.26 and 4.27 is apparently correct. However, the equivalent load based solution underestimates the SCF value at the dent center.

The FEM and semi-analytical solutions in Fig. 26 appear to differ by a constant

Fig. 25. Comparison of finite element and semi-analytical, equivalent load based, solutions for the outer surface SCF profile of a $\phi_0 = \pi/24$, $\xi = 0.9$ dent in an 18″ diameter, 1/4″ thick cylinder.

factor. Agreement between models is probably best judged in terms of predicted deviation from the unit stress concentration value. This adjustment is helpful because the unit SCF value consistently offsets inner and outer SCF values. Thus, the ratio C is used to measure disagreement:

$$C = \frac{SCF_{FEM} - 1}{SCF_{ELM} - 1} \tag{4.30}$$

In Eq. 4.30, the terms SCF_{FEM} and SCF_{ELM} refer to the SCF values at $\phi = 0$ obtained using the finite element and semi-analytical, equivalent load based approaches. For the complete set of inner and outer SCF values for the eight d/D values considered in Fig. 26 the average value of C is 1.512. The standard deviation from this average is 0.275%. Thus, the error parameter C is essentially constant over the range of d/D for $\phi_0 = \pi/8$.

Fig. 26. Comparison of finite element and semi-analytical, equivalent load based, solutions for the outer and inner surface SCF values predicted for a range of ξ or d/D values at the dent center, $\phi = 0$, for a $\phi_0 = \pi/8$ dent in an $18''$ diameter, $1/4''$ thick cylinder.
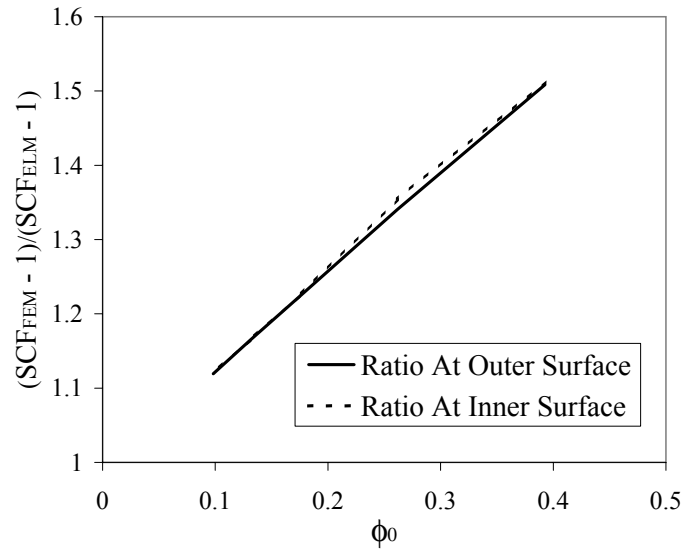
Fig. 27. Variation of the parameter C in terms of ϕ_0 for $d/D = 1\%$ or $\xi = 0.180$ in an 18″ diameter, 1/4″ thick cylinder.

It remains to be seen whether or not C is constant with respect to ϕ_0. In fact, it is not, as seen in Fig. 27. However, C appears to vary linearly with ϕ_0. Furthermore, the C function appears to be the same for both inner and outer surface SCF values.

A linear fit can be made of the C-ϕ_0 dependence. As ϕ_0 approaches zero the imperfection must disappear and SCF_{FEM} and SCF_{ELM} must approach 1.0. The limit of Eq. 4.30 as these terms approach 1.0 is 1.0. In Fig. 27, the y-intercept value indeed appears to be 1.0. Using this y-intercept value the slope of C with respect to ϕ_0 is determined from Fig. 27 for both the inner and outer surface curves. The average C slope values are 1.337 and 1.352 for outer and inner surface cases respectively. Taking the slope of C to be 1.34 the following expression appears to describe the dependence of C in terms of ϕ_0:

$$C = 1 + 1.34\phi_0 \tag{4.31}$$

The adjusted semi-analytical SCF solution is then given as:

$$SCF_{ELM,adjusted} = 1 + (1 + 1.34\phi_0)\left(SCF_{ELM} - 1\right) \qquad (4.32)$$

The semi-analytical solution values used to generate the curve of the error function in Fig. 27 may be adjusted using Eq. 4.32 and compared again to the finite element prediction. The resulting root–mean–squared error between adjusted semi–analytical and finite element solutions is 0.0094. Relative to the stress concentration values, ranging from 1 to 5 in this case, this error indicates a good fit.

The question remains as to whether or not adjusting the semi-analytical solution to match the more accurate finite element solution at one point significantly worsens the overall agreement between predicted SCF profile shapes. If so, then the adjusted semi–analytical solution should not be used to investigate the behavior of the entire two-dimensional dent SCF profile. Figs. 28 and 29 show the adjusted semi–analytical and finite element predictions of the outer SCF profile for the $\pi/12$ and $\pi/24$ cases. These figures can be compared to the unadjusted semi-analytical situation shown in Figs. 24 and 25.

The profile comparison made in Figs. 28 and 29 shows that the adjusted semi-analytical solution does a better job at predicting the SCF profile in the dent interior, or in the region of the central SCF peak. In addition, the profile agreement away from the dent where no significant peaks are present is similar to that seen for the unadjusted case in Figs. 24 and 25. The main problem with the adjusted solution is agreement at the peripheral peak. The semi-analytical solution is less successful at predicting the shape of this region of the SCF profile regardless of whether or not magnitude adjustments have been made. Magnitude adjustments based on the center stress value lead to an increased overestimate of the magnitude of the peripheral SCF peak.
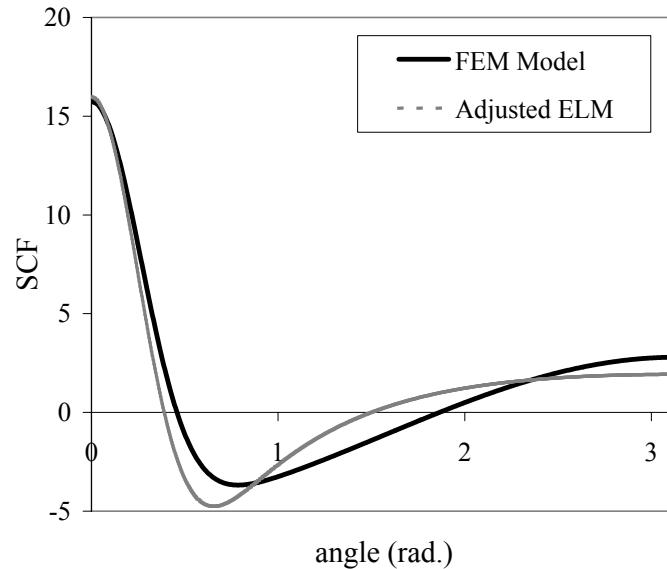
Fig. 28. Comparison of finite element and adjusted semi-analytical, equivalent load based, solutions for the outer surface SCF profile of a $\phi_0 = \pi/12$, $\xi = 0.9$ dent in and 18″ diameter, 1/4″ thick cylinder.

One final check of the accuracy of the semi-analytical solution is necessary. Equations 4.26 and 4.27 describe a linear relationship between the stress concentration factor and the pipe diameter to thickness ratio, D/t. Four D/t cases with $\phi_0 = \pi/24$ and $d/D = 1\%$ were analyzed both with the semi-analytical solution and the finite element method. The semi-analytical solution was adjusted according to Eq. 4.32. Results for the four cases, in which t was 1/4″ and D was 12″, 16″, 18″, 24″, or 30″ are shown in Fig. 30. The finite element model confirms the linear relationship between SCF and D/t predicted by Eqs. 4.26 and 4.27 and adjusted using Eq. 4.32. In addition to correctly predicting the qualitative nature of the relationship, actual accuracy is maintained over the range of D/t ratios.

Comparisons with more accurate finite element estimates of the SCF profiles arising in two-dimensional dented cylinders suggest that the semi-analytical equivalent
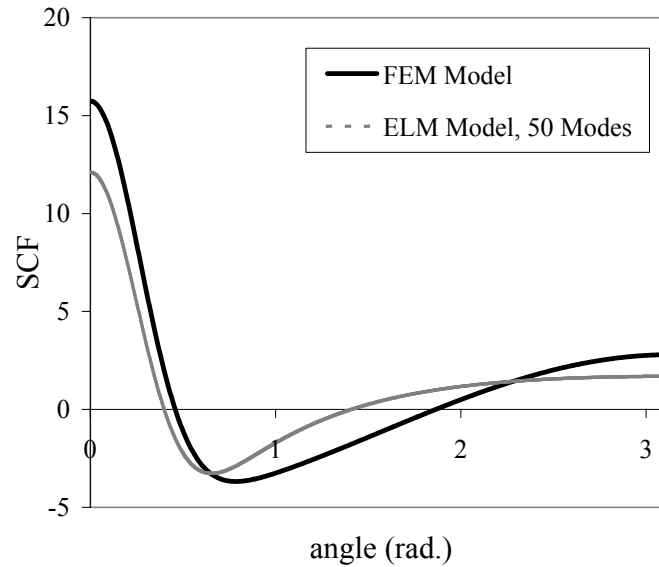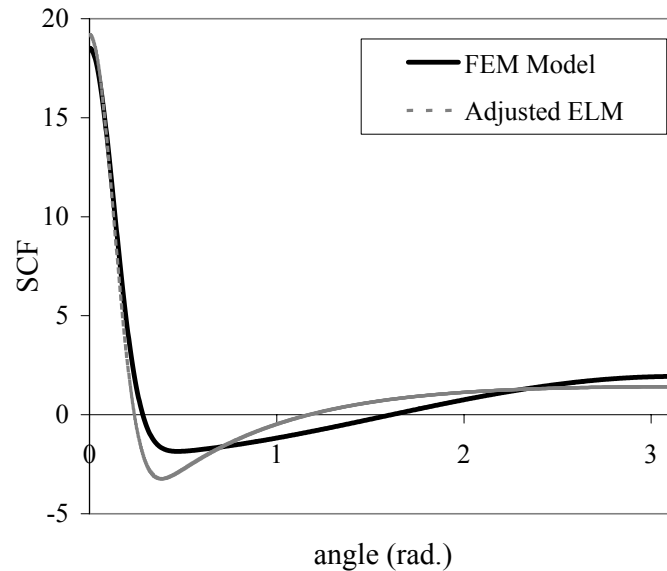
Fig. 29. Comparison of finite element and adjusted semi-analytical, equivalent load based, solutions for the outer surface SCF profile of a $\phi_0 = \pi/24$, $\xi = 0.9$ dent in an $18''$ diameter, $1/4''$ thick cylinder.

load based solution to the problem is a reasonable solution. This conclusion is especially true given the fact that the solution is based on an approximate approach to the problem. In particular, estimates of the magnitude of the dent center SCF seem reasonable. Only rough estimates of peripheral SCF behavior can be made using the semi-analytical solutions. Accepting its limitations, the semi-analytical model can be used to study aspects of the functional dependency of two-dimensional dent SCF behavior on dent characteristics.

3. Discussion of Solution

As noted in Chapter II, current understanding of dent stress behavior is typically either qualitative in nature or consists of case-specific, empirical results. The underlying mechanics of dent stress behavior have not been extensively developed. Other
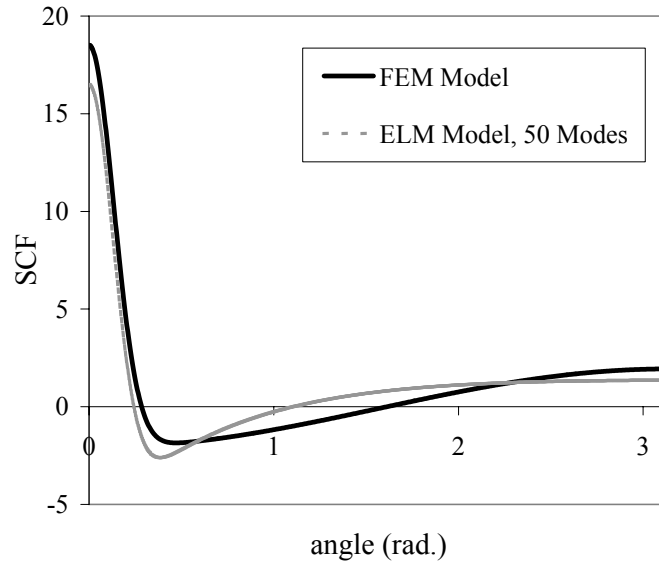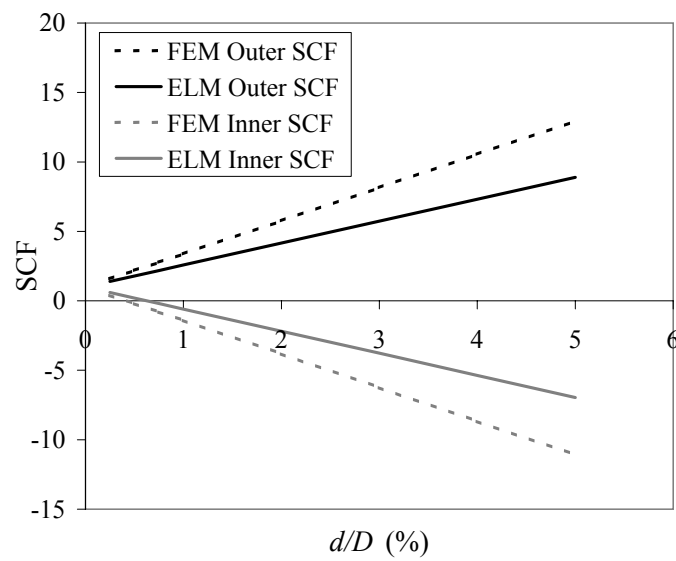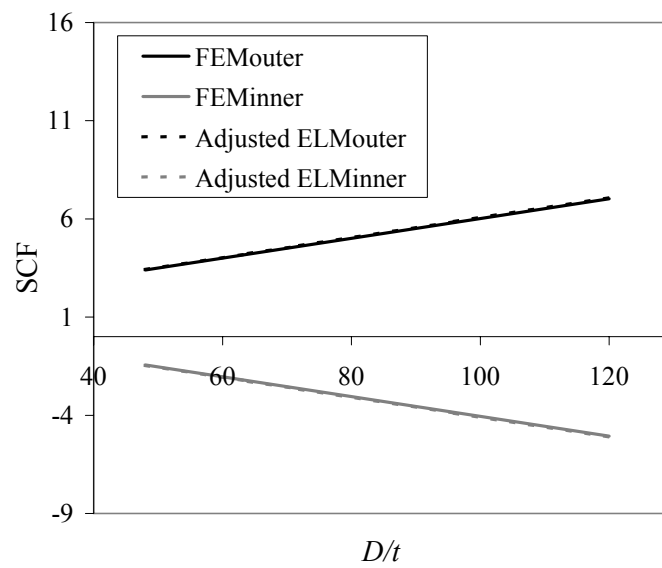
Fig. 30. Comparison of finite element and adjusted semi-analytical, equivalent load based, solutions for the outer and inner surface SCF profile of a $\phi_0 = \pi/24$, $\xi = 0.9$ dent for pipes with D/t values of 48,64, 72, 96, and 120 where $t = 1/4''$.

work has emphasized the analysis of imperfections in thin shells [17, 20] and has used mechanics to develop the equivalent load approach to the problem. However, this work has not payed a great deal of attention to the mechanics of the imperfection itself once the analytical approach has been developed to study it.

The semi-analytical solution of Eqs. 4.26 and 4.27 appears to be accurate enough to offer reasonable insight into the mechanics of two-dimensional dents. In their basic form, Eq. 4.26 describe SCF dependency in terms of dent depth, ξ, dent width, ϕ_0, pipe radius-to-thickness ratio, R/t, and angular location, ϕ. The relations in Eqs. 4.26 and 4.27 can be adjusted for accuracy via Eq. 4.32, combined, and simplified:

$$k_{inner}^{outer} = 1 + \left(\frac{\xi}{R}\right)\left(\frac{1 + 1.34\phi_0}{\phi_0^2}\right)\left(1 \mp 6\frac{R}{t}\right)f\left(\phi, \phi_0\right) \tag{4.33}$$

The superscript "outer" and subscript "inner" on k refer to which SCF is obtained based on whether a minus or plus sign is used for the minus-plus symbol. The term $f(\phi, \phi_0)$ represents the more complicated term:

$$f\left(\phi, \phi_0\right) = \left[\frac{1 + 2k}{1 + k}I_0 + \sum_{m=1}^{M} I_m \frac{1 - m^2}{m^4 + 2m^2 + 1}cos\left(m\phi\right)\right] \tag{4.34}$$

This term can be evaluated numerically.

Given conventions used elsewhere in other chapters, it is consistent to rewrite the Eq. 4.33 replacing ξ and R with d and D as depth and pipe size indicators. In this form Eq. 4.33 becomes:

$$k_{inner}^{outer} = 1 + 2\left(\frac{d}{D}\right)\left(\frac{1 + 1.34\phi_0}{\phi_0^2}\right)\left(1 \mp 3\frac{D}{t}\right)f\left(\phi, \phi_0\right) \tag{4.35}$$

Several important aspects of two-dimensional dent behavior can be obtained from Eq. 4.35. First, as alluded to in the previous subsection, SCF magnitude is depth dependent. In particular it varies linearly with depth. The fact that depth is important is not surprising, given the emphasis it has been given by existing approaches to

assessing three-dimensional dents [11, 12, 9].

It has never been clear whether or not pipe diameter-to-thickness ratio plays a role in determining dent behavior. Linear SCF dependency on D/t shown in Equation 4.35 and validated in Fig. 30 indicates that D/t plays a meaningful role in determining SCF behavior. In particular, larger D/t ratios lead to increased SCF magnitudes. While the result determined here applies only to two-dimensional dents it seems likely that D/t plays a role in three-dimensional dent stress behavior. It will be shown in Chapter V that D/t values do influence at least some aspects of three-dimensional dent stress behavior.

Equation 4.35 also indicates that circumferential location, ϕ, influences SCF value. This result is not surprising given that dent geometry varies with ϕ. As seen in Figs. 25 and 24 or Figs. 29 and 28, SCF peaks occur at $\phi = 0$ and at some peripheral, nonzero value of ϕ. As ϕ_0 increases, the SCF value at $\phi = 0$ decreases while the peripheral value appears to remain fixed or may even increase. Fowler *et al.* [9] reported what appears to be circumferential peripheral cracking in many of the dents tested in their study. These dents were wider and flatter than the narrow dents studied by Keating and Hoffmann [8] that experienced cracking along the $\phi = 0$ center-line. It is possible that decreased center SCF values predicted by the semi-analytical model combine with some other stress feature present in wider dents to lead to a circumferential peripheral crack location. More work on the wide dent problem is warranted.

The circumferential decay rate, ϕ_0, a measure of dent width, also plays a role in determining dent SCF values. The nature of this role is not immediately clear because the influence of ϕ_0 is given through $f(\phi, \phi_0)$ or Eq. 4.34 and must be evaluated numerically. Due to the present interest in narrow dents SCF behavior at $\phi = 0$ is of

primary interest. The function $f(\phi, \phi_0)$ is simplified for this case:

$$f(\phi = 0, \phi_0) = \frac{1 + 2k}{1 + k} I_0 + \sum_{m=1}^{M} I_m \frac{1 - m^2}{m^4 + 2m^2 + 1} \tag{4.36}$$

The terms I_0 and I_m do not simplify for $\phi = 0$ and are still given by Eqs. 4.28 and 4.29.

Equation 4.36 can be further simplified with a slight approximation. In the present case, attention is limited to a certain range of pipe D/t ratios. For instance, a range of diameters from $12''$ to $30''$ with a thickness of $1/4''$ is reasonable. Using Eq. 3.30 the value of the term $(1 + 2k)/(1 + k)$ in Eq. 4.36 may be determined. Where the pipe diameter is $12''$ this term has a value of 1.00159 and where diameter is $30''$ this term is 1.000254. Thus, it seems safe for the range of application considered here to assume $(1 + 2k)/(1 + k) = 1.0$. Thus, Eq. 4.36 is reduced to:

$$f(\phi = 0, \phi_0) = I_0 + \sum_{m=1}^{M} I_m \frac{1 - m^2}{m^4 + 2m^2 + 1} = \sum_{m=0}^{M} I_m \frac{1 - m^2}{m^4 + 2m^2 + 1} \tag{4.37}$$

A variant of the computer program in Appendix A may be used to find $f(0, \phi_0)$ as it is given in Eq. 4.37. Figure 31 shows how f varies over ϕ_0. Values of ϕ_0 in Fig. 31 are varied from 0.001 to 0.700. The range of practical interest, as seen in Fig. 17, is limited to a range of about $\pi/36$ to $\pi/8$ or 0.087 to 0.392. Values of ϕ_0 outside of this range may not have clear physical meaning as two-dimensional dents. However, it is reassuring that f approaches roughly zero as ϕ_0, or dent width, approaches zero. This result means that the limit of Eq. 4.35 as ϕ_0 goes to zero, or as the dent disappears because width goes to zero, is an SCF value of 1.0.

As noted, for practical purposes attention in Fig. 31 should be restricted a limited ϕ_0 range. In the ϕ_0 range 0.1 to 0.4, f becomes almost linear. In fact a linear regression fit of f in this range has an R value of 0.999579 and gives f in terms of ϕ_0 to be:

$$f = 9.659e^{-3} - 0.1706\phi_0 \tag{4.38}$$
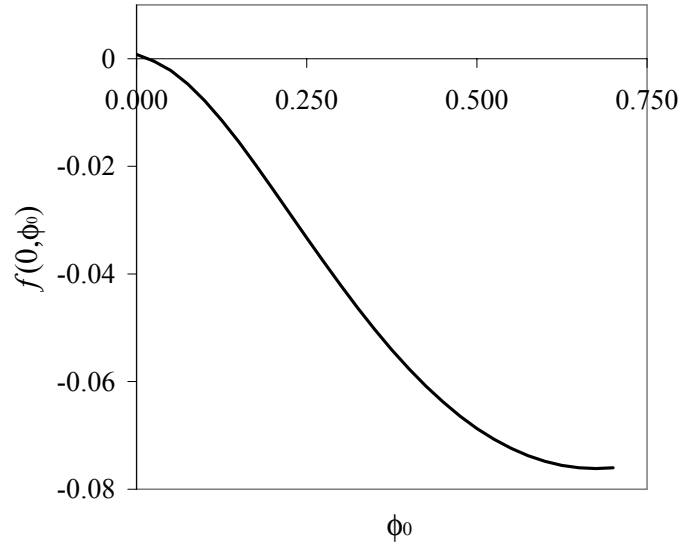
Fig. 31. Plot of $f(0, \phi_0)$, Eq. 4.37 over a range of ϕ_0 values.

Figure 32 shows both the actual f result and the fit given in Eq. 4.38. Use of the fitted f function seems reasonable for $0.1 <= f < 0.4$. This range corresponds to a ϕ_0 range of about $\pi/30$ to $\pi/8$, which, as seen in Fig. 17, covers a considerable range of dent width.

Although is it empirical, Eq. 4.38 gives a closed form version of f. Thus, the functional influence of ϕ_0 on two-dimensional dent SCF behavior can now be determined by substituting Eq. 4.38 into the adjusted two-dimensional SCF equation Eq. 4.35. The resulting empirical expression is a solution for the SCF in a two-dimensional dent:

$$k_{inner}^{outer} = 1 + \frac{d}{D} \left(\frac{0.01932 - 0.3154\phi_0 - 0.4572\phi_0^2}{\phi_0^2} \right) \left(1 \mp 3\frac{D}{t} \right) \qquad (4.39)$$

As discussed, the two-dimensional dent SCF depends linearly on relative dent depth d/D and the pipe diameter-to-thickness ratio D/t. The term in Eq. 4.39 describing ϕ_0 dependence is plotted in Fig. 33 so that the effect of ϕ_0 can be judged.
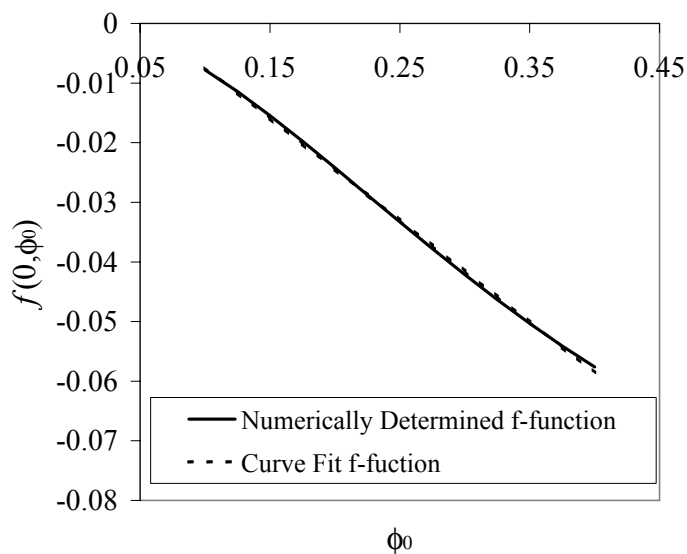
Fig. 32. Plot of $f(0, \phi_0)$, Eq. 4.37, and a linear fit of $f(0, \phi_0)$, Eq. 4.38 over a range of ϕ_0 values corresponding to a range of about $\pi/30$ to $\pi/8$.
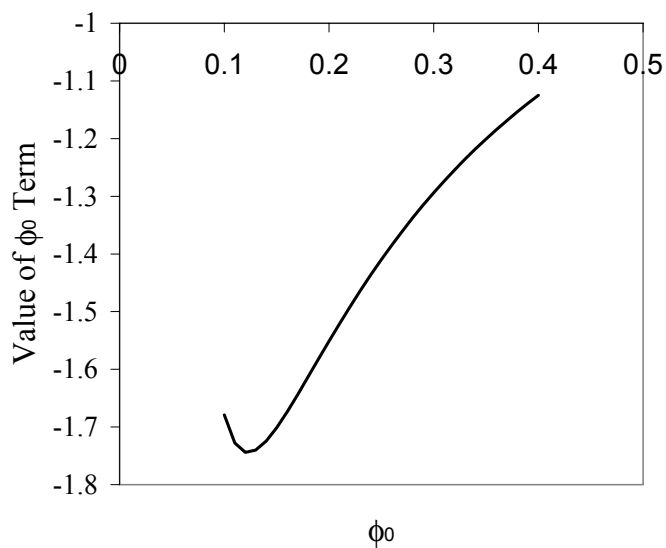
Fig. 33. Plot of term containing ϕ_0 in the empirical closed-form dent SCF model Eq. 4.39 over a range of ϕ_0 values corresponding to a range of about $\pi/30$ to $\pi/8$.

Figure 33 shows that the value of ϕ_0 has a significant influence on dent SCF behavior. Over the range of practical interest, the ϕ_0 term varies as a multiplier from about 1.1 to 1.7. Narrow dents, characterized by low ϕ_0 values, result in larger SCF values. A peak in this influence is seen at a ϕ_0 value of about 0.12 or $\pi/26$. Values of ϕ_0 less than this value, in other words, narrower dents, have less of an effect on the SCF value. A primary result of Fig. 33 is that wider dents appear to have decreased center SCF values. This result lends credence to the idea that dent width is a significant and almost completely unexplored factor in dent mechanics.

A solution for the SCF produced by a two-dimensional dent in a pipe has been developed in this section. A semi-analytical version of the solution is given in Eq. 4.35. A closed-form, slightly empirical version of the solution describing the SCF at the dent center is given in Eq. 4.39. The solution, based on the equivalent load method, appears to be fairly accurate in comparison with more accurate finite element results. The solution provides insight into the mechanics of two-dimensional dents. In particular, functional relationships between dent SCF and dent geometry are predicted.

In reality, dents are not likely to be two-dimensional. However, it is possible that the behavior of very long three-dimensional dents might be described by the solution obtained in this section. In addition, other pipe imperfections, such as weld misalignments, could be considered to be two-dimensional and could be treated in a manner similar to that used here.

In addition to solving two-dimensional problems, two key results obtained from the two-dimensional model inform the study of three-dimensional dents. First, the pipe diameter-to-thickness ratio influences two-dimensional SCF magnitude. Presumably this influence remains in the three-dimensional case. This influence has not been clearly noted in the past. Second, dent width, in the form of ϕ_0, has a significant influence on dent SCF. The significance of dent width has seemed likely given the

established importance of dent length [8, 16]. A width effect might also help account for some clear differences that exist between the experimental results reported by Fowler *et al.* [9], who studied relatively wide dents, and Keating and Hoffmann [8], who studied narrower dents. Thus a two-dimensional solution has value in its own right and also informs understanding of three-dimensional dent behavior. However, it would be worthwhile to investigate three-dimensional dent behavior.

B. Limitations of the Equivalent Load Method in Studying Three-Dimensional Localized Damage

Given its success in developing a semi-analytical solutions for two-dimensional dents, the equivalent load method might successfully be applied to the problem of three-dimensional dents. This problem is much more complicated. First, since dent geometry varies in two directions, ϕ and x, dent geometry must be represented by a double Fourier series. Second, the matrix relation, Eq. 3.36, between load and displacement Fourier coefficients is complicated by the presence of all six terms. Third, relations between stresses, forces and moments, and displacements are complicated by the presence of more terms. The possibility exists that functional information about three-dimensional dent SCF behavior may be difficult to determine.

In addition to practical implementation considerations, the following examination of the literature uncovers a discrepancy that suggests that the equivalent load method may not accurately model all three-dimensional imperfections. Much of the reported use of the equivalent load method has involved analyzing cases with one dimension of imperfection [17, 19, 18, 41]. As seen in the previous section, two-dimensional dents, which are situations with one-dimension of imperfection, appear to be handled fairly well by the equivalent load method.

Several authors have applied the equivalent load method to specifically study localized, three dimensional imperfections in shell structures [46, 44, 43]. Tam and Croll [46] reported success in applying the equivalent load method to study localized three-dimensional dents. They noted that as an imperfection becomes more localized the magnitude of the local stress concentration increases. This effect was noted in the previous section when two-dimensional dent SCF values increased as dent width decreased. Tam and Croll did not verify their results with an independent model.

Godoy considered localized, three-dimensional imperfections in spheres [44]. He notes that the equivalent load method is successful in studying localizations as long as the imperfection amplitude is on the order of the shell thickness. It is not specifically noted what occurs when imperfection depth is deeper than the shell thickness. It is assumed that a loss of accuracy develops with increasing depth. A change in the shape of the stress profile itself was not specifically noted. In this paper, the equivalent load method is compared to an independent finite element analysis. In a later work [47] it is suggested that a nonlinear implementation of the equivalent load method eliminates inaccuracies for deeper imperfections.

In their analysis of cooling towers with local imperfections, Han and Tong [43] also conclude that the equivalent load method is an acceptable approach to analyzing "dimple" shaped imperfections as long as the imperfection is shallow. They verify their results with independent finite element analysis and indicate that the equivalent load method accurately predicts the stress profile but is somewhat inaccurate in predicting magnitudes.

Thus, the equivalent load literature suggests that the equivalent load method will treat general localized, three-dimensional damage with acceptable accuracy. Imperfection geometry is noted to alter the magnitude and extent of the stress concentration profile. However, a change in profile shape, such as that seen in studies of long and

short dents and illustrated in Fig. 3, does not occur. This constant stress stress profile shape result does not correspond to results obtained by research in the area of pipeline dent stress behavior [14, 8, 15, 16]. As noted in Chapter II of the present work, otherwise similar dents of different lengths can develop very different stress concentration profile shapes. Equivalent load research has not noted this effect.

There are at least two possibilities for the apparent discrepancy between predictions of SCF profile shape changes. One possibility is that equivalent load work did not note the shape change because it did not investigate imperfection geometries in the region where SCF shape transitions occur. This possibility would seem likely, since important pieces of dent fatigue literature have also not noted this stress profile change [9, 7, 13]. A second possibility is that the equivalent load method is not well-suited to analyze all classes of localized imperfections.

Questions regarding the general applicability of the equivalent load method to three-dimensional dents have been raised. Thus, this matter should be explored more thoroughly. A simple dent model will permit the predictive success of the equivalent load method to be gauged. If this model validates use of the equivalent load method, a more advanced model specialized to study the dent stress problem can be developed with confidence. To validate the equivalent load method, a simple-to-implement, smooth, periodic imperfection profile is needed. The simplest such profile for a cylinder might be the double-cosine profile:

$$r\left(\phi, x\right) = R - \xi cos\left(m\phi\right) cos\left(\frac{n\pi x}{L}\right) \tag{4.40}$$

The double-cosine profile, Eq. 4.40, does not generate a single localized imperfection but rather an entire imperfect surface. For high values of the harmonics m and n the imperfection is small compared to the length and radius of the cylinder. Imperfection magnitude is given by ξ. The double-cosine does not describe a single
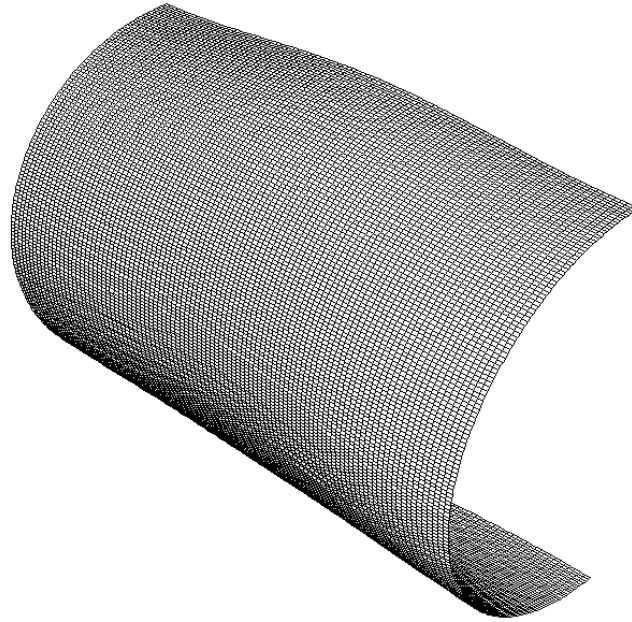
Fig. 34. ABAQUS VIEWER image of mesh generated using double-cosine imperfection profile, Eq. 4.40, in $18''$ diameter cylinder with $\xi = 0.360$, or $d/D = 2\%$ $m = 2$, and $n = 2$.

local dent. Instead, the resulting surface contains a set of multiple localized imperfections. These imperfections have the features necessary to determine whether or not the equivalent load method accurately analyzes general localized imperfection behavior. Examples of finite element meshes generated to contain double-cosine imperfection profiles are shown in Figs 34 and 35. These meshes correspond to $18''$ diameter pipes with double-cosine imperfection profiles with equal m and n values of 2 and 10, respectively.

To explore method accuracy, the equivalent load method is implemented in the numerical manner described in Fig. 14 of Chapter III. The equivalent load distribution is generated either in a computer program or using a spreadsheet and is pasted into an ABAQUS input file as a set of nodal forces. These equivalent nodal forces are
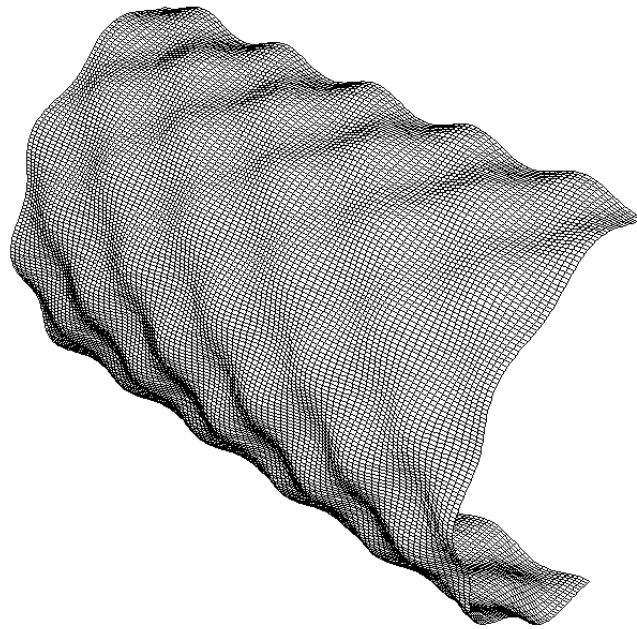
Fig. 35. ABAQUS VIEWER image of mesh generated using double-cosine imperfection profile, Eq. 4.40, in 18″ diameter cylinder with $\xi = 0.360$ or $d/D = 2\%$, $m = 10$, and $n = 10$.

applied to a perfect cylindrical mesh. The resulting stresses are added to the nominal stresses developed by the perfect shell under uniform internal pressure.

The validating finite element model performs an elastic analysis of a mesh generated using Eq. 4.40. The analysis is geometrically nonlinear. In both cases of analysis, the mesh is 100 elements long and 180 elements in the circumferential direction. Symmetry is used. Elements are $0.25''$ in the longitudinal direction and have an angular extent of $\pi/180$ or 0.0174 radians. Other, more complicated finite element models that model both contact and inelastic rerounding have been discussed elsewhere [8, 21, 22, 16] and have been demonstrated to have reasonable convergence with $0.5''$ by 0.0262 radian elements. Because the mesh is finer in the present model and because the modelling issues are more straightforward, convergence is assumed to exist. The boundary conditions of this three-dimensional finite element model are shown in Fig. 36. It should be noted that the figure does not indicate the fact that the bottom nodes of the model are free to translate in the longitudinal direction.

With both a means of implementing the equivalent load method in three-dimensions and a means of validating the results, the discrepancy between equivalent load and dent fatigue literature regarding stress behavior of localized damage can be investigated. The primary measure of stress behavior will be the outer surface hoop stress behavior. This measure is selected because it is central to the dent fatigue problem. In particular, outer surface hoop stress along the longitudinal meridian at the top of the cylinder will be examined.

A general model of dent behavior must be applicable over a range of depths and relative dent sizes. Thus, the applicability of the equivalent load method will assessed for a series of imperfection depths with relatively large $(m, n = 2)$ and relatively small $(m, n = 10)$ imperfection sizes. An $18''$ cylinder with $1/4''$ wall is studied. According to [44] the equivalent load method will be successful if imperfection depth is of the

Top View

Side
View
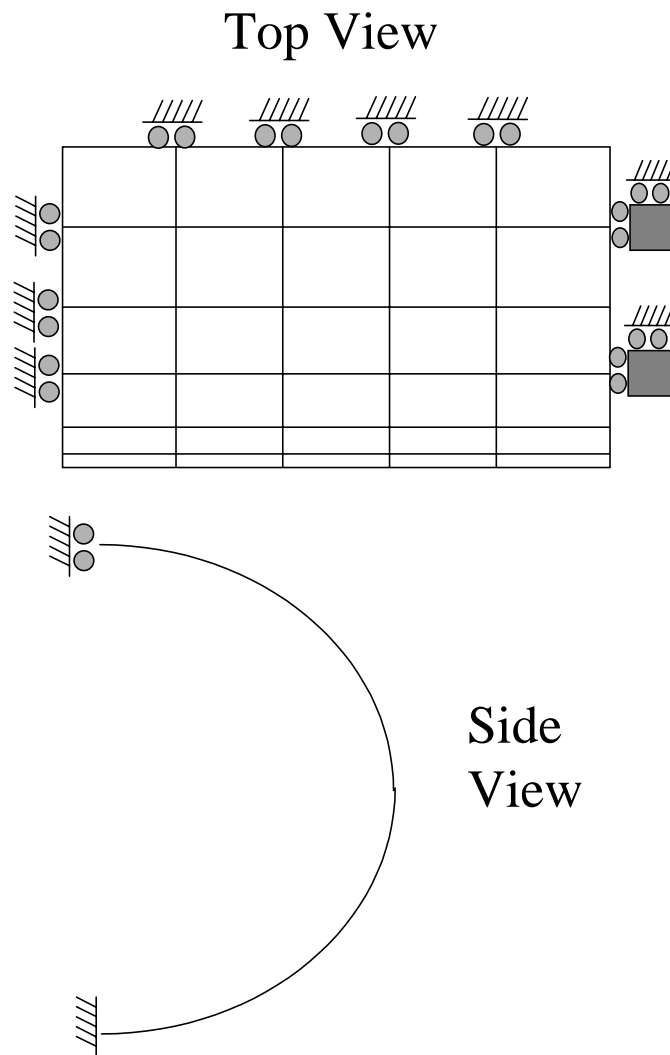
Fig. 36. Illustration of boundary conditions used for three-dimensional finite element model.
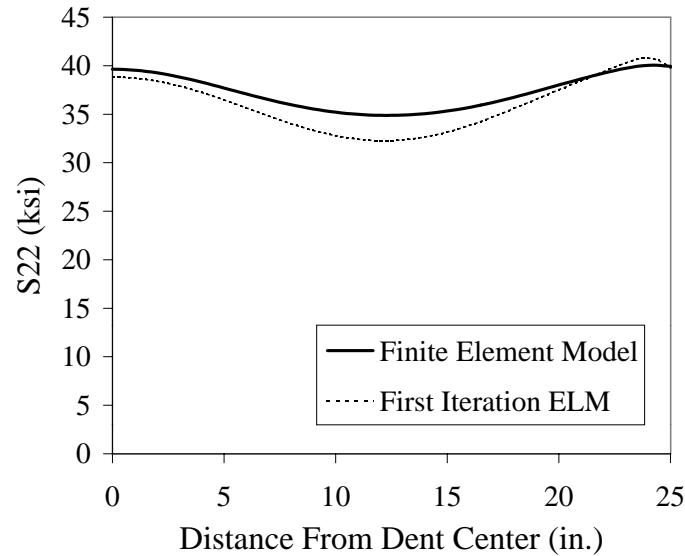
Fig. 37. Hoop stress profiles along center meridian predicted using equivalent load method and finite element analysis for $\xi = 0.180$ or $d/D = 1\%$, $m, n = 2$ double-cosine imperfection.

order $0.25''$ or $d/D = 1.39\%$.

An imperfection depth of $0.18''$, corresponding to $d/D = 1\%$, is considered first. Hoop stress profiles along the center-line meridian are shown in Figs. 37 and 38 for $m, n = 2$ and $m, n = 10$, respectively. It should be noted that profile non-uniformities apparent at the far end of the profiles result from end conditions present in the finite element model.

Several features are apparent in Figs. 37 and 38. For the relatively large imperfection case, Fig. 37, the equivalent load method makes an overall underestimate of the result predicted by the finite element model. This result is consistent with underestimates found in the previous section using the two-dimensional equivalent load based solution. In the smaller imperfection case, Fig. 38, the equivalent load method actually overestimates the magnitude of the stress deviation resulting from

Fig. 38. Hoop stress profiles along center meridian predicted using equivalent load method and finite element analysis for $\xi = 0.180$ or $d/D = 1\%$, $m, n = 10$ double-cosine imperfection.

the imperfection. In both cases, the equivalent load method provides reasonably accurate estimates of the stress profile shape. Magnitude accuracy problems were noted previously in the application of the two-dimensional model. In that case, a correction factor was determined and was found to depend on the defect size parameter ϕ_0. Thus, the results of Figs. 37 and 38 would seem to indicate at first inspection that the equivalent load method, with adequate correction, offers a reasonable approach to study general three-dimensional localized damage.

Further analysis using the equivalent load method indicates problems, however. Figures 39 and 40 show hoop stress profile plots like those in Figs. 37 and 38. For Figs. 39 and 40 d/D is 2% and m and n are either 2 or 10. Thus, imperfection depth is $0.360''$ which is above the thickness value of $0.250''$ advocated by [44] as a method limit. Indeed, for the larger, $m = n = 2$ imperfection case of Fig. 39 method accuracy

Fig. 39. Hoop stress profiles along center meridian predicted using equivalent load method and finite element analysis for $\xi = 0.360$ or $d/D = 2\%$, $m = n = 2$ double-cosine imperfection.

has deteriorated compared to Fig. 37. In the two-dimensional case, the equivalent load method's accuracy seemed correctable even for deep imperfections.

A more serious problem is seen in the small, $m = n = 10$ imperfection situation. A comparison of the finite element solutions in Figs. 38 and 40 indicates that the hoop stress profile undergoes a change in shape as dent depth increases. In particular, the sinusoidal stress profile predicted for the $d/D = 1\%$ case is replaced by a profile shape in which the positive outer stress peaks have become flattened and even begin to have slight peaks at the edges. These positive peak regions of the stress profile correspond to the stress in the depression portion of the imperfection profile. Thus, the finite element solution predicts the loss of central stress peaks and the development of stress peaks at the periphery of the depression region. These peripheral stress peaks have been noted in the pipeline dent literature [14, 8, 15, 16] for relatively small dents.

Fig. 40. Hoop stress profiles along center meridian predicted using equivalent load method and finite element analysis for $\xi = 0.360$ or $d/D = 2\%$, $m = n = 10$ double-cosine imperfection.

However, the development of the trend as depth increases, as seen in comparing Figs. 38 and 40, has not been noted. Importantly, this change in profile shape is not predicted by the equivalent load method, which continues to predict a sinusoidal stress profile that corresponds strictly to the imperfection profile shape.

The loss of a single, central stress peak for a given imperfection segment increases with further dent depth for the small imperfection case. Figure 41 shows stress imperfection profile predictions for the 3% d/D case. The equivalent load solution continues to predict a sinusoidal stress profile. On the other hand, the finite element solution now predicts clear outer stress peaks at the periphery of the concave portions of the imperfection profile. For the larger imperfection case, shown in Fig. 42, both methods continue to predict the same stress profile, however agreement in terms of accuracy continues to deteriorate.

Fig. 41. Hoop stress profiles along center meridian predicted using equivalent load method and finite element analysis for $\xi = 0.540$ or $d/D = 3\%$, $m = n = 10$ double-cosine imperfection.
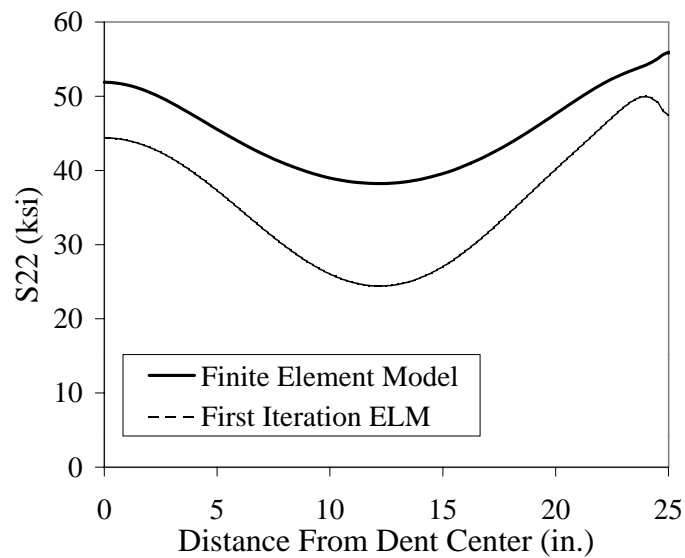
Fig. 42. Hoop stress profiles along center meridian predicted using equivalent load method and finite element analysis for $\xi = 0.540$ or $d/D = 3\%$, $m = n = 2$ double-cosine imperfection.

In the above discussion, the finite element method, which is presumed to be accurate, predicts a clear shift in stress profile behavior for the smaller imperfection case when d/D is 2% and 3%. These depths are admittedly deeper than the wall thickness, which has been advocated as a bound on the equivalent load method [44]. However, the fact that the equivalent load method still does a reasonable job predicting profile shape for the large imperfection case and the fact that accuracy problems were not insurmountable for the two-dimensional case suggests that this depth bound given in the literature is accuracy based. No remarks appear to be present in the equivalent load literature that suggest the presence of a size effect in imperfection stress behavior. In fact, localized imperfection size was studied [46]. The results were similar to those seen for the two-dimensional dent situation of the previous section. In [46], predictions of peak magnitude vary with imperfection size but the general shape of the stress profile remains unchanged. Thus, it would seem that a previously unknown limitation of the equivalent load method has been found.

The phenomenon of a size related shift in imperfection stress behavior is interesting in its own right. In addition, it is relevant to the problem of dent fatigue behavior as it appears to determine, in large part, whether or not dents are dangerous center cracking dents or more benign peripheral cracking dents [15, 16]. The relationship between stress profile features and defect size and depth will be explored more fully in the next chapter where a practical resolution to the problem of size based dent type determination is sought. In the remainder of the current chapter the source of the shortcoming of the equivalent load method in dealing with three-dimensional imperfections will be explored. This exploration will indicate some fundamental aspects of the size effect problem.

The outer hoop stress profile, while practical from a fatigue standpoint, is perhaps not the best indicator of the mechanisms at work in shell behavior. The force and

moment resultants give a much better indication of how a shell actually resists load. The force resultant is a measure of the presence of membrane action while the moment resultant is an indicator of the presence of bending action. These values can be determined from inner and outer surface stress values, $\sigma_{\phi,inner}$ and $\sigma_{\phi,outer}$. For the case of hoop membrane and bending components, N_ϕ and M_ϕ can be found in terms of inner and outer hoop stress values as follows:

$$N_\phi = \frac{t}{2} \left(\sigma_{\phi,inner} + \sigma_{\phi,outer} \right) \tag{4.41}$$

$$M_\phi = \frac{t^2}{12} \left(\sigma_{\phi,inner} - \sigma_{\phi,outer} \right) \tag{4.42}$$

Figures 43 and 44 show resultant profiles predicted with finite element analysis and equivalent load analysis for $m, n = 2$ double-cosine profiles with d/D values of 1% and 3%. These plots present both membrane and moment results. Care must be taken to note that the two types of resultants have different y axes. Also, one must realize that boundary effects obscure the behavior at the right of the cylinder, so that resultant plots should be examined in the first half of the length range. In both cases, the equivalent load method seems to accurately predict the shape of the resultant profiles. When one emphasizes the portion of the plots from $0''$ to $12.5''$ where boundary effects don't come into play, both resultants have similar sinusoidal deviations from a uniform value. For the perfect version of the shell in question there should be no moment and the membrane hoop force should be 9 k/in. In Fig. 43, the finite element results indicate that some mix of membrane and bending action develops in response to the presence of a shallow imperfection. In the deeper imperfection case, shown in Fig. 44, the variation in moment resultant drops while the membrane force deviation increases, indicating that more membrane action results from a deeper, relatively large imperfection.
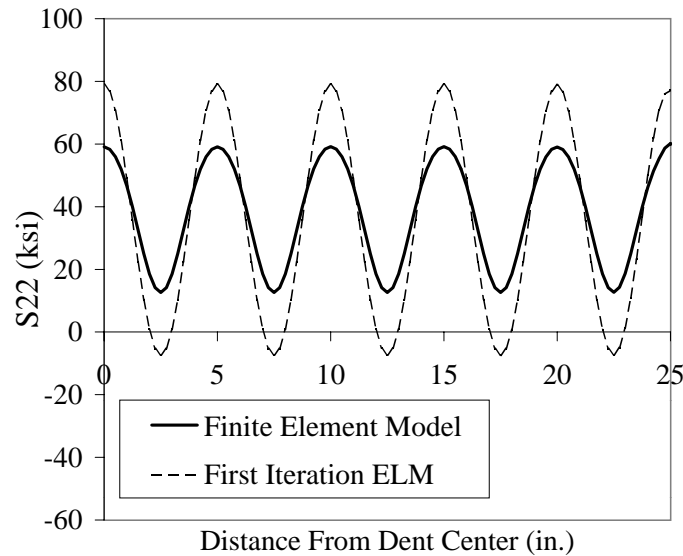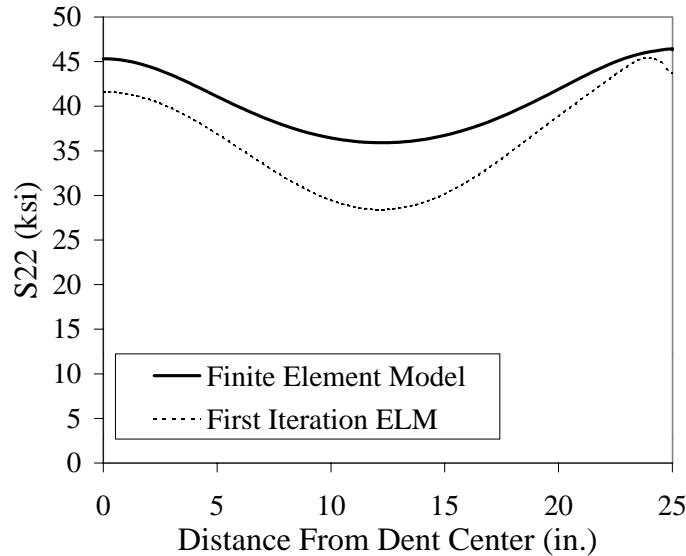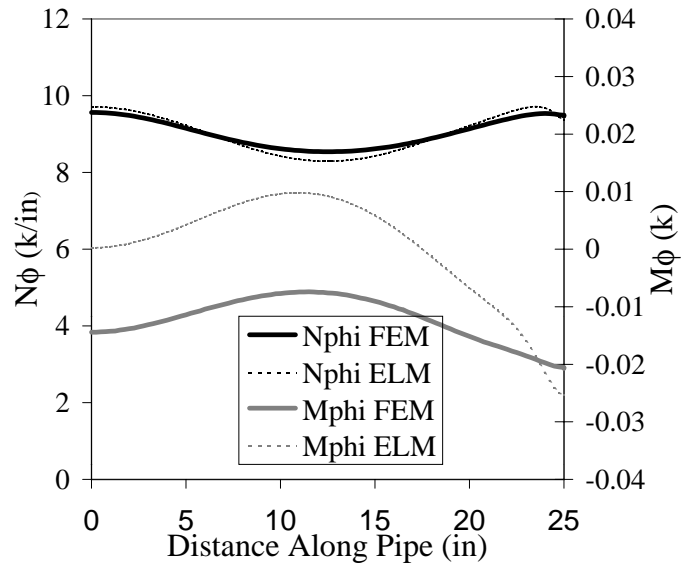
Fig. 43. Hoop membrane and bending resultant force profiles along center meridian predicted using equivalent load method and finite element analysis for $\xi = 0.180$ or $d/D = 1\%$, $m = n = 2$ double-cosine imperfection.
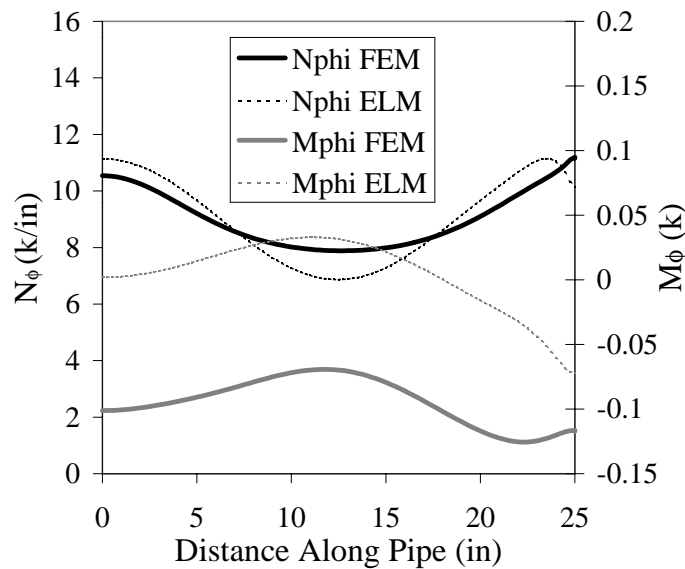
Fig. 44. Hoop membrane and bending resultant force profiles along center meridian predicted using equivalent load method and finite element analysis for $\xi = 0.540$ or $d/D = 3\%$, $m = n = 2$ double-cosine imperfection.
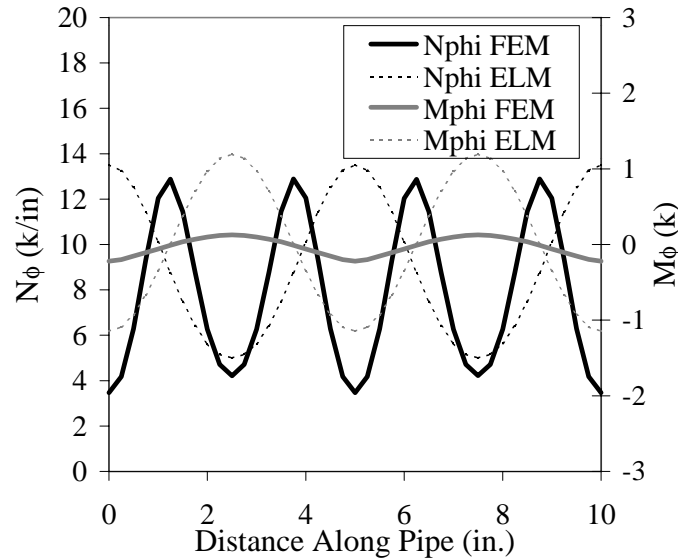
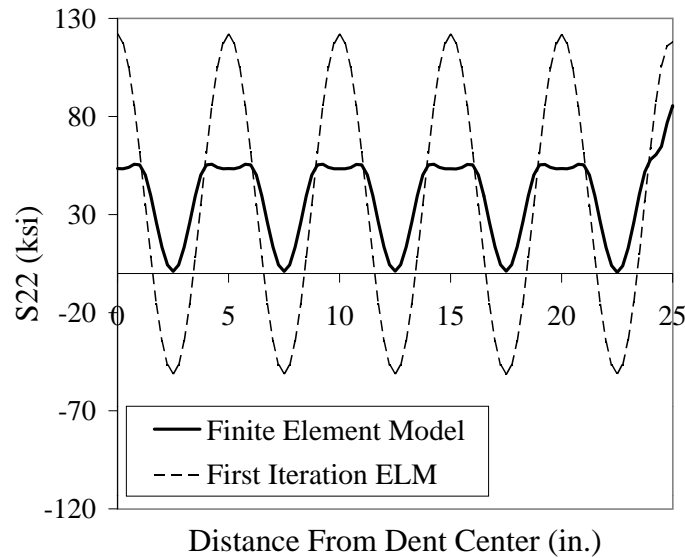Fig. 45. Hoop membrane and bending resultant force profiles along center meridian predicted using equivalent load method and finite element analysis for $\xi = 0.540$ or $d/D = 3\%$, $m = n = 10$ double-cosine imperfection.

It has been established that imperfection-induced stress behavior shifts as the imperfection becomes smaller and deeper. It remains to establish the corresponding change in resultant force action that occurs. Figure 45 shows hoop resultant forces for the $d/D = 3\%$, $m = n = 10$ case. This case was shown in Fig. 41 to have a definite loss of outer surface stress at the imperfection depression center. The distance axis of Fig. 45 has been limited so that profile features can be examined more closely. A sense of the dent profile shape can be obtained from the curves predicted by the equivalent load. They have a period of $5''$ which corresponds to the $n = 10$ situation. The equivalent load method does a poor job predicting magnitude for either resultant and predicts the wrong shape for the membrane force resultant.

In Fig. 45, the finite element solution is assumed to be the most accurate predictor of actual imperfect shell behavior. The finite element solution predicts low

membrane forces in the dent center regions and heightened membrane forces in the region where one imperfection transitions to the next. In other words, deep, relatively small imperfections appear to develop heightened membrane forces at the periphery. At the same time, bending moment does not appear to play a significant role as a load resisting action in this case. Results for relatively large imperfections, shown in Figs. 43 and 44 indicate that while moment also is not particularly significant, membrane action is and that membrane action arises primarily in the centers of the imperfections. Thus, a fundamental shift in membrane stress takes place as defects become smaller.

The equivalent load method does not anticipate the shift in membrane stress behavior that takes place for highly localized imperfections. As discussed in Chapter II, in the case of pipeline dent fatigue, a geometry dependent shift in dent stress behavior occurs. This shift from a dent SCF profile having a center peak to having a peripheral peak results in certain dents developing short lived center fatigue cracks and others developing long-lived peripheral cracks [8, 15, 16]. Thus, it is of central importance to be able to predict this behavior. The equivalent load method fails to accurately predict this shift in stress behavior. Thus, it cannot be used to explore important aspects of general dent behavior.

The present study based on the double-cosine imperfection model has shown that the equivalent load method does not appear to be as general as believed for studying geometric imperfections. However, this study may also have some more constructive insights. In particular, a preliminary assessment of the role of depth and imperfection size in determining imperfection behavior has been made. Also, fundamental understanding of the mechanics of center stress and peripheral stress behavior of imperfections has been improved.

Having established a characteristic behavior of relatively small imperfections, it
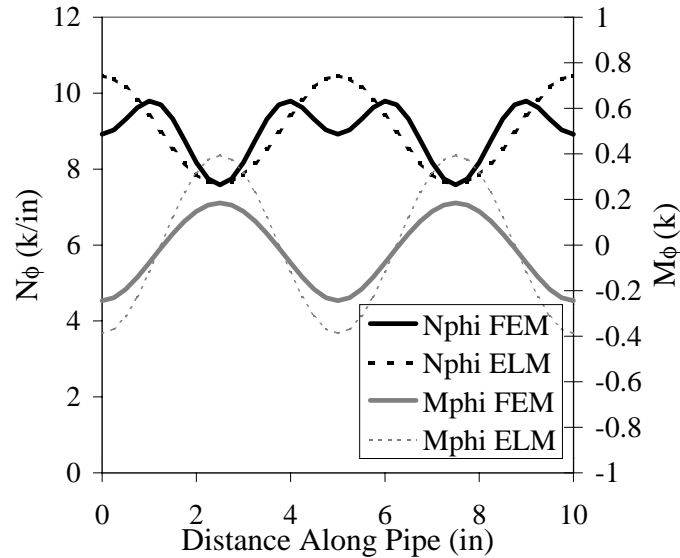
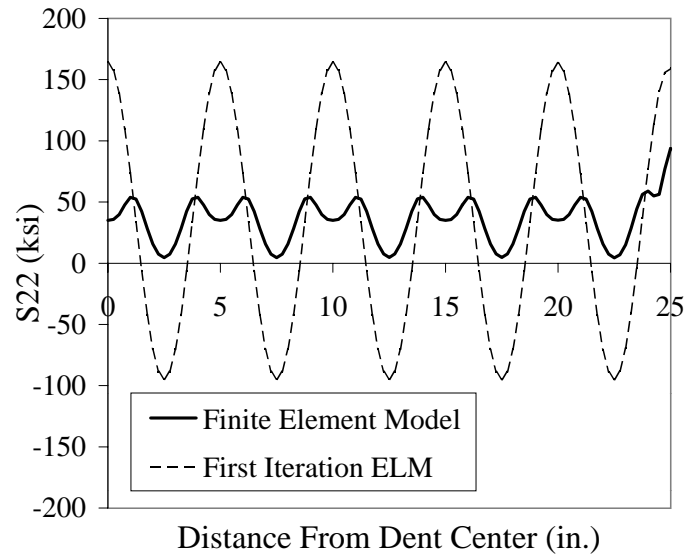Fig. 46. Hoop membrane and bending resultant force profiles along center meridian predicted using equivalent load method and finite element analysis for $\xi = 0.180$ or $d/D = 1\%$, $m = n = 10$ double-cosine imperfection.

remains to be seen whether defects need to be *both* deep *and* small in order to develop peripheral stress features. The hoop stress profile of the 1 %, $m = n = 10$ case did not indicate a clear presence of a size effect. Figure 46 shows the equivalent load and finite element predicted resultants for this case. In fact, the membrane force resultant predicted using finite elements in Fig. 46 has clearly been influenced by the smaller defect size. This profile contains peak membrane resultant values at dent periphery locations along with reduced values at the imperfection centers. The behavior seen in this case seems to be a transitional situation falling between center membrane resultants seen for larger imperfection and clear peripheral membrane resultants seen for smaller, deeper imperfections.

Thus, it appears that center stress behavior transitions gradually to peripheral stress behavior. Qualitative work in the literature has shown that relative imperfec-

tion size plays a role in determining whether the dominant imperfection stress mode is center stress or peripheral stress [8, 15, 16]. A comparison of the resultant force profiles, shown in Figs. 45 and 46, of 3% and 1% deep $m = n = 10$ double-cosine imperfections demonstrates that the tendency toward peripheral dent stress behavior increases with depth for a given defect size. Thus, depth seems to play a previously unnoticed role in determining dent stress behavior.

Up to this point, analysis has been restricted to comparing the hoop stress profiles predicted along the center line at the top of the pipe. Hoop stress behavior shifts as damage becomes deeper and/or smaller relative to pipe diameter. More insight into the problem may be gained by examining overall pipe stress behavior. Figure 47 shows a contour plot of the outer surface hoop stress distribution predicted by finite element analysis in an $18''$, $1/4''$ pipe subject to a 1 ksi pressure. The pipe in Fig. 47 contains a double-cosine imperfection with $d/D = 2\%$ and a relatively large, $m = n = 2$, spatial extent. As anticipated by Fig. 39, peak hoop stress values develop at the centers of the dents in Fig. 47. Large, possibly shallow, imperfections lead to the development of bending stresses, as seen in the alternation of red and blue portions of the stress contour plot in Fig. 47.

As damage becomes more localized, the stress behavior shifts. In the $d/D = 2\%$ case, it was seen in Fig. 40 that hoop stresses along the meridian start to lose their peaks at the dent center and develop peripheral stress features when m and n change from 2 to 10. Figure 48 shows an overall view of outer surface hoop stresses developed for the $d/D = 2\%$, $m = n = 10$ case. A clearer picture of the local dent stress behavior is seen in Fig. 49, a magnified portion of Fig. 48. In this magnified view, the outer surface peripheral hoop stress features that arise in the dent center region are seen. These stress localizations might be interpreted as being slightly interconnected from dent depression to dent depression.
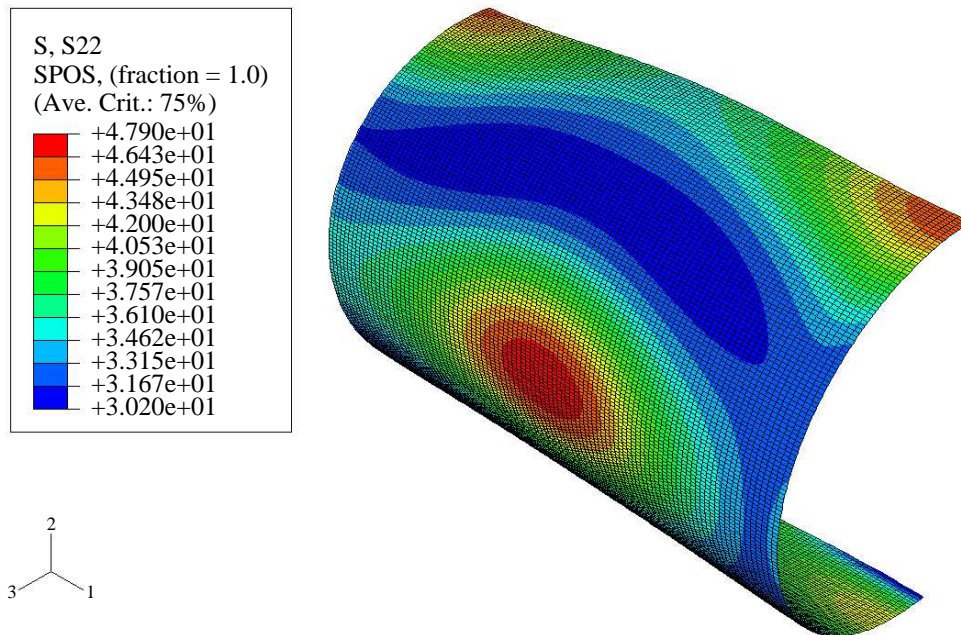
Fig. 47. Stress contour plot from ABAQUS VIEWER made of outer surface hoop stress distribution predicted using finite element analysis for $18''$, $1/4''$ pipe with $\xi = 0.360$ or $d/D = 2\%$, $m = n = 2$ double-cosine imperfection.
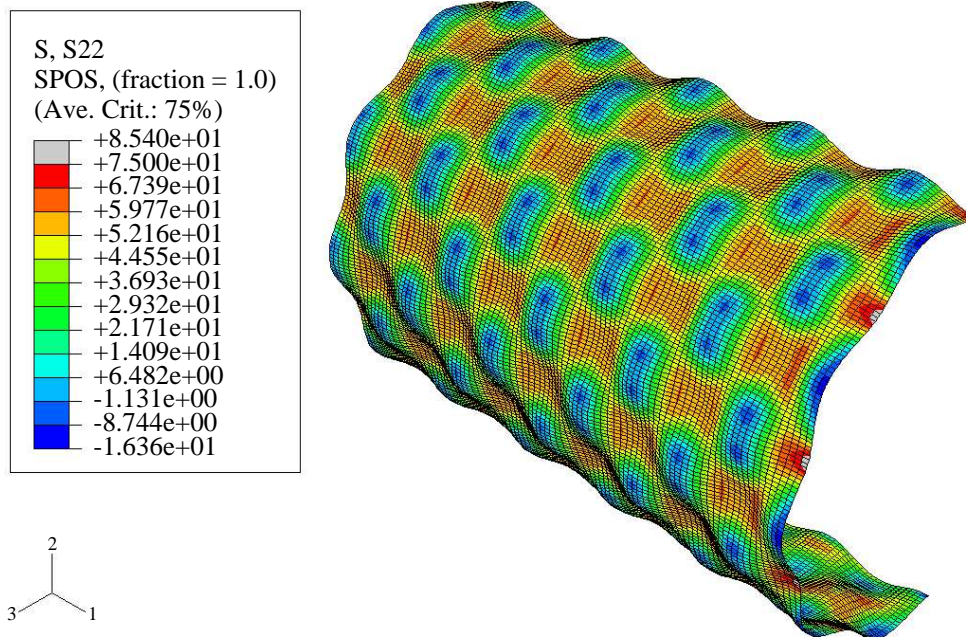
Fig. 48. Stress contour plot from ABAQUS VIEWER made of outer surface hoop stress distribution predicted using finite element analysis for $18''$, $1/4''$ pipe with $\xi = 0.360$ or $d/D = 2\%$, $m = n = 10$ double-cosine imperfection.
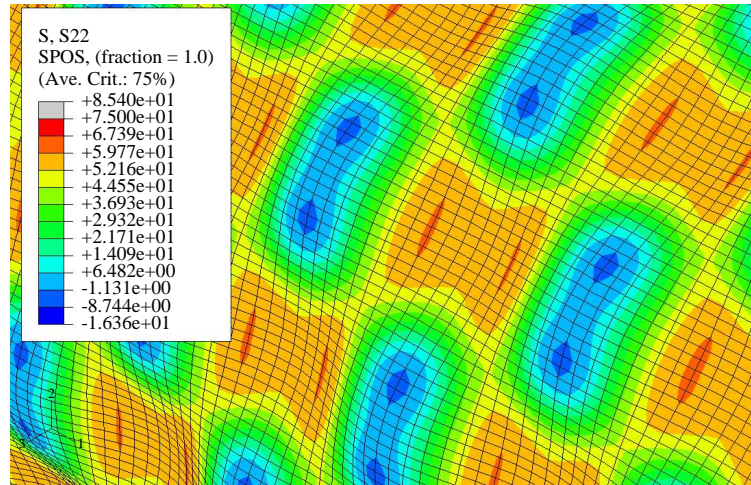
Fig. 49. Magnified stress contour plot from ABAQUS VIEWER made of outer surface hoop stress distribution predicted using finite element analysis for $18''$, $1/4''$ pipe with $\xi = 0.360$ or $d/D = 2\%$, $m = n = 10$ double-cosine imperfection.

The interpretation that hoop stress peaks at the periphery of relatively local double-cosine imperfections become interconnected is supported by Figs. 50 and 51. These figures show full and magnified contour stress plots for deeper $m = n = 10$ dents, this time with $d/D = 3\%$. In Figs. 50 and 51, peak hoop stress values are clearly located in the transition regions between dents. In fact, the zones with heightened levels of hoop stress connect to form a sort of tensile lattice that flows around the imperfections. Thus, pipes with deep, highly local imperfections seem to resist pressure load not by developing bending moment and membrane force in the dent center but by shifting membrane load so that it flows around the imperfections. This phenomena has been noted in the past [8, 15] and has been compared to the way in which load flows around a hole in a plate.

The behavior transition that takes place as imperfections go from being relatively shallow and large to being deeper and more localized appears to have at its root
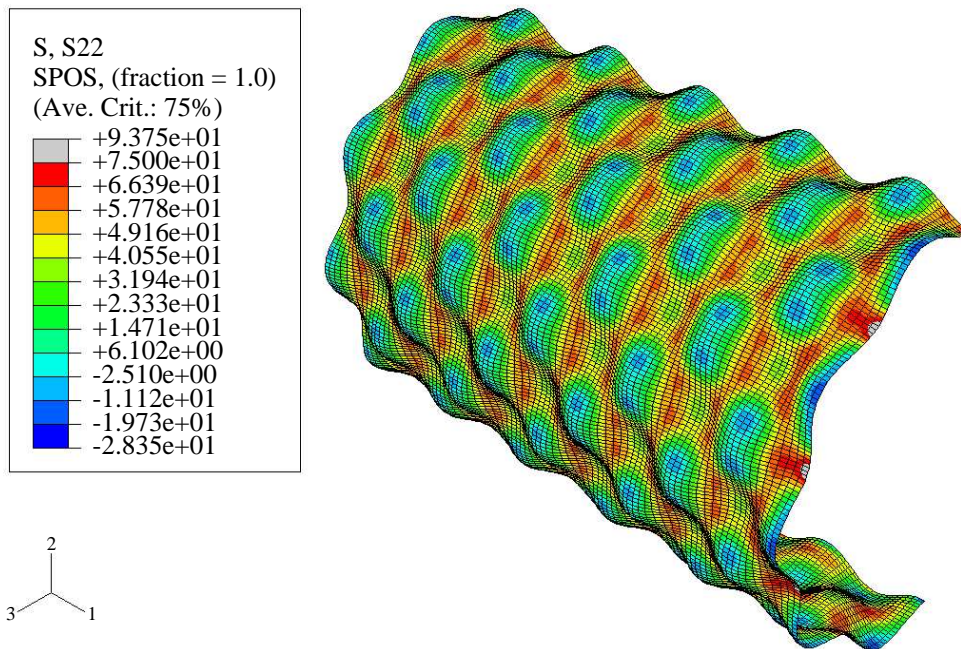
Fig. 50. Stress contour plot from ABAQUS VIEWER made of outer surface hoop stress distribution predicted using finite element analysis for $18''$, $1/4''$ pipe with $\xi = 0.540$ or $d/D = 3\%$, $m = n = 10$ double-cosine imperfection.
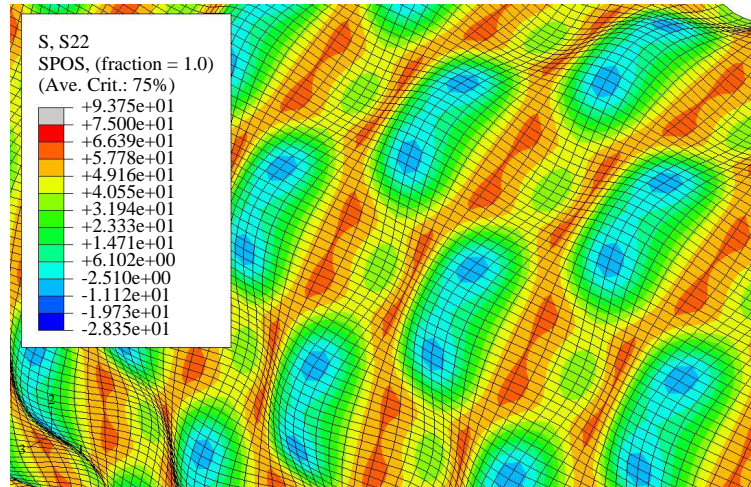
Fig. 51. Magnified stress contour plot from ABAQUS VIEWER made of outer surface hoop stress distribution predicted using finite element analysis for $18''$, $1/4''$ pipe with $\xi = 0.540$ or $d/D = 3\%$, $m = n = 10$ double-cosine imperfection.

a change in the way the imperfect shell redistributes load. Some combination of increased moment and membrane force at the center of the dent results from shallow, broad imperfections. In more localized imperfections, membrane force appears to flow around the imperfection. It is believed that ultimately the relative membrane stiffness is the fundamental source of the imperfection size effect explored here. This idea has been posited in previous work [8, 15]. Geometric imperfections exist in a displacement controlled environment. Shallow, broad imperfections have a load-displacement response, or stiffness, that is similar to that of surrounding undamaged shell. Thus, adequate imperfection deformation can occur to develop load in the center of the imperfection. Deeper, more localized imperfections are less stiff owing to their increased local curvature. As a result, the global deformations associated with a pressure load are inadequate for the imperfection to develop equilibrating forces in the center. The neighboring shell material must then accommodate the imperfection

by developing increased local stresses at the imperfection periphery.

The equivalent load method does not predict the imperfection size-effect on stress behavior. This shortcoming is a result of assumptions made in its formulation. Calladine derived the equivalent load formulation by assuming that variations in geometry and force were inter-related at a given point [17]. He determined the nature of this inter-relationship by considering the effect of these variations on the membrane equilibrium equation as was shown in Eq. 3.2. It has been shown here that in the case of broad imerfections there is a direct relation between the geometric deviation of a point in a shell and the force deviation experienced by that point. However, in more localized imperfections, the force deviation caused by the geometric deviation is at a different location than the actual geometric deviation. Thus, the basic assumption of the equivalent load method appears to break down. Support for this idea can be seen in a situation such as that shown previously in Fig. 41. In the actual shell stress profile, predicted by the finite element method, the stress profile differs significantly from the geometry profile as peripheral stress features develop. At the same time, however, the equivalent load method continues to predict a stress profile that essentially follows the imperfection profile.

In contrast to the three-dimensional situation studied in this chapter, the equivalent load method appears to work well even for deep, localized imperfection in the two-dimensional case studied in Chapter III. This difference is a result of the fact that shell three-dimensionality is what leads the stress distribution to differ from the imperfection shape. In the two-dimensional case there is no mechanism for load to redistribute as the dent localizes and deepens. Thus, no size effect results.

In the first section of this chapter is was shown that the pipe diameter-to-thickness ratio also plays a role in determining imperfection stress behavior. Thus, three-dimensional imperfection stress behavior is influenced by at least three param-

eters: size, depth, and pipe geometry. It was seen that a size effect exists for three-dimensional dent damage. Relatively broad, shallow dents develop stress deviations in the dent center. Deeper, more localized dents, on the other hand, develop stress features at the dent periphery. It will be left for the next chapter to determine the details of this transition in behavior for the specific case of pipeline dents.

The equivalent load method was shown in Chapter III to be a useful tool for studying the behavior of two-dimensional imperfections. However, this chapter has shown that it is of limited value in studying three-dimensional defects. In fact, underlying assumptions appear to limit the application of the equivalent load method to situations in which imperfection profile is essentially the same shape as the resulting stress deviation profile. As a result, the equivalent load method is poorly suited to studying relatively localized imperfections.

CHAPTER V

A METHOD FOR PREDICTING DENT TYPE

A. Introduction

In Chapter II, the fact that dents of differing geometry may differ significantly in terms of fatigue and rerounding behavior was discussed. In particular, it was noted experimentally by Keating and Hoffmann [8] that unrestrained longer dents tend to have relatively short fatigue lives, develop cracks in the dent center, and experience large amounts of post-indentation rerounding. On the other hand, shorter dents tend to have longer fatigue lives, develop cracks at the dent periphery, and experience only some post-indentation rerounding.

The most important practical aspect of the geometry effect on dent fatigue behavior is that it can produce a large disparity between the fatigue lives of different dent types. Table III compares measured fatigue lives of otherwise similar long and short dents studied in [8]. The data in Table III are for dents in 24″ diameter, 1/4″ thick API 5L X60 pipe. All dents were subjected to the same pressure history and started at the identical initial depths indicated. Type A indentors were about 6″ long while Type BH-T indentors were about 3/8″ long in the direction of the pipe. The orientation of the longitudinal axis of these two indentor types was perpendicular, as indicated in Table I of Chapter II. However, the overall dent geometry of these cases corresponds to long and short narrow dents for Type A and Type BH-T indentors, respectively. Figures 5 and 6 are pictures of dents produced by the Type A and Type BH-T indentors respectively.

In Table III, dents that differ initially only in terms of length are seen to have significantly different fatigue lives. Testing in [8] was halted at approximately 100,000

Table III. Comparison of fatigue behavior for long Type A and short Type BH-T dents in 24″ diameter 1/4″ API 5L X60 pipe seen in data taken from [8].

Indentor Type	Induced Defect	Initial d/D (%)	Failure Mode	Cycles to Failure
A	scratch	5	crack, center of dent	30,108
A	scratch	7.5	crack, center of dent	18,608
A	scratch	10	crack, center of dent	12,711
BH-T	none	5	no cracking	109,332+
BH-T	none	7.5	peripheral crack, post-proof test	109,332+
BH-T	none	10	peripheral crack, post-proof test	109,332+

cycles and a final proof test to 77% of yield pressure was run. The failure modes indicated for Type BH-T dents in Table III are either "no cracking" or describe the development of visible short dent type peripheral cracking only after the final proof test. On the other hand, Type A dents all failed in the first 30,000 cycles of testing. This contrasting behavior indicates that long dent fatigue lives in Table III are about an order of magnitude less than those of otherwise similar short dents. Because long dents pose an apparent heightened fatigue risk compared to short dents it would be beneficial to be able to distinguish long dents from short dents in the field.

Work has already been done that explains qualitatively the fundamental mechanism that prompts long dent fatigue behavior to differ from short dent fatigue behavior. This work was reviewed in Chapter II. Work by Beller [14] and by Rinehart and Keating [16, 15, 21, 22] has established that dent geometry has a strong effect on dent type because dent geometry has a fundamental effect on the stress environment that develops in the dent region. In particular, longer dents develop elastic stress concentrations profile peaks in the dent center while while shorter dents develop stress concentrations at the dent periphery. The location of fatigue failure and the relative presence or absence of dent rerounding can be associated with the location of the

dent stress concentration factor peaks.

Furthermore, long dent stress concentration factors tend to be larger than those of short dents and tend to contain more bending stress. These long dent stress concentration features, coupled with the likelihood of sharpened defects in the long dent center, may account in part for the relative shortness of long dent fatigue lives. However, as noted in Chapter II, dent fatigue behavior is significantly influenced by residual stress as well as by stress concentration features. In addition, it seems likely that some inelastic bending behavior may sometimes take place in the center of long dents. These large inelastic stress concentrations may result in Region III fatigue behavior instead of the Region II behavior assumed in the power law model introduced in Chapter II. Thus, the complicated overall mechanics of long dent fatigue behavior make it difficult to establish the exact magnitude of the influence that elastic SCF behavior has on accounting for shorter long dent fatigue lives. However, elastic SCF behavior certainly is an important factor in this problem.

In Chapter IV it was shown that the dent type dependency in elastic dent stress behavior is due to a general size effect feature of dent behavior. In particular, broader, shallower dents developed elastic stress concentration distributions with peaks in the dent center. In more localized, deeper dents elastic SCF behavior shifts and SCF peaks arise at the dent periphery. This behavior was seen in shells containing dent patterns where the elastic hoop stress distribution shifted from having magnitude peaks in the center, as seen in Fig. 47 of Chapter IV, to having a tensile lattice, as seen in Fig. 50 of Chapter IV.

Work has also investigated criteria for use in distinguishing long dents from short dents. Most notably, Rinehart and Keating [16] showed that fatigue lives of unrestrained dents in [8] have an inverse relationship with the nondimensional parameter Ld_fw/D^2t. This relationship is shown in Fig. 52 where d is taken to be final, post-
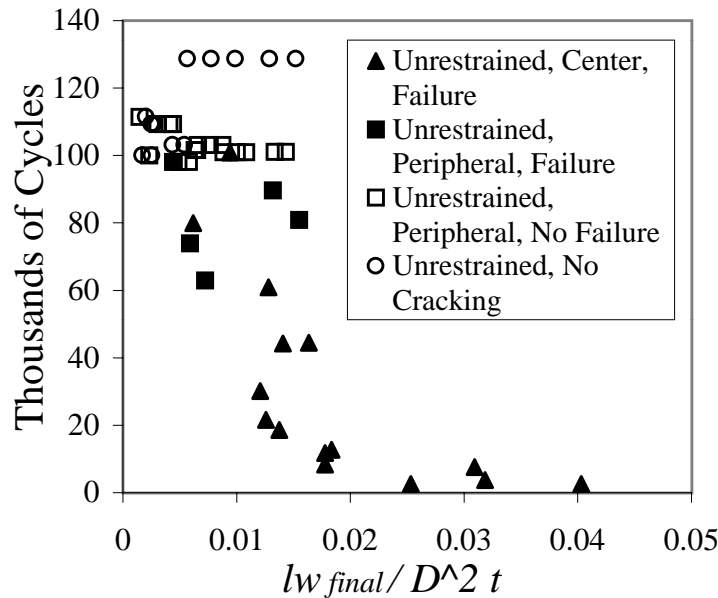
Fig. 52. Fatigue life data taken from [8] plotted in terms of the non-dimensional ratio $Ld_f w/D^2 t$ where L and w are indentor width and d_f is final, rerounded dent depth (taken with permission from [16] courtesy of ASME).

rerounding dent depth, d_f. A better correlation exists between fatigue data from [8] and the parameter $Ld_f w/D^2 t$ than exists with the traditional d_f/D parameter, as shown in Fig. 7 of Chapter II. In fact, criteria can be developed from Fig. 52 for distinguishing long dents from short dents.

Although the $Ld_f w/D^2 t$ parameter proposed in [16] appears to offer a somewhat successful approach to distinguishing long and short dents it has several drawbacks. First and foremost, it is completely empirical and is specific to the data set in [8]. As a result, uncertainty exists regarding its applicability to cases with circumstances and pressure histories deviating from those used in [8]. Such limiting circumstances include the need for similar levels of damage in the contact region, similar material types, and similar residual stress features resulting from pressure history details.

In addition, the dents in [8] are rather narrow in the transverse direction. Other

sets of test results are available in [9] that indicate that wider dents may have a different mode of failure than narrower dents. The parameter $Ld_f w/D^2 t$ does a poor job of distinguishing between the effects of dent length L and dent width w. For example, holding D, t, and d_f fixed, the factor $Ld_f w/D^2 t$ would return the same value for short, wide and a long, narrow dents having the same Lw, length-width product. At the same time, it appears that wide dents may have a different failure mode compared to long narrow dents. Dents studied by Fowler *et al.* [9] were relatively wide and may have developed cracks at the circumferential dent periphery. Also, the two-dimensional dent stress concentration model of Chapter IV suggests that wide dent stress concentration profiles have lower central stress peaks than those of narrow dents. The possible role played by dent width means that it is important to be able to distinguish length from width in a dent categorization model.

The $Ldw/D^2 t$ parameter of [16] is case specific and may confuse the length and width indicators that possibly distinguish categories of dent behavior. In addition, this model is data-specific. Thus, a more general approach to dent classification is desirable. It would also be interesting to determine how to classify dents based on elastic stress concentration behavior because these mode bounds would also define limits on the equivalent load method, which was shown in Chapter IV to be unable to analyze relatively short, deep dents with peripheral stress features.

B. Experimental Insights and Modelling Issues

It was noted above and previously in Chapter II that dent stress behavior is the most significant parameter influencing dent fatigue behavior. In particular, geometry dependent changes in dent elastic stress concentration behavior appear to account for the existence of geometry based modes of dent behavior. Thus, if one can deter-

mine dent geometry values that distinguish long and short dent stress behavior, the same geometry values can be used to distinguish between long and short dent fatigue behavior.

It has been shown in Chapter III, and illustrated in Fig. 3 of that chapter, that short dents and long dents have type-specific peaks in elastic stress concentration profile present along the top longitudinal axis of the pipe. In particular, short dents have peripheral peaks in their outer surface stress ranges and long dents have a center peak in their surface stress ranges. Presumably, in a given pipe diameter there is some dent length range that marks a transition from short dent to long dent type stress behavior. This length range has yet to be quantified.

In [8], Type A dents typically behaved as long dents while Type BH-T and BH-L dents were typically short dents. However, in the largest specimen tested, a 36″ diameter, 3/8″ thick pipe, this correspondence was not observed. The results for all 36″x3/8″ specimens are shown in Table IV. In Table IV, two of three Type A dents have long-life peripheral cracking. A large diameter was present in this case. Thus, the Type A dent was relatively short in terms of the pipe diameter compared to other situations in [8] involving smaller diameter pipes. The shift in fatigue behavior of Type A dents in 36″ pipe indicates that the long dent-short dent transition problem involves relative length.

Another feature of dent stress behavior can be observed in the data of Table IV. It is not immediately clear why some Type A dents in the 36″ pipe behave like long dents and others behave like short dents. One possibility is that relative length is not the only parameter involved in distinguishing long dents from short dents. The shallowest Type BH-L dent was reported to develop a groove crack. While it is not entirely clear what is meant by "groove crack," elsewhere in [8] "groove crack" usually refers to center cracks. If this dent developed center cracking, then both dents

Table IV. Fatigue failure data for Type A and Type BH-L dents in $36''$x$3/8''$ Gr. B pipe taken from [8].

Indentor Type	Induced Defect	Initial d/D (%)	Failure Mode	Cycles to Failure
A	scratch	5	crack, center of dent	79,975
A	scratch	10	peripheral cracking	101,125+
A	scratch	10	peripheral leak, post-proof	101,125+
BH-L	none	5	groove crack, 2390 large cycles after proof test	111,42++
BH-L	none	10	peripheral leak, post-proof test	111,425+
BH-L	none	15	no cracking	111,425+

in Table IV with initial d/D ratios of 5% developed center cracking. On the other hand, deeper dents in Table IV, with initial d/D values of 10% and 15%, developed peripheral cracks. Thus, it appears that relative dent depth also plays a role in determining whether dents are "long dents" or "short dents".

The role of depth in determining dent mode was also seen in Chapter IV. Three-dimensional dent patterns with a given amount of localization actually developed more pronounced peripheral stress features as dent depth increased. For example, compare the $m = n = 10$ stress profiles shown in Figs. 38 and 42 of Chapter IV.

Because dent type appears, based on experimental evidence, to be influenced by relative length *and* relative depth the designators "short dent" and "long dent" no longer appear appropriate. Dents exhibiting center cracking, short life, and significant rerounding will subsequently be called Mode C dents, in reference to their center stress feature and center mode of cracking. Dents exhibiting peripheral cracking, long life, and low levels of rerounding will subsequently be called Mode P dents, in reference to their peripheral stress feature and peripheral mode of cracking.

The fact that relative dent depth and relative dent length play a role in distin-

guishing Mode C and P dents can also be shown by considering the effect of these geometry values on dent stress. While this effect was shown in Chapter IV, a more thorough investigation of the behavior of a single dent will be carried out here. Approaches to studying dent stress have been explored in earlier chapters. Finite element analysis appears to offer the most direct approach and will be used in this chapter.

The discussion in Chapter III of the equivalent load approach led to a significant conclusion. Namely, elastic dent stress concentration features are a direct result of the geometric imperfection of the dent. This imperfection leads to a redistribution of stress in the pipe wall and can lead to plate bending. Subtle differences in the features of this imperfection no doubt lead to differences in stress behavior. However, as a first approximation, it seems reasonable to assume that if one uses a typical dent profile model then one should get a prediction of the typical stress behavior of a range of dent configurations in which local profile features differ slightly from this ideal profile. As a result, analysis of a simple profile that is easily modelled can lead to an understanding of what dent geometry values distinguish Mode C and P dents.

The dent analysis problem is also complicated by the evolutionary nature of the dent life-cycle. After indentor removal, unrestrained dents that are the focus here rebound to a different, stable configuration [8, 24]. Dents undergo a significant change in geometry during rerounding. Figure 53 illustrates typical changes in longitudinal profile produced by rerounding for Mode C and P dents. Mode C dents undergo a relatively large geometry change.

Dent stress behavior is largely a result of profile shape. It would be useful to vary dent length in an analysis of dent stress behavior and to determine when the hoop stress concentration profile shifts from having a central peak to having a peripheral peak. However, in the post-rerounding configuration, Mode C and Mode P dents have very different profile shapes. These differences make it difficult to formulate a
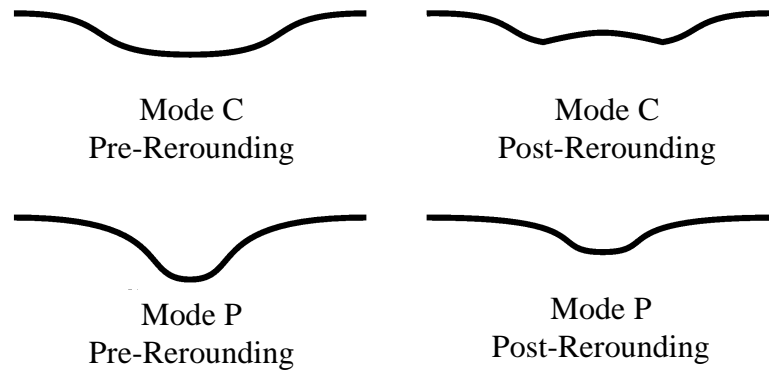
Fig. 53. Illustration of change in longitudinal profile from pre-rerounding to post-rerounding state for Mode C ("long") and Mode P ("short") dents.

single dent profile model that can be used to find the transition geometry.

Unlike the post-rerounding profiles, the pre-rerounding profiles in Fig. 53 of Mode C and P dents have very similar features. Furthermore, the fact that Mode C dents undergo large amounts of dent center rerounding indicates that a central SCF peak is still present in the pre-rerounding configuration. Mode P dents don't experience significant dent center rerounding. This observation suggests Mode P dents don't have central SCF features. Furthermore, because they always have the same approximate shape, Mode P dents can be expected to have peripheral stress peaks in the pre- and post-rerounding configurations.

Using a detailed, full life-cycle finite element model that considers indentation and rerounding phases of dent life and that is described in [8, 16, 22, 21] it is possible to demonstrate more rigorously that central and peripheral stress features result from more easily modelled pre-rerounding dent profiles. Figures 54 and 55 show outer surface hoop stress concentration profiles determined using this finite element model. In both cases, a longitudinal dent was formed to a depth of 10% in an 18″x1/4″ X60
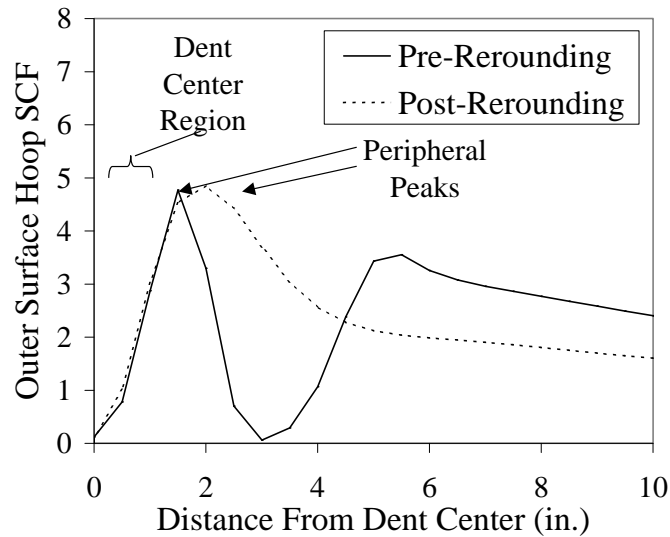
Fig. 54. Pre- and post-rerounding outer surface hoop stress concentration factor profiles from complete life-cycle FEM analysis of 18″x1/4″ X60 pipe with 1″ indentor.

pipe. The models used to generate Figs. 54 and 55 had 1″ and 7″ indentors respectively. Indentation occured when the pipe was unpressurized. After the indentor is released, residual stress is determined and pressure is applied. The pre-rerounding hoop stress concentration factor is based on the stress change that occurs during this initial pressure ramp-up. Rerounding is modelled by two 0% to 70% to 0% pressure ramp-ups cycles. Post-rerounding residual stress values are then determined and stress concentration factors are determined from a third pressure ramp-up.

Although the SCF profiles in Figs. 54 and 55 differ considerably from the prerounding state to the post-rerounding state, at least one important feature remains consistent between the two states. Namely, the Mode P peripheral stress feature is present in both the pre-rerounding and post-rerounding situations shown in Fig. 54. Likewise, in Fig. 55 a definite center SCF feature is present in both the pre- and
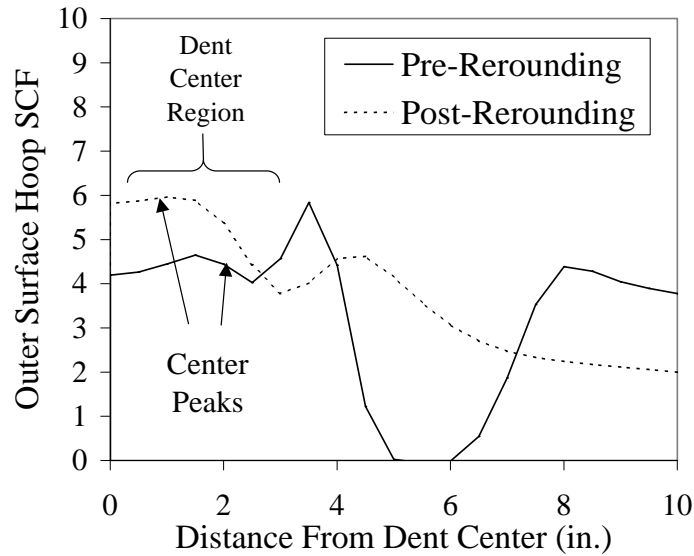
Fig. 55. Pre- and post-rerounding outer surface hoop stress concentration factor profiles from complete life-cycle FEM analysis of 18″x1/4″ X60 pipe with 7″ indentor.

post-rerounding configuration.

A study seeking transition geometry values does not need highly accurate stress magnitude information, only an accurate sense of whether a dent will have center or peripheral stress features. Detailed finite element analysis as well as physical arguments suggest that a simple, single-depression model of dent geometry will provide information that can be used to predict whether a certain dent geometry is a Mode C or P geometry.

C. A Simple Model

It appears likely that the main aspects of long and short dent stress features are not highly dependent on precise details of dent geometry or pressure history. In addition, one doesn't necessarily need completely accurate magnitude information if one only

seeks to distinguish Mode P dents from Mode C dents. These two facts suggest that a simple finite element model can be used to determine dent length and depth values that designate the transition zone between Mode C and P dents. These models need not account for all stages of the dent life cycle. Instead, if a pipe with a dent imperfection is meshed and analyzed as an elastic situation, an indication of whether the dent behaves as Mode C or P should result.

The finite element package ABAQUS [37] is used to perform an elastic finite element analysis. A doubly-symmetric model is used with boundary conditions like those shown in Fig. 36 of Chapter IV. Four noded linear Type S4R elements are used with an elastic material model. A Young's Modulus of 29,000,000 ksi and a Poisson Ratio of 0.30 are used as material properties. Because the influence of geometry on elastic stress concentration behavior is being studied and because the purpose of this study is not to obtain accurate stress magnitudes, inelastic material behavior is not studied. The elements have 11 integration points and a geometrically nonlinear analysis option is used. For every model, a uniform internal pressure of 1 ksi is applied. These models are simple and as a result can be used to efficiently generate data for a range of dent geometry cases.

The dent profile is included directly in the mesh geometry. A FORTRAN 77 code was written that generates the mesh. The dent profile is based on a normal distribution similar to that used in the equivalent load analysis discussed in the previous chapter. This profile model generates single depression dents. Dent profile r is determined over the longitudinal coordinate x and circumferential angle coordinate ϕ. Given a pipe radius R, a dent depth ξ, and longitudinal and circumferential "decay" terms x_0 and ϕ_0, the pipe wall profile can be written as:

$$r = R - \xi \exp\left(-\frac{1}{2}\left(\frac{x}{x_0}\right)^2\right) \exp\left(-\frac{1}{2}\left(\frac{\phi}{\phi_0}\right)^2\right) \qquad (5.1)$$
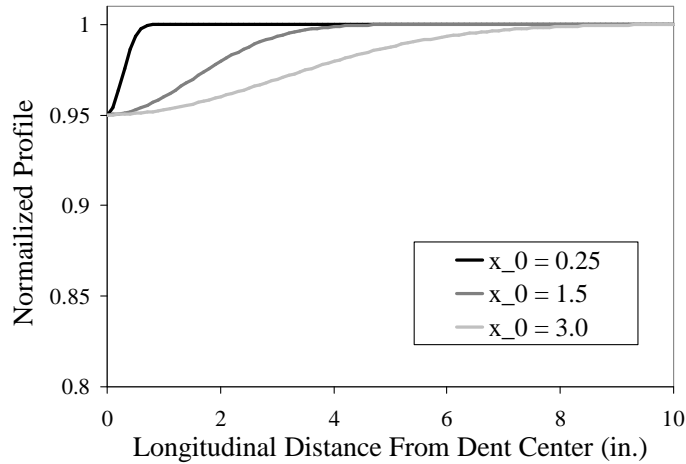
Fig. 56. Normalized longitudinal dent profiles developed using Eq. 5.1 with d/D ratios of 5% and three values of x_0.

This model of dent profiles was shown in Chapter IV to be capable of generating a wide range of circumferential cross-sections. It is also capable of generating single depression dents of a variety of lengths. Dent length is controlled through the value of x_0, essentially a spatial decay rate. The value of x_0 can be related to actual dent length. Figure 56 shows three longitudinal dent profiles generated using Eq. 5.1. These profiles are normalized against pipe diameter. All three cases have a depth-to-diameter ratio of 5%. While Eq. 5.1 can't model a long flat dent it is capable of representing long depressions. Because it requires only a single parameter, x_0, to describe a considerable range of dent lengths, Eq. 5.1 offers a simple means of easily developing models for studying a range of dent configurations.

Finite elements used in this analysis have a longitudinal dimension of $0.25''$ and an angular extent of $\pi/180$ or 0.0174 radians. Other, more complicated finite element models of dent behavior that model both contact and inelastic rerounding have been discussed elsewhere [8, 21, 22, 16] and have been demonstrated to have reasonable
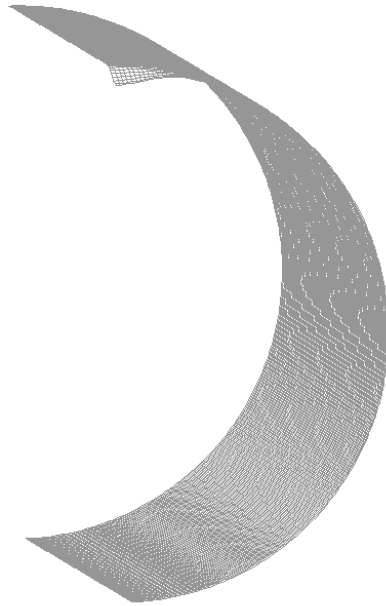
Fig. 57. Front view taken from ABAQUS VIEWER of mesh generated for the case $\phi_0 = \pi/24$, $x_0 = 0.25$, $\xi/D = d/D = 0.05$.

convergence with $0.5''$ by 0.0262 radian elements. Because the mesh is finer in the present model and because the modelling issues are more straightforward here than they are in the more complicated model, convergence is assumed to exist.

Images of example meshes generated using a mesh generation routine that implements Eq. 5.1 are found in Figs 57 through 60. Figures 57 and 58 are front and side views of a mesh containing a dent with $x_0 = 0.25''$. Figures 59 and 60 are front and side views of a mesh containing a dent with $x_0 = 4.5''$. Both pairs of figures were generated using the ABAQUS post-processer ABAQUS VIEWER and show front and side views of typical generated meshes used in determining Mode C to P transition dent geometries. In both cases $\phi_0 = \pi/24$, a narrow dent situation.
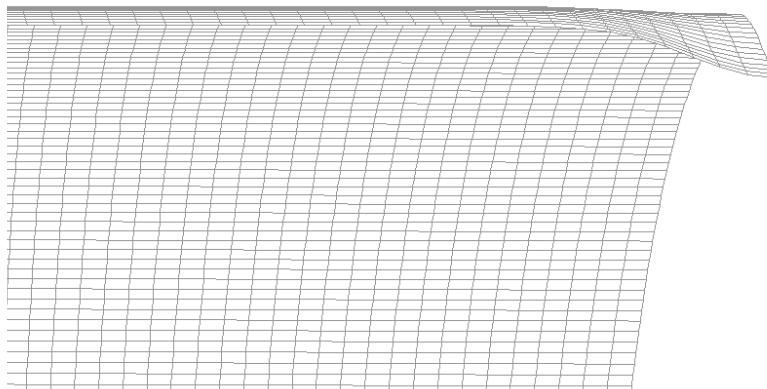
Fig. 58. Side view taken from ABAQUS VIEWER of mesh generated for the case $\phi_0 = \pi/24$, $x_0 = 0.25$, $\xi/D = d/D = 0.05$.
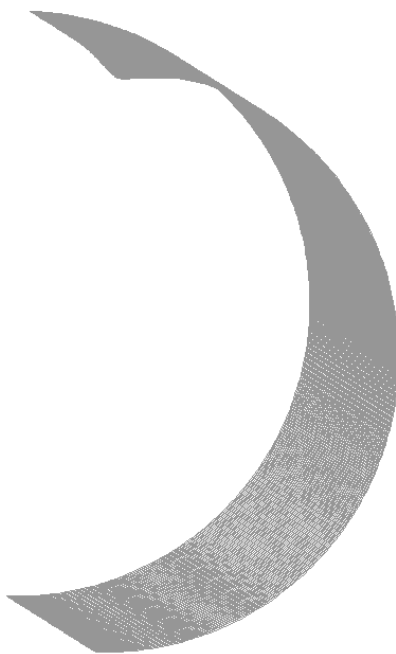
Fig. 59. Front view taken from ABAQUS VIEWER of mesh generated for the case $\phi_0 = \pi/24$, $x_0 = 4.5$, $\xi/D = d/D = 0.05$.
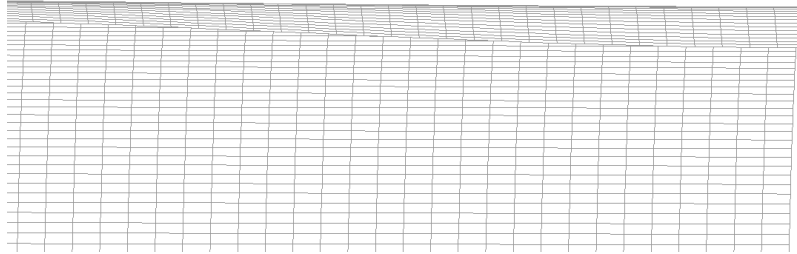
Fig. 60. Side view taken from ABAQUS VIEWER of mesh generated for the case $\phi_0 = \pi/24$, $x_0 = 4.5$, $\xi/D = d/D = 0.05$.

D.   Aspects of Stress Effects of Dent Geometry Features

Using the finite element model described in the previous section, a general sense of the effects of certain geometry features on dent stress behavior can be developed. It is important to remember that the simplified approach used in this chapter does not offer a fully accurate picture of stress magnitudes. However, the approach can be used to determine what role different parameters play in determining whether a dent is Mode C, Mode P, or belongs to some other mode, perhaps associated with wider dents.

Existing experimental data [8, 9] covers a wide range of dent situations. However, details about dent geometries in [9] are somewhat unclear. More information is available about the dent geometries studied in [8]. As a result, analytical efforts will focus on geometries for which there is data available in [8]. This approach is used to avoid analysis results that can't be judged in terms of experimental data. One problem with the data set available in [8] is that it is confined to rather narrow dents. As a result of both this fact and the need to focus analysis on cases for which exper-

imental data is available, this study will be primarily restricted to a consideration of narrow dents.

Although they will not be studied in detail here, wide dents are an important class of damage. In fact, the possibility exists that they have their own dent fatigue mode not covered by Mode C or P. Experimental work reported in [9] by Fowler, *et al.* shows that many of the wider dents studied actually failed at what appears to be the circumferential dent periphery. More analysis is needed to explore the relative threat posed by this failure mode.

Using the finite element model and dent profile model described in the previous section, qualitative aspects of the effect of dent geometry on dent stress behavior can be studied. The stress behavior of a dent is complicated. Post-processor applications like ABAQUS VIEWER can be used to look at color contour plots of stress over the entire surface of a pipe model. These plots are useful to judge locations of interest and general trends as was done in Chapter IV. However, these sorts of plots are highly qualitative and, in the present case, tend to contain far more information than necessary.

In the case of narrow dent fatigue, the location of interest is the longitudinal centerline of the dent. This line falls on the approximate location where all Mode C and P fatigue cracks were observed to develop in experiments. The dent fatigue model [21, 22] discussed in Chapter II is based solely on hoop stress behavior behavior at this location. While some multi-axial fatigue effects are no doubt present, the overall accuracy of the fatigue model presented in [21, 22] suggests that hoop stress behavior is the stress feature that plays the predominant role in driving dent fatigue. Both residual stress and stress concentration factors are important. However, it is hypothesized that the dent length effect on fatigue is largely due to dent length effect on SCF behavior. As a result, this study will focus on understanding the influence

Fig. 61. Illustration of definition of dent length: the shortest straight-line distance between the two closest points on the longitudinal axis that are not noticeably part of the local dent depression.

of dent geometry on hoop stress features present along the longitudinal centerline of the dent.

Before hoop stress effects of dent geometry can be explored, one issue related to the dent model in Eq. 5.1 must be addressed. Dent length and width are determined in Eq. 5.1 through two spatial decay terms, x_0 and ϕ_0. These terms must be related to actual dent geometry. The term x_0 relates to dent length. An accurate measurement of dent length is probably somewhat subjective. In this case, dent length is defined as illustrated in Fig. 61. As shown in Fig. 61, dent length is defined as the straight-line distance between the two closest longitudinal points that are not noticeably in the dent depression. This measurement seems practical since it can be done with some degree of accuracy and repeatability by laying a straight ruler along the longitudinal axis of the pipe and reading the distance between the two points of the ruler that first come in contact with the pipe.

To relate the spatial decay term x_0 to actual dent length it is assumed that the two closest points not noticeably part of the dent depression occur when the dent profile term accounting for deviation from perfect radius R is 5% of its maximum

value. In other words, the dent length L occurs when:

$$\exp\left(-\frac{1}{2}\left(\frac{x}{x_0}\right)^2\right) = 0.05 \quad \text{for} \quad x = L \tag{5.2}$$

This condition can be shown to be satisfied when:

$$L = 2.4477\,(2x_0) \tag{5.3}$$

Use of Eq. 5.3 provides a simple way to relate results obtained using the normal distribution dent model in Eq. 5.1 to actual dent sizes measured using the definition illustrated in Fig. 61.

With a dent model, an analysis approach, and a means of relating model parameters to physical parameters it is now possible to explore aspects of the influence of dent geometry parameters on dent stress behavior. It makes sense to first demonstrate that this approach indeed predicts the length dependent, Mode C to P transition seen in Chapter IV and in the experimental results of [8]. Figure 62 shows elastic hoop stress concentration factor profiles for increasing values of dent length. In Fig. 62, an 18″ diameter 3/8″ thick pipe is modelled. In all cases, the dent width descriptor ϕ_0 is held fixed at $\pi/24$. All dents have a deepest depth of 0.540″ or 3% of the pipe diameter. As expected, for shorter dent situations, $L = 1.33″$ and $L = 4.90″$ ($L_0 = 0.5″$ and $L_0 = 2.5″$), clear peripheral stress features indicative of Mode P dent behavior are exhibited. For long dent lengths, $L = 9.79″$ and $L = 14.69″$ ($L_0 = 4.0″$ and $L_0 = 6.0″$), center peak SCF profiles corresponding to Mode C behavior are seen.

Another feature worth pointing out in Fig. 62 is the fact that as dent length increases, the peak hoop stress concentration magnitude increases. While the behavior of real dents is considerably more complicated than the simplified problem being considered here, this result is still interesting. It has been discussed in Chapters II
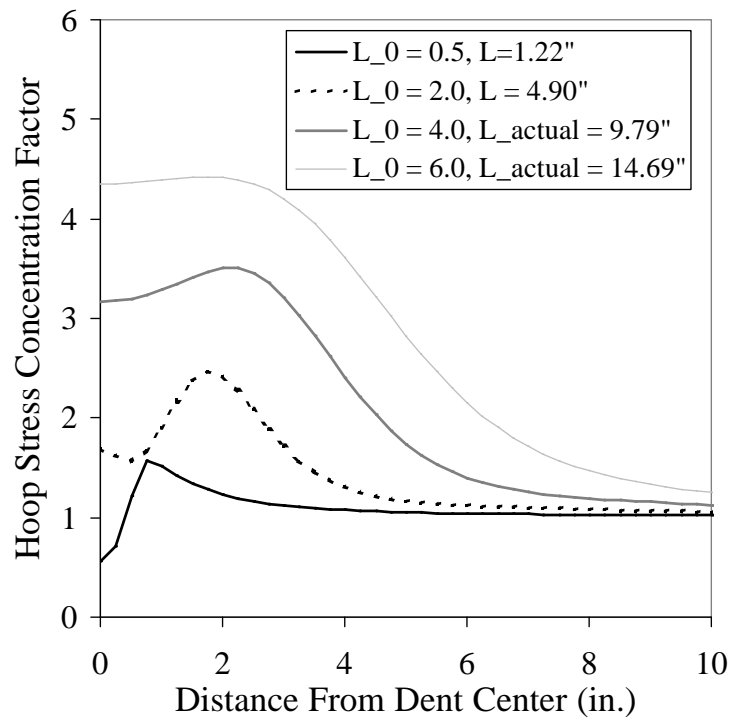
Fig. 62. Hoop stress concentration profiles calculated for 18″ diameter, 3/8″ thick pipe containing dent profiles based on Eq. 5.1 with increasing dent length parameters and fixed dent depth (d/D = 3%) and width ($\phi_0 = \pi/24$).

and III that imperfections in shells lead to stress deviations. Presumably, longer dents are actually larger deviations from the standpoint of hoop stress and lead to a greater overall disturbance in the stress system associated with a given dent. From a practical standpoint, increases in stress concentration magnitude associated with increases in dent length help account for the fact that relatively long dents with center stress peaks studied in [8] tended to have much shorter lives than shorter dents, as was illustrated in Table III.

Another feature evident in Fig. 62 is the continued presence of a slight peripheral peak even in some longer dent cases where central SCF levels indicate Mode C behavior. This feature is most evident in the curve for the $L_0 = 4.0$, $L = 9.79''$ case shown in Fig. 62. However, a peripheral peak appears to remain as length increases. At the same time, as length increases, the central region of the SCF zone increases in magnitude until it achieves a magnitude on the same order of the peripheral peak. This apparently gradual transition from Mode P to C behavior raises a question. Namely, one must determine what ratio of center SCF value to peripheral SCF value marks the transition from Mode P to Mode C behavior. This issue will be addressed in the next section.

Discussion in a previous section of this chapter and work presented in [16] shows that the significant dent length parameter in terms of fatigue effects is *relative* dent length with respect to pipe diameter. This feature of dent fatigue behavior may be motivated by the elastic nature of dent SCF behavior. If the dent SCF problem is essentially elastic, then two pipes with differing absolute dimensions containing dents will have the same elastic behavior if the relative sizes of all of the pipe and dent features are kept consistent. This fact is illustrated by returning to finite element analysis results. Figure 63 shows Mode C hoop SCF profiles predicted for $12''x1/4''$ and $18''x3/8''$ pipes containing dents that have an angular extent of $\phi_0 = \pi/24$. For

Fig. 63. Hoop stress concentration profiles calculated for 18″x3/8″ and 12″x1/4″ pipe containing dents with $\phi_0 = \pi/24$ and $x_0 = 6.0''$ and $x_0 = 4.0''$ respectively and plotted in terms of absolute length in inches from dent center.

the SCF profiles shown, $x_0 = 4.0''$ for the 12″x1/4″ pipe and $x_0 = 6.0''$ for the 18″x3/8″ pipe. The pipe and dent geometry values are chosen to maintain consistent aspect ratios. In both cases, the diameter-to-thickness ratio, D/t, is 48, the length to diameter ratio is 1/3, and the width to diameter ratio is $\pi/24$. The resulting SCF profiles in Fig. 63 do not match because the "Distance From Dent Center" axis on the graph is still in absolute terms. In Fig. 64, this axis is put in relative terms with respect to pipe diameter. The resulting hoop SCF profiles in Fig. 64 overlap. Thus, the expected linear scaling of elastic dent models is demonstrated. Also, the importance of relative dent geometry measurements is reinforced.

The preceding discussion has established several important aspects of the effect of dent length on dent hoop SCF behavior using a simple finite element analysis

Fig. 64. Hoop stress concentration profiles calculated for $18''$x$3/8''$ and $12''$x$1/4''$ pipe containing dents with $\phi_0 = \pi/24$ and $x_0 = 6.0''$ and $x_0 = 4.0''$ respectively and plotted in relative terms of length from dent center divided by pipe diameter.

approach. First, as expected, shorter dents result in Mode P stress behavior while longer dents result in MOde C stress behavior. In addition, as analysis of data in [8] indicates, dent length is considered long or short depending on its relative value with respect to pipe diameter. This result is essentially due to the linear scaling of elastic dent SCF behavior. While the current discussion has contributed to existing qualitative understanding, one important practical question remains to be answered. Namely, it is still not clear how to distinguish Mode C and Mode P dents over a range of general cases. This problem will be addressed in the next section. However, another aspect of the effect of dent geometry on dent stress behavior needs to be explored first.

Conventionally, a great deal of attention has been given to dent depth. Existing approaches for assessing dent damage in pipelines specify depth-to-diameter ratios that indicate whether or not a dent requires repair [11, 12, 13]. Experimental research has indicated that dent depth is an indicator of dent severity. This result was a conclusion of the study conducted by Fowler *et al.* Although not a major conclusion of the study by Keating and Hoffmann [8], the final observed dent depth-dent severity relationship is still evident within a given dent mode in data taken from [8]. Consider Table III, appearing earlier in this chapter and containing measured fatigue lives taken from [8] for a 24″x1/4″ pipe. Within the set of Mode C dents in Table III, in this case resulting from Type A indentors, fatigue life decreases as relative initial depth of indentation increases.

Because no Mode P failures are shown in Table III, a different data set, taken from [8] for a 12″x1/4″ pipe and Type BH-T indentors, is used. Table V shows initial and final relative dent depths, cycles to failure, and final condition for these dents. In Table V, deeper dents, specifically those with final d/D values of 6.58% and 7.75%, fail due to fatigue while the shallower dents do not. For the two dents that failed in

Table V. Experimentally observed fatigue behavior reported in [8] for Type BH-T
dents exhibiting Mode P behavior in 12″x1/4″ X60 pipe.

Initial d/D (%)	Final d/D (%)	Failure Mode	Cycles to Failure
5	4.41	Shallow Periph. Post-Proof	100,943
7.5	5.00	Shallow Periph. Post-Proof	100,943
10	5.42	Shallow Periph. Post-Proof	100,943
12.5	6.58	Peripheral Leak	89,684
15	7.75	Peripheral Leak	80,880

fatigue the deeper dent had the shorter life.

Tables III and V indicate that deeper dents within a failure mode appear experimentally to have shorter lives. This result was anticipated by the results of the two-dimensional equivalent load model reported in Chapter III. This model predicted that, at least in two dimensions, dent hoop SCF values increase linearly with dent depth. Thus, deeper dents, particularly deeper Mode C dents, are predicted to have shorter fatigue lives.

Data from [8] shown in Table IV indicates that dent depth may influence more than just stress magnitude. As discussed previously, the shallowest dents in Table IV appear to behave as Mode C dents while deeper dents appear to behave as Mode P dents. This fact appears to hold true for both Type A and Type BH indentors in the case of the 36″ pipe data set in [8]. Because only a very limited set of experimental evidence is available that exhibits this depth effect on dent mode type and because some questions surround the terminology used in [8] to report one of these failures, it makes sense to explore the problem further using the simple elastic finite element dent model.

Figure 65 shows SCF profiles obtained from models of a 18″x3/8″ pipe containing dents with $x_0 = 4$, $\phi_0 = \pi/24$, and increasing values of depth. The depth value ξ
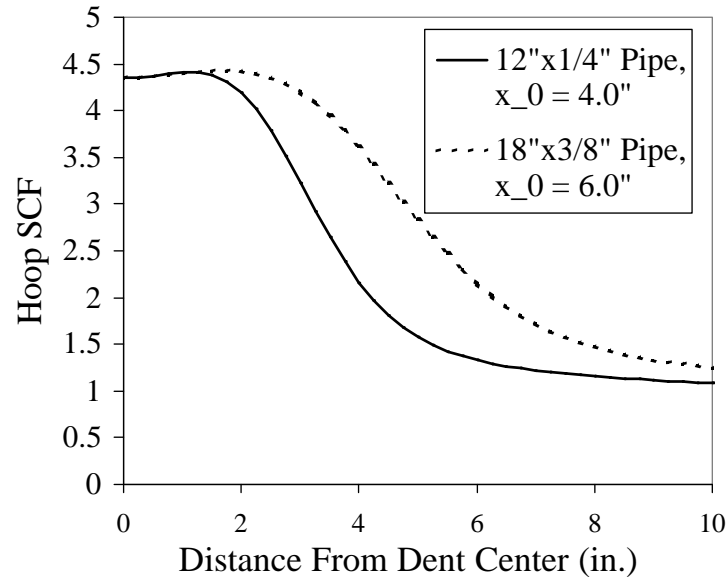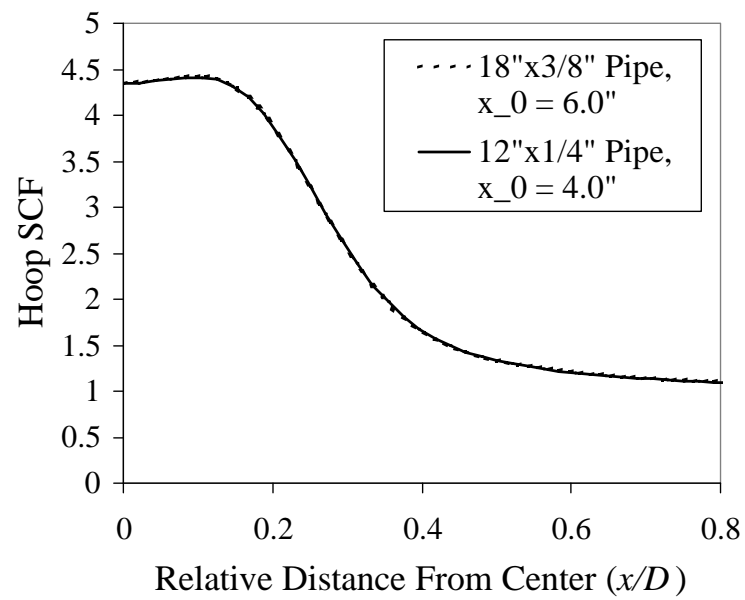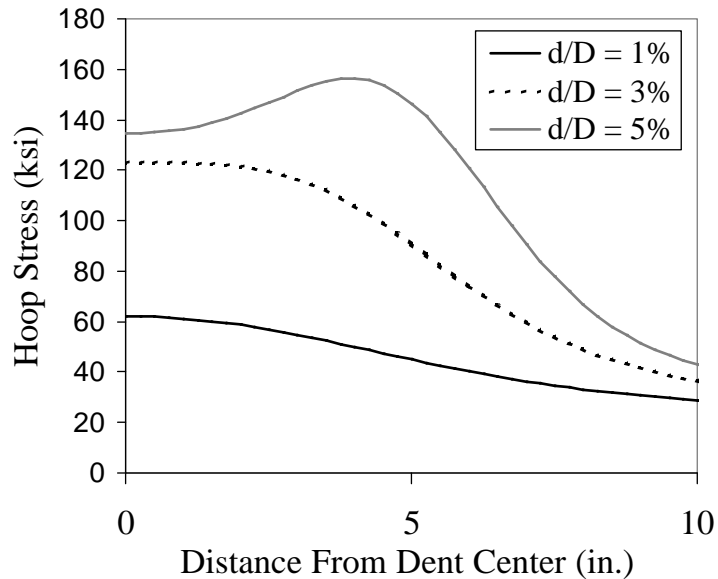
Fig. 65. Hoop stress concentration profiles calculated for 18″x3/8″ pipe containing dents with $\phi_0 = \pi/24$ and $x_0 = 4.0″$ and three increasing values of dent depth d/D.

is converted to a relative dent depth value d/D. In Fig. 65, a clear Mode C SCF profile is apparent for d/D values of 1% and 3%. In fact, the magnitude of the SCF increases with depth for these cases. This increase was as anticipated by the preceding consideration of experimental results [8], existing dent acceptance approaches, and the equivalent load approach discussed in Chapter 3. However, when d/D becomes 5%, the center SCF peak in Fig. 65 disappears and a peripheral peak feature typical of Mode P dents in Fig. 62 appears. Thus, at a fixed dent length, as dent depth increases, stress behavior shifts from Mode C center stress peak behavior to Mode P peripheral stress peak behavior. Limited experimental evidence introduced in Table IV indicates that this shift in stress behavior is accompanied by a shift in fatigue behavior.

The way in which the parameters of depth and length influence dent categoriza-

tion can be understood in terms of a simple hypothesis that has been presented in the past by Keating and Hoffmann [8] and by Rinehart and Keating [15]. Essentially, dent geometry differences can be viewed as leading to fundamentally different mechanical responses. Dents have two features that distinguish them from the surrounding pipe material. As shown in the overview of the equivalent load method presented in Chapter II, dents alter the geometry of the pipe's shell structure. These alterations perturb the normal stress flow in the shell. For example, bending moments may arise. At the same time, dents are also localized zones of reduced stiffness compared to the stiffness of the surrounding, undamaged pipe material. If the dent geometry is especially deep and abrupt the stiffness loss in the dent region becomes so large that membrane loads will begin to flow around the dent as seen in the tensile lattices that developed in Figs. 48 and 50 of Chapter IV. Intuitively, a round, short dent would be expected to begin to behave like a hole in a plate as its depth approached some large value.

This two-part view of dent mechanics means that dents that are fairly long compared to the pipe size and that are fairly shallow will act like structural imperfections, developing bending stresses in the center. These situations are Mode C situations. On the other hand, relatively localized, deep damage behaves like a lower stiffness inclusion in the pipe material and develops peripheral stress features. These situations result in Mode P behavior. The transition between these limiting situations does not appear to be abrupt.

This section has attempted to demonstrate several aspects of dent hoop stress concentration behavior using a simple elastic finite element model. Dent residual stress behavior, although important to understand the complete dent fatigue problem, was not explored. First, dent behavior can be better understood if it is categorized by length , as first suggested in [8]. Mode C dents have center cracking associated with center SCF peaks and Mode P dents have peripheral cracking associated with

peripheral SCF peaks. Other categories of dents may also exist. Dent categorization is geometry dependent. For a fixed depth of dent, dent behavior transitions from Mode P to Mode C as dent length increases. For categorization purposes, dent length should be measured relative to pipe diameter. For a fixed length dent, dent SCF behavior transitions from Mode C to Mode P as relative depth increases. Thus, in order to know whether a dent is Mode C or Mode P one needs to know both the dent length and the dent depth. This combined influence has not been remarked upon in the past by other investigators.

E.   A Simple Method for Distinguishing Mode C and P Dents

Mode C dents have much shorter fatigue lives than to Mode P dents [8]. Therefore a simple means of determining, before failure, whether a given dent in the field is Mode C or P would be of great practical value. It was established in the previous section that this determination depends on the relative length and depth of the dent. In fact, one could draw a map of dent behavior in terms of dent geometry, as illustrated in Fig. 66. The map shown in Fig. 66 only describes whether a given dent falls into Mode C or Mode P. No information is given regarding actual fatigue life, stress values, or relative differences between dents within a mode. However, earlier discussion has demonstrated that Mode C dents have much shorter fatigue lives than Mode P dents and should be considered a definite repair priority.

A preliminary check of the merit of this "dent mapping" approach is possible by referring to the experimental record. Figure 67 shows dent fatigue results taken from [8] and plotted in terms of relative dent length L/D and final relative dent depth d_f/D. The only aspect of dent fatigue plotted is whether a given dent falls into Mode C or Mode P. Mode C dents developed visible center fatigue cracking. Mode P
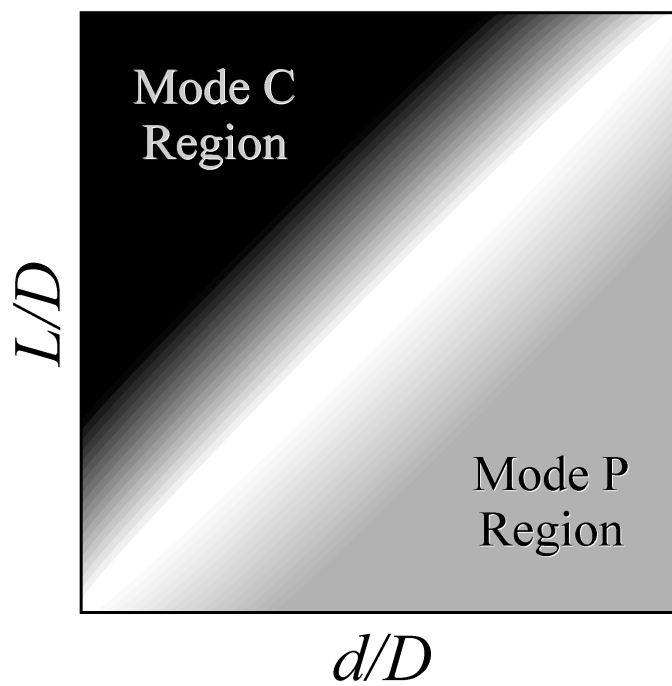
Fig. 66. Schematic representation of "map" used to distinguish Mode C and Mode P dents based on relative length L/D and relative depth d/D measurements of dents.
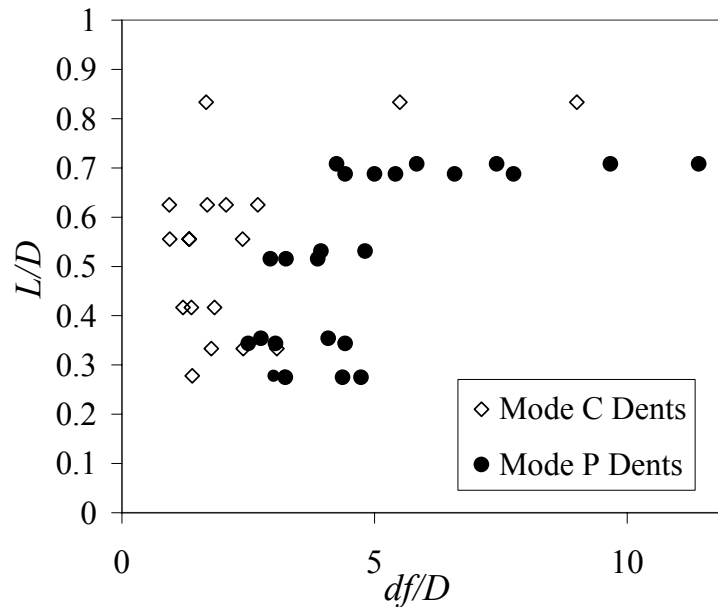
Fig. 67. Complete set of unrestrained dent data from [8] grouped into either Mode C or Mode P and plotted in terms of measured L/D and d_f/D values.

dents are all remaining unrestrained dents that either had visible peripheral cracking or no cracking at all. Dent depth is taken from records in [8] that contain values of dent depth at the dent center. For Mode C dents this value is probably not the deepest possible measurement that could be obtained from a rerounded dent given the local convexity resulting from high levels of rerounding associated with these dents. Length measurements were taken from several available dent specimens based on the definition illustrated in Fig. 61. Type A dents were roughly 10″ long, Type BH-T dents were roughly 8.25″ long, and Type BH-L dents were roughly 8.5″ long.

The data plotted in Fig. 67 is the complete set of unrestrained dent data in [8]. Possible effects of depth-to-diameter ratio, relative differences in width, and other variables are not taken into account in Fig. 67. However, for almost the entire data set, Mode C dents form a cluster in the left and upper-left region of the map while

Mode P dents cluster in the right and lower-right regions of the map. This clustering is similar to that predicted intuitively in Fig. 66

The existing experimental data set is limited. For example, only a limited range of dent lengths are considered and only two types of pressure histories were applied. In addition, it is not entirely clear how to move from Fig. 67 towards a reliable dent categorization approach. It would be worthwhile to develop an analytical means of determining dent type and to validate this approach with existing experimental data. A validated approach could then be used to develop assessment tools that are much broader in application than those permitted by relying only on existing test data.

The mode characterization analysis used here relies on elastic stress predictions developed using the simple elastic finite element model of a normal distribution type dent that was introduced earlier in this chapter. Earlier analysis showed that dents with clear peripheral elastic SCF peaks are Mode P dents while dents with a single central elastic SCF peak are Mode C dents. However, many dents fall into a transition region of behavior and have both noticeable peripheral peaks and significant central SCF values. These three types of SCF plots are shown, in normalized form, in Fig. 68. All three plots were taken from models of $16''$x$1/4''$ pipes containing dents with $d/D = 3.0\%$ and $\phi_0 = \pi/24$. For the Mode P, transitionary, and Mode C cases, x_0 values were 0.75, 2.5, and 4.5 respectively. Figure 68 raises the question of how one demarcates the boundary between Mode C and Mode P dents.

One approach to distinguishing Mode C and P dents is to determine the values of the outer surface elastic SCF profile at the dent center and at the peak peripheral value. A measure of the dent mode would then be the ratio of the center elastic SCF value and the peripheral elastic SCF value. For example, a low ratio indicates that the center elastic SCF is relatively low compared to the peripheral elastic SCF and that the dent is likely going to behave as a Mode P dent. Using the information
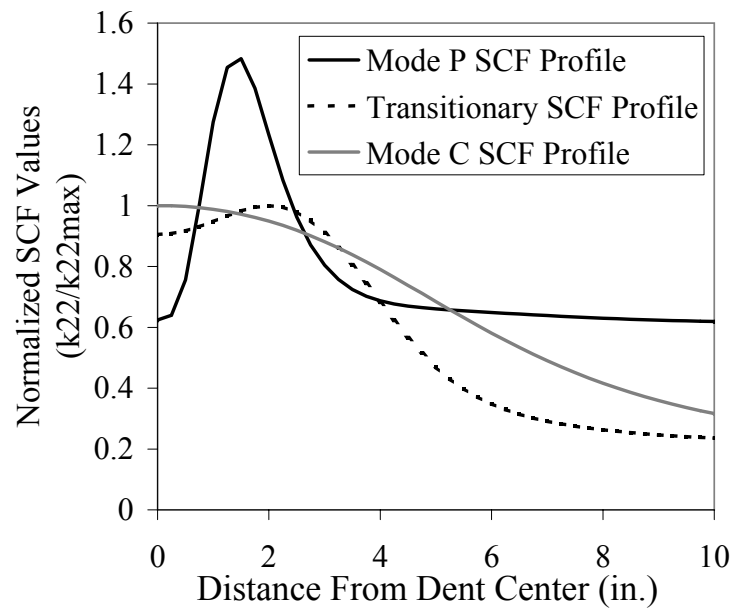
Fig. 68. Three normalized outer surface SCF profiles illustrating clear Mode C and P behavior and a typical transitional profile. Profiles are based on models of 16″x1/4″ pipes containing dents with $d/D = 3\%$, $\phi_0 = \pi/24$, and variable values of x_0.

generated by finite element models, ratio values can be easily calculated for a variety of different dent configurations. This ratio of center SCF to periphery SCF value is called the C-P ratio here.

For each fixed center/periphery SCF ratio value a curve can be drawn on the L/D-d/D map shown in Fig. 66. If a set of these curves is drawn for different constant values of the C-P ratio, a "topographic" type of plot would result. Such a map could provide a sophisticated understanding of the C-to-P transition zone and would provide insight into the mechanics of dents.

Given the fact that this study is in many ways a first attempt at understanding dent categorization and given the interest in practical dent assessment tools, a complete center/periphery SCF ratio topography is not developed here. Instead, only certain "elevations" on the dent topography map are sought. In particular, sets of ratios of center SCF to periphery SCF are evaluated in terms of their ability to distinguish Mode C and P behavior. A single ratio line on the L/D-d/D map that distinguishes dent mode is sought.

It is not entirely clear how to pick a single value of the ratio between the peak center SCF and peak peripheral SCF that can be used to distinguish Mode C and P dents. In reality, a range of these ratio values probably correspond to transitionary cases. A center/peripheral SCF ratio value of 1.0 might be used as an indicator. This value would select only situations without any peripheral stress features as Mode C. However, a Mode C dent is clearly more of a fatigue threat than a Mode P dent so it is important to pick a ratio value that is somewhat more conservative. A range of ratio values and their relation to experimental results are considered here.

A fixed value C-P ratio line is determined by using linear interpolation to analyze a matrix of SCF results obtained using finite element analysis. The SCF values are obtained here using the simple elastic finite element model to analyze a variety of

Table VI. Center SCF / Peripheral SCF values and corresponding C-P ratio values
predicted using elastic FEM model of normal distribution dent profiles for
indicated L_0 and d/D values in a $12''$x$1/4''$ pipe.

L_0	d/D (%)					
	1	2	3	4	5	7
0.5	31.00/31.37 =99.0%	27.29/38.16 =71.5%				
2.5			71.85/80.50 =89.2%	60.58/90.57 =66.9%		
4.0			104.3/105.8 =98.5%	103.9/119.9 =86.7%	96.66/133.1 =72.6%	
6.0				144.8/147.4 =98.2%	150.1/164.6 =91.2%	146.2/197.4 =74.1%

meshes generated using the normal distribution dent model. For example, Table VI shows center SCF, peripheral SCF, and C-P ratio results for a $12''$x$1/4''$ pipe containing dents with d/D values ranging from 1% to 7% and L_0 length parameters ranging from 0.5 to 7.0.

As apparent in Table VI, it is not possible to know the exact L_0 and d/D combinations that will lead to a given C-P ratio. It is possible, by varying parameters adequately, to bound the value that is being sought. To then determine the actual L_0 and d/D values that would result in a given C-P ratio value, linear interpolation is used. The L_0 value is typically held fixed and the slope of the C-P ratio is found in terms of the change in d/D. The d/D value that results in the desired C-P ratio value for a given L_0 is then found. Table VII illustrates this process for a C-P ratio of 75% based on the results shown in Table VI. An important feature apparent in Table VII is that the C-P value slope is not fixed and decreases with increasing L_0 values. In addition, it is not clear even for a given L_0 value that C-P ratios vary linearly with d/D. As a result, the use of linear interpolation is expected to only produce

Table VII. Illustration of method used to calculate dent geometries corresponding to C-P ratios of 75% using results of the type presented in Table VI for a 12″x1/4″ pipe.

L_0	d range	C-D slope	C-D start	Δd	$d_{75\%}$
0.5	$1\% \Rightarrow 2\%$	-27.5%	99%	0.873	1.873%
2.5	$3\% \Rightarrow 4\%$	-22.3%	89.2%	0.637	3.637%
4.0	$4\% \Rightarrow 5\%$	-14.1%	86.7%	0.830	4.830%
6.0	$5\% \Rightarrow 7\%$	-8.55%	91.2%	1.894	6.894%

an approximate 75% C-P curve. However, inaccuracies in this line seem likely to be reasonable given other uncertainties in the analysis.

Knowing L_0-d/D combinations at which the C-P ratio is a given value, a curve can be plotted and used to distinguish Mode C and P dents for the case in question. The plotted C-P curve is most useful if it is presented in terms of actual dent length L instead of L_0 and the 2.4477 L_0 to L conversion is used to affect this change. Figure 69 shows the resulting 90%, 75%, and 60% C-P curves on a C-P map. The curve is fairly linear and does not cross through the origin.

It was suggested in Fig. 66 that a type of map could be developed that would classify dents in terms of Mode C or P behavior based on relative dent length, L/D, and depth, d/D, measurements. Figure 67 demonstrated that experimental data from [8] does indeed seem to fall into the sort of layout suggested in Fig. 66. Next, a predictive method for developing criteria for distinguishing Mode C and P dents was introduced and used to develop a line, shown in Fig. 69, that divides the C-P map into Mode C and P regions. The next issue is whether or not the predictive approach successfully predicts experimental results.
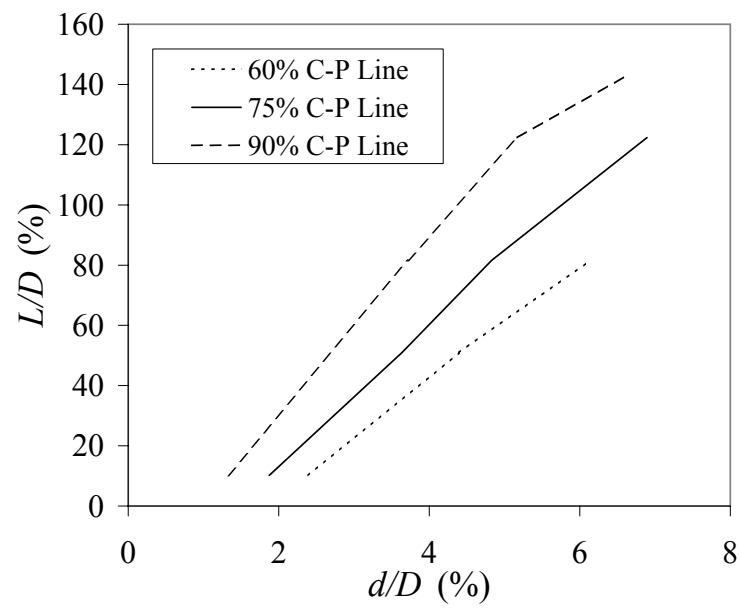
Fig. 69. C-P map showing 90&, 75%, and 60% C-P curves plotted in terms of actual dent length and dent depth ratios L/D and d/D generated from finite element results interpolated in Table VII for a $12''$x1-4$''$ pipe.

Table VIII. List of pipe diameters and thicknesses along with corresponding D/t ratios for pipes studied experimentally in [8].

D (in.)	t (in.)	D/t
12″	3/8″	32
12″	1/4″	48
16″	1/4″	64
18″	1/4″	72
24″	1/4″	96
30″	3/8″	80
36″	3/8″	96

Dent fatigue failure data is available in [8] for seven pipe situations. These seven situations and the corresponding diameter-to-thickness, D/t, ratios are listed in Table VIII. Typically both Type A and either Type BH-T or BH-L indenters were used in each pipe type. Dents that developed center cracks are considered Mode C dents and all other unrestrained dents that either developed peripheral cracks or no cracks at all are considered Mode P dents. Because dents with no cracks do not possess clear peripheral cracks there is some question about assuming they fall into Mode P. However, the relatively short life of typical Mode C dents suggests that, in the typical case, a dent that did not develop a center crack in 100,000 cycles is a longer-lived Mode P dent. One might question whether the lack of peripheral cracking is an indication of a third dent type. It is believed here that the consistently narrow width of all dents in [8] means that non-Mode C dents are very likely all members of Mode P.

Parametric studies of each of the seven pipe situations listed in Table VIII were
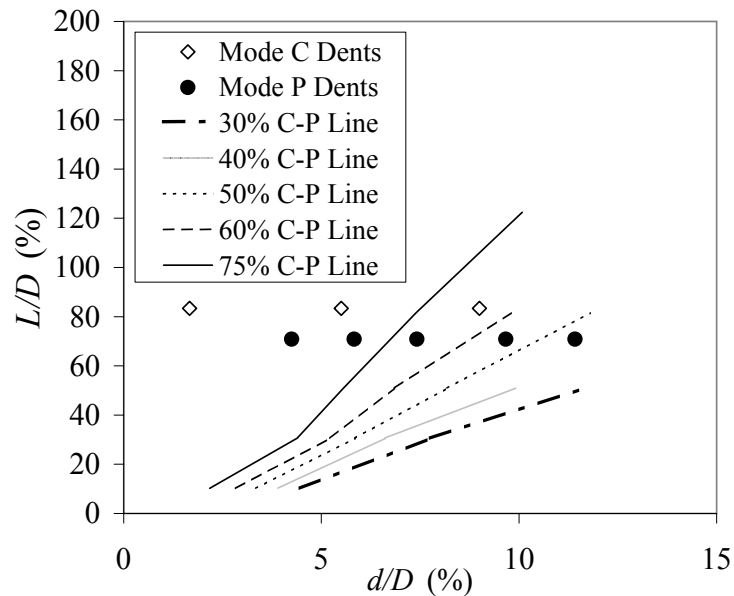
Fig. 70. C-P map showing test results from [8] by failure mode for 12″, 3/8″ ($D/t=32$)
X60 pipe with a low-high pressure history and corresponding 75%, 50%, 40%,
and 30% C-P curves generated with interpolated finite element results.

carried out. As described above and as illustrated in Tables VI and VII, the results
of these studies were used to calculate the location of the C-P lines of several fixed
values on the C-P map for each pipe case. The resulting C-P lines are plotted along
with the appropriate experimental data in Figs. 70 through 76. The C-P ratio curves
shown in Figs. 70 through 76 are D/t case specific.

It is important to remember that the lines and points in Figs. 70 through 76
should not be viewed as curve fits. Rather, the correct C-P line should divide the
Mode C data points, shown as open diamonds, from the Mode P data points, shown
as solid circles. If the C-P line correctly distinguishes the experimental data points
by type, then it would seem to offer an accurate prediction of dent type for the given
situation.

Figures 70 through 76 indicate C-P lines that are successful indicators of dent
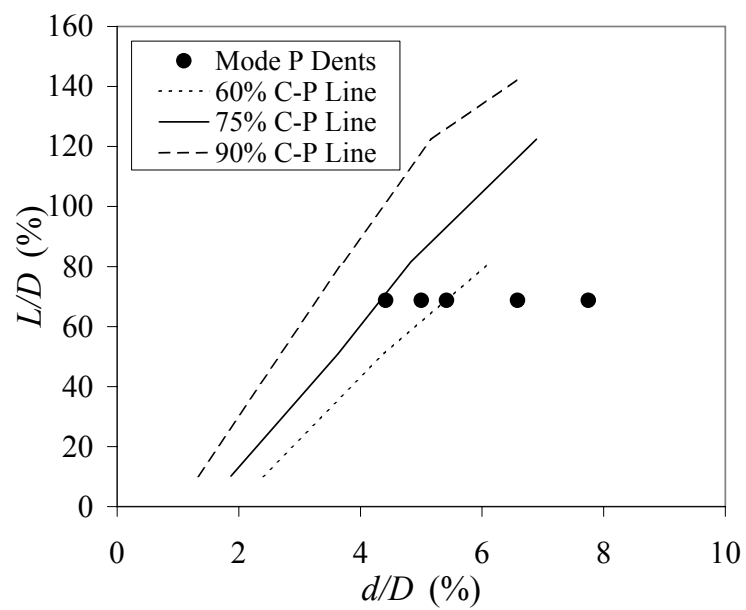
Fig. 71. C-P map showing test results from [8] by failure mode for 12″, 1/4″ (D/t=48) X42 pipe with a low-high pressure history and corresponding 90%, 75%, and 60% C-P curves generated with interpolated finite element results.

Fig. 72. C-P map showing test results from [8] by failure mode for 16″, 1/4″ (D/t=64) and corresponding 90%, 75%, and 60% C-P curves generated with interpolated finite element results. Mode C dents were in a X60 pipe with a low-high pressure history and Mode P dents were in X42 pipe with a high-low pressure history.
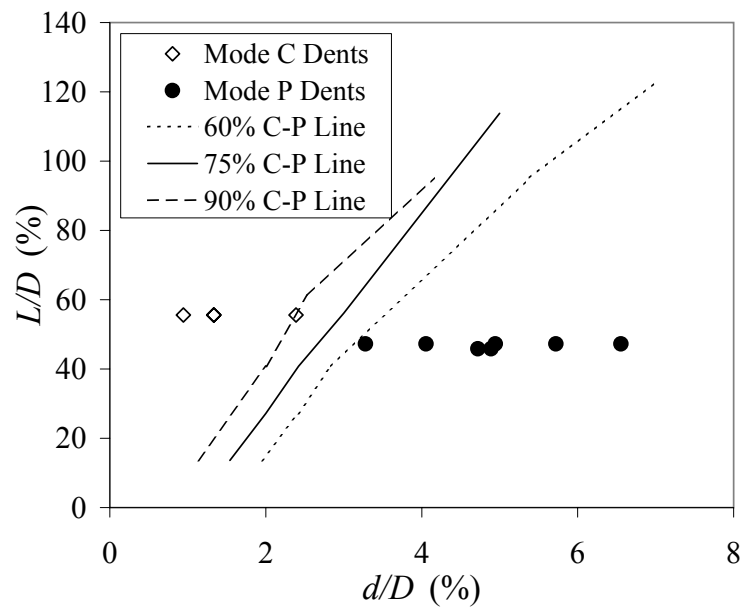
Fig. 73. C-P map showing test results from [8] by failure mode for 18″, 1/4″ (D/t=72) and corresponding 90%, 75%, and 60% C-P curves generated with interpolated finite element results. Mode C dents were in a X42 pipe subjected to a high-low pressure history and Mode P dents were in either X42 or X60 pipes with low-high pressure histories.
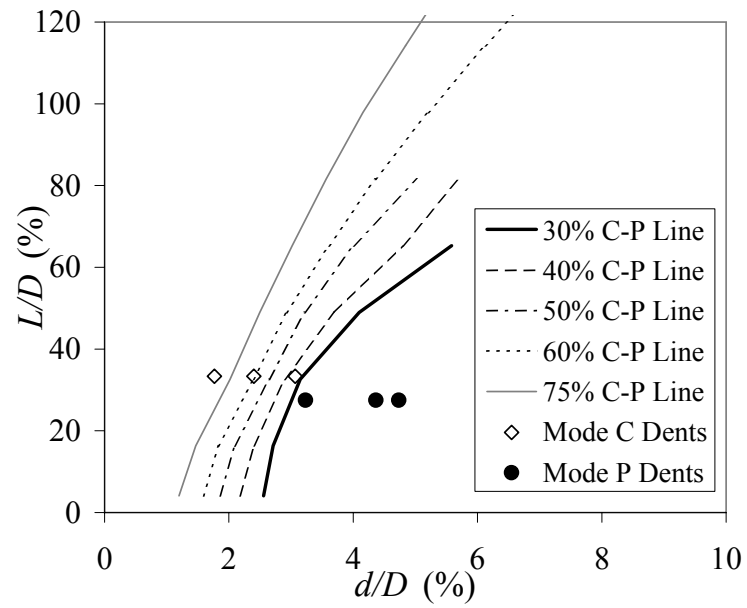
Fig. 74. C-P map showing test results from [8] by failure mode for 30″, 3/8″ (D/t=80) and corresponding 75%, 60%, 50%, 40%, and 30% C-P curves generated with interpolated finite element results. All dents were in Gr. B pipes with high-low pressure histories.
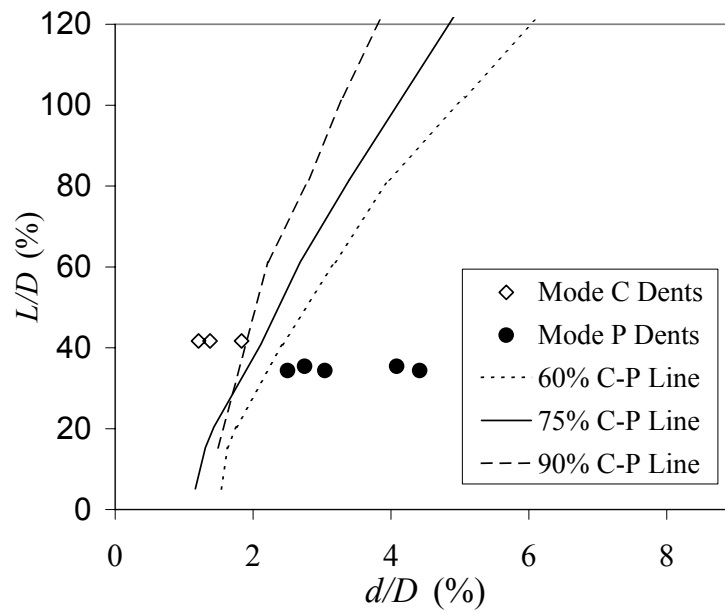
Fig. 75. C-P map showing test results from [8] by failure mode for 24″, 1/4″ (D/t=96) and corresponding 90%, 75%, and 60% C-P curves generated with interpolated finite element results. All dents were in X60 pipes with high-low pressure histories.
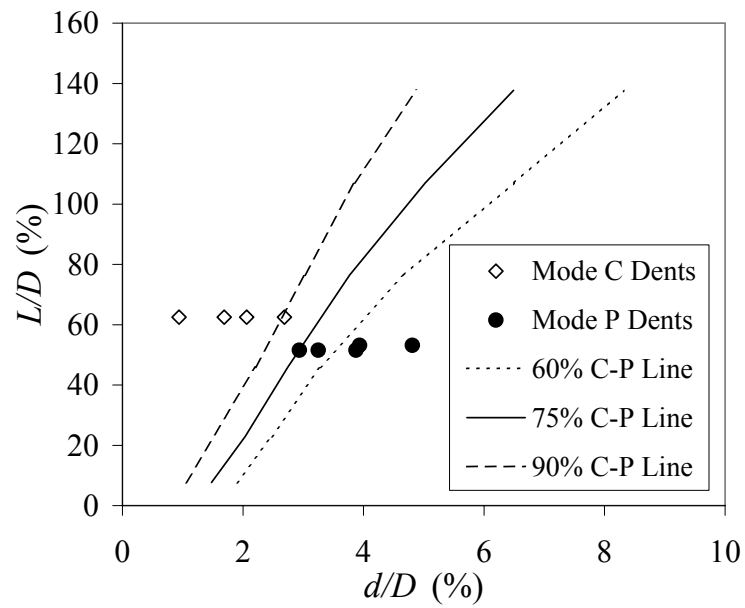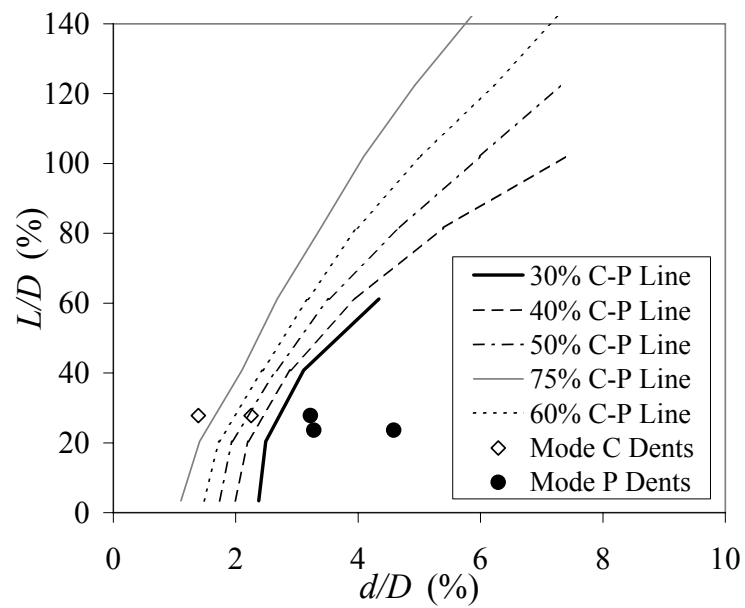
Fig. 76. C-P map showing test results from [8] by failure mode for 36″, 3/8″ (D/t=96) and corresponding 75%, 60%, 50%, 40%, and 30% C-P curves generated with interpolated finite element results. All dents were in Gr. B pipes with high-low pressure histories.

type for each pipe case studied in [8] except for the 12″ by 3/8″ situation. In fact, the 75% C-P line successfully distinguishes Mode C and P dents in every case where the pipe wall thickness was 1/4″, as seen in Figs. 71, 72, 73, and 75.

In three instances, the 75% C-P curve is not successful. These situations are the 12″″ by 3/8″, 30″ by 3/8″, and 36″ by 3/8″ cases. It is important to establish what distinguishes these cases from the 1/4″ cases. While these three cases all have a common thickness of 3/8″ other reasons for the lack of success of the 75% C-P line in these instances must be explored for the sake of completeness.

The three situations where the 75% C-P line fails to distinguish dent type occur at edges of the diameter-to-thickness spectrum for which test data is available in [8]. One possible source of this failure is that the 75% C-P line has a limited range of application in terms of D/t values. However, this idea is questionable when it is noted that the 75% C-P curve works for one case where $D/t = 96$, namely the 24″ by 1/4″ case, but not another, namely the 36″ by 3/8″ case. These contrasting mode predictions are seen in comparing Figs. 74 and 75. Because the $D/t = 96$ situation is the extreme D/t situation for which data is available and because the 75% C-P line succeeds in one instance of this case, it appears that the method has not necessarily reached an upper D/t limit.

The contrasting mode predictions for the $D/t = 96$ cases are interesting when it is seen that C-P curves are identical for a given D/t value. Figure 77 plots the 75% C-P curves calculated for the 24″, 3/8″ and the 36″, 3/8″ cases shown in Figs. 75 and 76 respectively. Whatever small deviations that are present between the two C-P curves in Fig. 77 are presumably due to errors introduced by the interpolation process. Thus, for the two cases in question, the C-P curve is the same but the outcome of the dent mode prediction is quite different. As a result, it seems difficult to attribute the failure of the 75% C-P curves in Figs. 70, 74, and 76 to a limitation in terms of
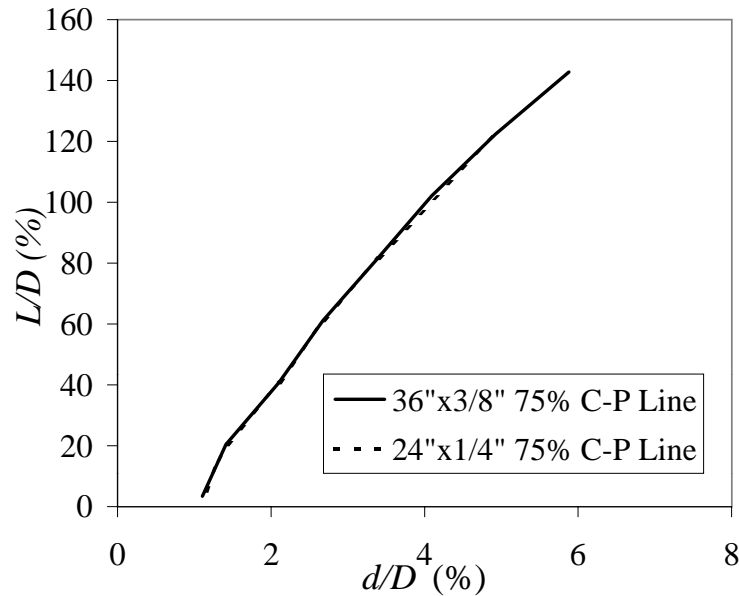
Fig. 77. 75% C-P curves predicted for $24''$ by $1/4''$ and $36''$ by $3/8''$ pipes ($D/t = 96$).

the $D - t$ spectrum.

The possibility also exists that the problems evident in Figs. 70, 74, and 76 stem from differences in steel type or pressure history. These factors are reported in the captions to Figs. 70 through 76. With regard to pressure history effects, cases can be found in which the 75% C-P line both fails and succeeds for instances of low-high and high-low pressure histories. With regard to steel type X60 and X42 steels are found in situations where the 75% C-P fails and succeeds. Grade B steel does appear only where the 75% C-P curve fails to predict behavior. Uniaxial tension test results are presented in [8] for many of the pipe specimens. The Gr. B stress-strain curve available for the $30''$ pipe doesn't differ significantly from those shown for other X42 pipes. The Gr. B stress-strain curve for the $36''$ pipe indicates much lower yield and ultimate strengths, both being around 30 ksi, compared to the 40 ksi and 60 ksi values for other Gr. B and X42 specimens. However, the lack of predictive success of

the 75% C-P line shown in Fig. 76 for the 36″ pipe with this lower yield steel is not markedly different from that shown in Fig. 74. As a result, it is not believed that the relative success or failure of the 75% C-P curve can be attributed to steel type.

Having considered other explanations, the fact remains that the 75% C-P curve fails to predict experimentally observed dent type for all 3/8″ wall thickness cases but succeeds for all 1/4″ wall thickness cases. This result suggests that the failure mode of dents is dependent not only on D/t but also on wall thickness. Having considered other sources of difference it appears that pipes with 3/8″ thick walls should be approached with a different C-P curve.

Examination of the 3/8″ cases in Figs. 70, 74, and 76 suggests that the 30% C-P line appears to successfully anticipate dent mode for the large diameter 3/8″ cases. In the 12″ case, Fig. 70, it would seem that no C-P line successfully predicts dent type. Two possibilities exist for this lack of success . First, all experimental data deemed to be Mode P was so classified due to the fact that these dents developed no visible cracking. This assumption was used for all cases studied here and seemed to result in good C-P mode predictions. However, if one were to exclude all data where no cracking occurred in the 12″, 3-8″ case then the 30% C-P line would successfully divide the remaining data. Another possibility is that for the low D/t ratio in question the C-P line categorization approach breaks down, perhaps because shell behavior begins to move away from the thin-shell regime. This matter cannot be resolved without more experimental data or a more thorough examination of the problem.

Finally, it has only been noted that the C-P transition occurs at different ratio values for different pipe wall thicknesses. It has been established that outer surface residual stress resulting from the indentation and rerounding process has a significant influence on dent fatigue behavior [21]. This result was discussed in Chapter II. It seems possible that wall thickness effects on outer surface residual stress
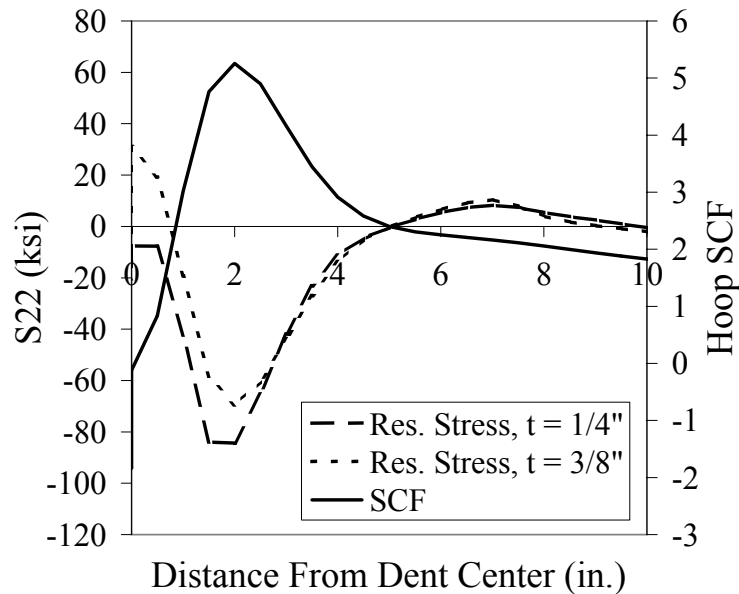
Fig. 78. SCF and residual hoop stress profiles predicted using complete finite element model for 18″ X60 pipes with 1/4″ and 3/8″ wall thicknesses indented with 1″ long, 1″ wide indentor.

magnitude could lead to the thickness dependent shift in the C-P curve value that distinguishes Mode C and P dents. Using a full life-cycle finite element model that considers indentation, inelastic rerounding, and elastic post-rerounding dent behavior, the residual stress profile of dents can be determined. This model has been discussed elsewhere [8, 15, 21, 22, 16].

Figures 78 and 79 show SCF and residual stress profiles predicted using the full finite element model for 18″ pipes composed of X60 steel. Indentors were 1″ wide, had round ends, and were 1″ long in Fig. 78 and 3″ long in Fig. 79. Residual stress profiles predicted for two wall thicknesses of 1/4″ and 3/8″ are shown. Both length cases are essentially Mode P cases with clear peripheral SCF features. The SCF profile can thus be used to determine which portion of the residual stress profile occurs in the dent center region.
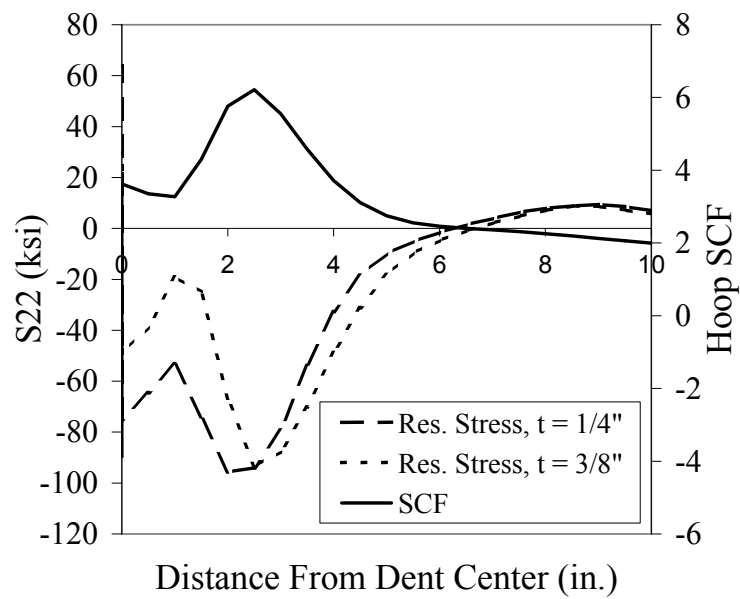
Fig. 79. SCF and residual hoop stress profiles predicted using complete finite element model for 18″ X60 pipes with 1/4″ and 3/8″ wall thicknesses indented with 3″ long, 1″ wide indentor.

It was noted previously that a center-peripheral SCF ratio of 75% marks the transition from center to peripheral cracking for $1/4''$ pipes while this ratio is only 30% for $3/8''$ pipes. In both cases, the center SCF value is less than the peripheral SCF value and the profile resembles those shown in Figs. 78 and 79. For the two thickness cases it takes relatively more center stress to shift the likely crack location to the dent center in the $1/4''$ case. Thus, some mechanism inhibits center crack growth in $1/4''$ pipes compared to $3/8''$ pipes. It can be seen in Figs. 78 and 79 that dent center residual stress is relatively more compressive for the $1/4''$ pipe wall case. In general, a situation with relatively higher compressive residual stress will tend to have less of a tendency to develop fatigue cracks. Thus, it would seem that thickness dependent residual stress differences in the dent center account for the thickness effect on the value of the transition C-P ratio.

F.   A Simple Dent Type Assessment Procedure

In the previous section it was shown that in almost all cases where experimental data is available a constant value C-P line can be selected that successfully distinguishes dangerous Mode C dents from less dangerous Mode P dents. This constant value C-P line represents dents with combinations of relative depth, d/D, and length, L/D, that result in a constant ratio of center and periphery SCF peak values. Furthermore, all dents in pipes with $1/4''$ walls can be distinguished using 75% C-P lines while those in large diameter $3/8''$ thick pipes can be distinguished using 30% C-P lines. It would be useful to develop a procedure based on this result that can be easily applied to distinguish dents.

The first matter of an assessment procedure is that of which dent parameters need to be obtained. The depth measurement used in the previous section corresponded

to the depth at the dent center relative to the undamaged pipe circumference as reported in [8]. This depth value is not believed to be the depth to the deepest portion of the dent. In many cases, rerounding results in a bulge in the dent center and since depths reported in [8] are given as "Rebound Dent Depth" it is believed that the depth recorded was that of the dent center. In fact, this measurement of dent depth will tend to favor Mode C classification. This classification tendency would be conservative, as Mode C dents are believed to pose the greatest threat to pipeline integrity due to their low fatigue lives [8]. Dent length is defined as shown in Fig. 61 as the distance between the closest undamaged portion of the longitudinal dent profile. In making this measurement it is conservative to overestimate length. Dent width seems to play a role in determining dent fatigue behavior. However, this role remains to be addressed. Thus, the results obtained here are limited to dents with angular extents of approximately $\pi/12$ or less. In addition, results are calibrated to dents that have already undergone rerounding. Thus, the behavior of dents that have not experienced a typical in-service pressure environment for at least a few cycles cannot be judged using the 30% and 75% C-P curves suggested here. A dent would have to be found at the time of indentation for this condition not to apply and so this circumstance is considered a special case.

Given dent measurements, one must determine dent mode. One approach would be to use an appropriate C-P diagram and determine the location in question based on measured geometry. Then, one could see whether the geometry combination is above or below the C-P transition line appropriate for the pipe thickness in question. For example, consider a 12″ long, 0.25″ deep narrow dent found in an 18″ by 1/4″ pipe. In this case, $L/D = 66.6\%$ and $d/D = 1.39\%$. When this point is found on the appropriate C-P map, as shown in Fig. 80, it appears that the dent in question is a Mode C dent and is likely to have a relatively short fatigue life.
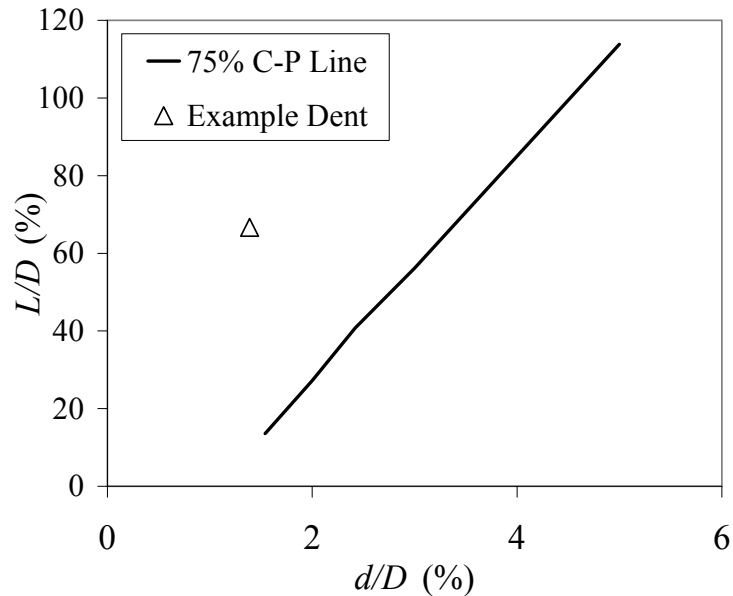
Fig. 80. Example of application of use of C-P curve for dent mode assessment.

In fact, a set of C-P curves appropriate to various pipe situations can be assembled on the same C-P map. Compiled C-P maps with curves validated in this study are shown in Figs. 81 and 82 for the cases of $1/4''$ and $3/8''$ walls, respectively. One could measure a dent and find its location on the appropriate chart. By determining the dent location relative to the diameter specific C-P line one could assess whether a given dent is Mode C or Mode P.

The 75% C-P curves in Fig. 81 appear to be roughly the same general shape, as do the 30% C-P curves in Fig. 82. These curves seem to vary mainly due to changes in pipe diameter D or diameter-to-thickness ratio D/t. These features and the fact that the important judgement is whether the dent geometry combination falls above or below the C-P line suggest that the curves might be combined into a more compact dent type assessment approach.

In the case of $1/4''$ thick pipes, the 75% C-P curves appear to be roughly linear
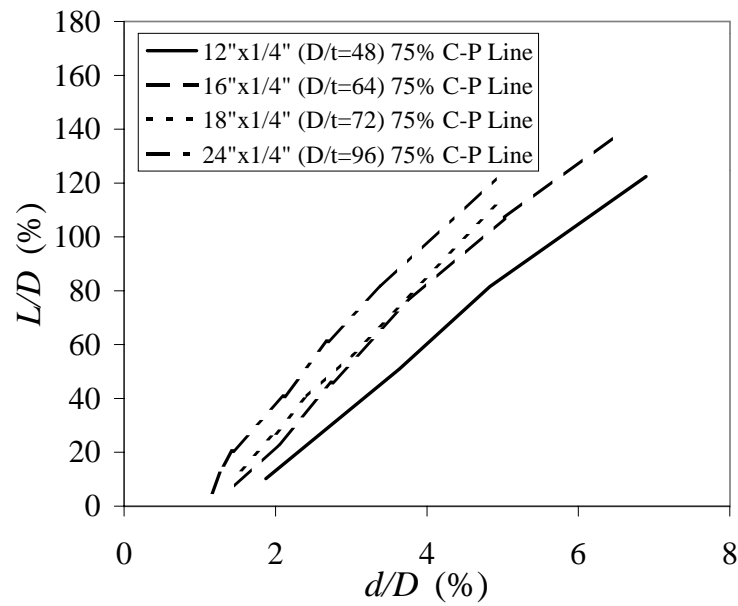
Fig. 81. Set of 75% C-P curves for all 1/4″ thick pipe cases studied here and found to be successfully characterized.
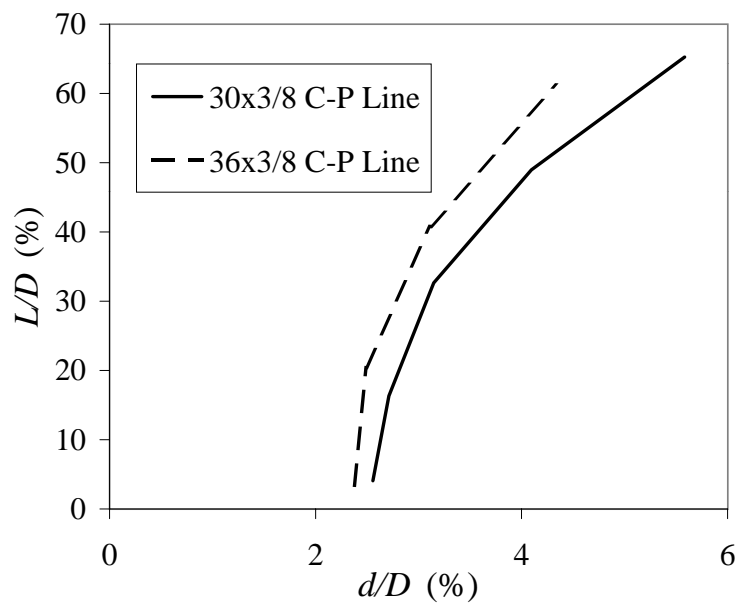
Fig. 82. Set of 30% C-P curves for all 3/8″ thick pipe cases studied here and found to be successfully characterized.

Table IX. Linear regression analysis results for C_1, C_2, and the R coefficient values for 12″, 18″, and 24″ 75% C-P curves in Fig. 81.

Diameter	D/t	C_1	C_2	R Coefficient
12″	48	-30.57	22.48	0.9986
18″	72	-28.29	30.26	0.9997
24″	96	-24.771	30.54	0.9967

and might be fit with two D/t dependent parameters, C_1 and C_2, and the simple function:

$$\left(\frac{L}{D} \right|_{75\%} = C_1 \left(D/t \right) + C_2 \left(D/t \right) \left(\frac{d}{D} \right|_{75\%} \tag{5.4}$$

Linear regression analysis of the curves shown in Fig. 81 is used to find the values of C_1 and C_2 for the diameter cases of 12″, 18″, and 24″. The results appear in Table IX

The coefficient C_1 is assumed to depend on D/t and a second linear regression establishes that:

$$C_1 \approx -36.58 + 0.1208 \frac{D}{t} \tag{5.5}$$

Thus, the relationship in Eq. 5.4 can be specified as:

$$\left(\frac{L}{D} \right|_{75\%} = -36.58 + 0.1208 \frac{D}{t} + C_2 \left(D/t \right) \left(\frac{d}{D} \right|_{75\%} \tag{5.6}$$

This expression can be rearranged so that the 75% C-P line can be specified as the D/t dependent ratio:

$$C_2^{75\%} = \frac{1}{(d/D|_{75\%}} \left((L/D|_{75\%} + 36.58 - 0.1208 \frac{D}{t} \right) \tag{5.7}$$

In Eq. 5.7 the values $(L/D|_{75\%}$ and $(d/D|_{75\%}$ describe the location of the 75% C-P line. The 75% C-P line has been reduced to the ratio value C_2. Values of C_2 were found previously for certain cases and are listed in Table IX for some D/t values

of interest. For an actual dent in a pipe the pair of L/D and d/D dent geometry measurements and the D/t value may be used to calculate the dent specific value of C_2^{dent}:

$$C_2^{dent} = \frac{1}{(d/D|_{dent}} \left((L/D|_{dent} + 36.58 - 0.1208 \frac{D}{t} \right) \qquad (5.8)$$

Knowing C_2^{dent} and $C_2^{75\%}$ the mode of the dent may be determined. Where the dent C_2 value is larger than $C_2^{75\%}$ the dent is Mode C and where it is smaller the dent is Mode P. Thus, a plot of $C_2^{75\%}$ in terms of D/t becomes a master curve by which dents in all $1/4''$ pipes may be categorized as type C or P.

Figure 83 illustrates the application of this master curve approach. The C_2^{dent} value is determined and plotted in terms of D/t for all available experimental cases in $1/4''$ pipes in [8]. The $C_2^{75\%}$ categorization curve is also plotted so that its ability to distinguish dent type may be assessed. It is seen in Fig. 83 that the compact C_2 ratio approach is reasonably successful at determining dent mode. In one or two cases Mode P data crosses the 75% line. However, this mis-characterization is conservative as it appears to favor classifying dents as more dangerous Mode C dents.

A similar analysis may be performed for the 30% C-P curves appropriate for assessing dents in $3/8''$ pipes. As seen in Fig. 82, these curves can probably not be modelled as straight lines. Instead a parabola with the following form is fit to the C-P curve data:

$$\left(\frac{d}{D} \bigg|_{30\%} = C_1 \left(D/t \right) + C_2 \left(D/t \right) \left(\left(\frac{L}{D} \bigg|_{30\%} \right)^2 \right) \qquad (5.9)$$

Values of C_1 and C_2 are found by fitting Eq. 5.9 to the 30% C-P curves in Fig. 82. Only two cases are available where the 30% C-P curve is known to work. Thus, C_1 and C_2 values are given on a case by case basis and a empirical version of C_1 is not determined. Table X contains $C_1^{30\%}$ and $C_2^{30\%}$ values found to describe the 30% C-P curves in Fig. 82
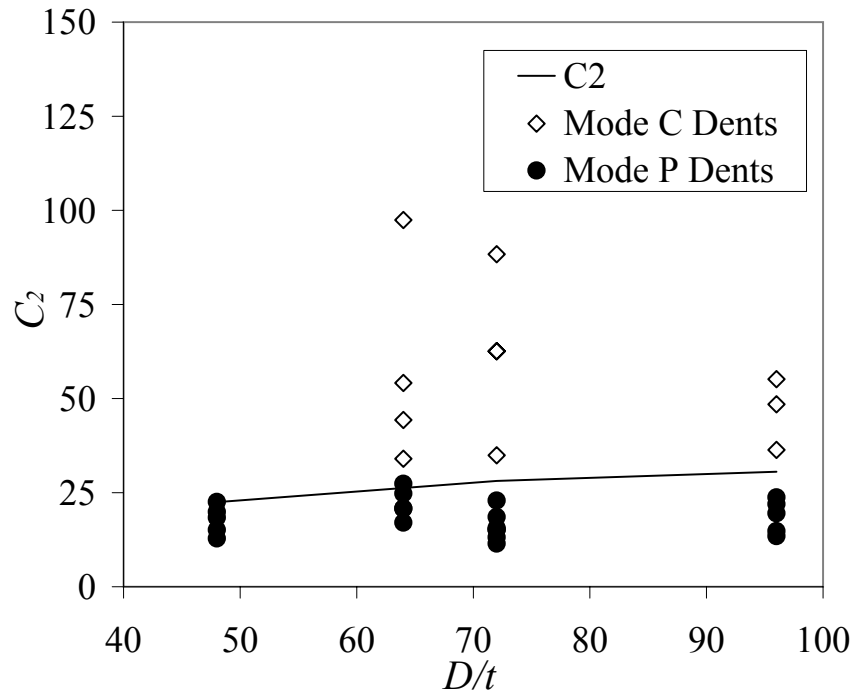
Fig. 83. Complete set of C_2 values of dents in $1/4''$ pipe studied by [8] plotted along with $C_2^{75\%}$ characterization curve.

Table X. Curve fit results for $C_1^{30\%}$ and $C_2^{30\%}$ values for $30''$, and $36''$ 30% C-P curves in Fig. 82.

Diameter	D/t	C_1	C_2
$30''$	80	2.49	0.000711
$36''$	96	2.258	0.000543
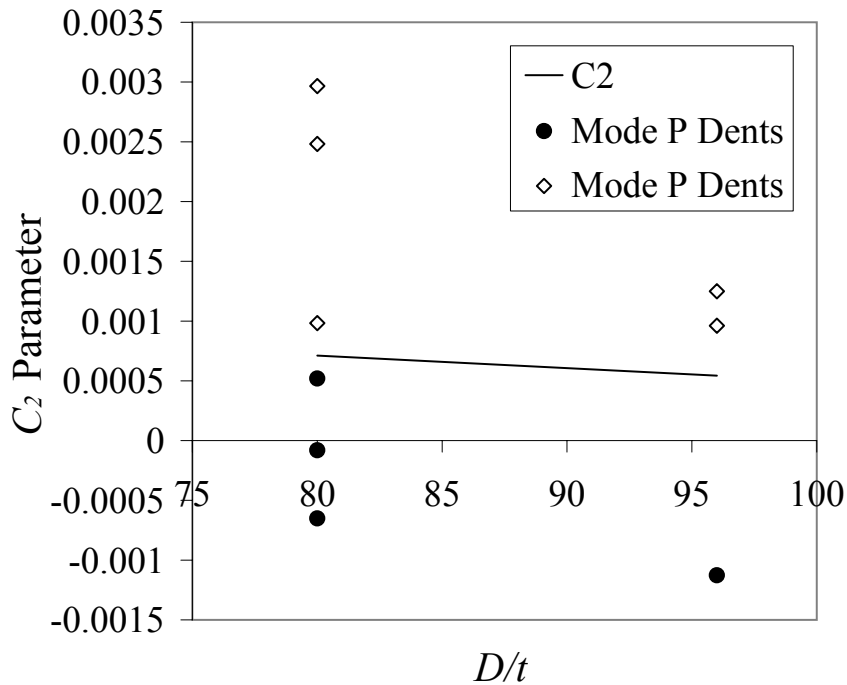
Fig. 84. Complete set of C_2 values of dents in $3/8''$ pipe studied by [8] plotted along with $C_2^{30\%}$ characterization curve.

Using the C_1 and C_2 values in Table X to describe the 30% C-P curve, dent mode may be assessed. Dent measurements are converted to C_2 values with the expression:

$$C_2^{dent} = \frac{\frac{d}{D} - C_1}{\left(\frac{L}{D}\right)^2} \tag{5.10}$$

Instead of using an empirical expression giving C_1 in terms of D/t, as was done in the $1/4''$ case, C_1 is found in Table X. As before, the dent C_2^{dent} value is compared to the $C_2^{30\%}$ value. If it is larger, then the dent is a Mode C dent. If it is smaller, then the dent is a Mode P dent. Figure 84 shows C_2^{dent} values for data taken from [8] plotted along with the predicted $C_2^{30\%}$ curve. This unified approach to dent acceptance again appears to give reasonable assessments of dent mode.

It was shown in Chapter IV that dent stress behavior undergoes a fundamental

shift as dents become deeper or more localized. This result was anticipated by earlier dent fatigue research [14, 8, 15, 16]. This shift in dent stress behavior is linked to a shift in dent fatigue performance. In particular, dents with center stress features have much shorter fatigue lives. Thus, there is practical value to understanding and being able to predict the size effect on dent stress behavior.

In the present chapter, it was assumed that the change in dent stress profile shape that accompanies a change in dent geometry could be studied with an elastic approach. A simple finite element model was used to explore how geometry changes influence dent stress behavior. A simple parametric model of dent geometry was introduced that is based on the normal distribution. Using this model, it was shown that the dent hoop stress profile changes shape across some range of dent depths and dent lengths. It was shown that the size of a dent relative to pipe diameter is what really determines the nature of the dent geometry effect.

A simple method for classifying actual dents as low-life, center-cracking or long-life, peripheral cracking dents was developed. This method is based on the ratio, called the C-P ratio, of the center stress value to the peripheral stress value predicted by a finite element model. By considering a wide range of dent parameters, curves with constant C-P ratio values may be calculated in the two-dimensional range of dent L/D and d/D values. Experimental data plotted on this L/D-d/D map shows that C-P curves with ratios of 75% and 30% correctly distinguish dents in $1/4''$ and $3/8''$ thick pipes, respectively. The set of C-P curves needed to distinguish dents in a range of pipe situations may be reduced to a single, thickness-specific master curve that varies with D/t. Using this curve, it appears that an accurate assessment of the approximate threat to pipeline integrity posed by a given dent may be made.

CHAPTER VI

CONCLUSIONS

A. Significant Findings

The preceding chapters have explored aspects of the behavior of dent imperfections in cylindrical shells. This problem has practical value, as discussed in Chapter II, in leading to a better understanding of an important mode of pipeline failure, namely the fatigue fracture of pipeline dents. In addition, the general mechanics of the behavior of shells with imperfections is fairly underdeveloped. As a result, any incremental improvement in the understanding of shell imperfections contributes to present overall understanding of shell behavior.

Because stress behavior, in large part, drives fatigue behavior, two main aspects of the relationship between dent geometry and dent fatigue behavior have been explored. First, semi-analytical solutions have been sought that describe the magnitude of elastic stress features of dents in terms of dent geometry features. Second, an attempt has been made to quantify the boundaries of two geometry-dependent categories of dent stress behavior. During this investigation, a previously unknown limit on an approximate method of shell imperfection analysis, the Equivalent Load Method, has been found.

A semi-analytical solution that predicts the stress concentration profile around a two-dimensional dented cylinder in terms of geometry values was found. This solution was formulated using a classical Fourier Series based approach to shell analysis and the Equivalent Load Method, an approximate method of shell imperfection analysis. The circumferential stress concentration profile of two-dimensional dents has two peaks, one at the center of the dent and one at the dent periphery. The solution was

calibrated so as to accurately predict dent center stress concentration values. Predictions of peripheral SCF peak values, while not strictly accurate, provide qualitative insight into behavior in this region.

The two-dimensional SCF solution contributes several specific results to current understanding of the behavior of two-dimensional shell imperfections:

- Stress concentration magnitude is linearly related to relative imperfection depth, d/D.

- Cylinder diameter-to-thickness ratio influences stress concentration value. This influence is linear.

- As implied by the experimental record [8, 9], dent width has a significant effect on the dent stress concentration profile. In particular, wider dents have lower dent center stress concentrations. At the same time, the peripheral dent stress concentration appears to be relatively uninfluenced by dent width.

The results obtained from the two-dimensional model are based on analysis of a single concavity in a two–dimensional cylindrical cross-section. However, these results provide insight about the behavior of a broader class of situations. First, the semi-analytical dent solution is based on Fourier Series representations of imperfection profiles. Thus, the solution could apparently be expanded to consider a wide range of two-dimensional imperfection geometries. In addition, defect depth is uncoupled from defect profile shape in the analysis. Thus, it follows that, in two-dimensions, stress concentration magnitude is always linearly related to imperfection depth. Second, the two-dimensional solution provides insight about three-dimensional problems where dent length is relatively long. In particular, the two-dimensional solution emphasizes the importance in three-dimensional dent behavior of two often overlooked parameters, dent width and pipe diameter-to-thickness ratio.

The equivalent load method was found to be unsuitable for studying relatively local and/or deep imperfections. Some equivalent load authors [46, 44, 43] have noted that the equivalent load method performs poorly in analyzing deeper imperfections. However, this reported shortcoming appears to be primarily an accuracy problem. In fact, as imperfections become more localized and deeper their stress behavior undergoes a fundamental change in distribution profile shape. It was demonstrated in Chapter IV that this change is not predicted by the equivalent load method. As a result, the general applicability of the equivalent load method as an analysis tool for three-dimensional shell imperfections becomes questionable.

It had been previously noted in the pipeline dent literature [14, 8, 15, 16] that longer imperfections develop stress concentrations in the center while shorter imperfections develop them at the dent periphery. This shift in stress behavior is of great practical importance because it is associated with a shift in fatigue performance from short life to long life. In Chapter IV this length effect on dent stress behavior was confirmed. In addition, the previously unknown fact that dent depth also influences this shift in stress behavior was introduced.

In Chapter V attention was focused on the problem of classifying three-dimensional dents in terms of whether they have center stress peaks or peripheral stress peaks. In particular, an emphasis was placed on making this classification based on simple measurements of dent geometry. Further evidence that both dent length and dent depth influence this transition in stress behavior was provided. It was also demonstrated that the influence of these values was based on their magnitude relative to cylinder diameter.

A method of mapping dent stress categories in terms of relative depth, d/D, and relative length, L/D was introduced in Chapter V. It was proposed that one can determine whether a dent is a center stress Mode C dent or a peripheral stress Mode

P dent by considering the dent location on this C-P map relative to a line defining transition geometry values.

A simple means of determining the transition line on a C-P diagram was developed. A simple elastic finite element model was used to determine the center and peripheral peak stress values of a dent imperfection of given depth and length. The ratio of these stress values was then determined. A line of dent geometry combinations with uniform center-to-periphery stress ratio values can be calculated and drawn on a C-P map. Actual dents plotted on the C-P map that fall above this line are Mode C dents. Those falling below the line are Mode P dents. As anticipated by the two-dimensional semi-analytical dent model, the C-P line location is specific to a given diameter-to-thickness ratio.

To provide a practical dent fatigue assessment tool, constant value C-P curves distinguishing short-lived, center cracking dents from longer-lived, peripheral cracking dents were found using existing experimental data from [8]. It was found that C-P curves representing geometry combinations with center-to-periphery peak stress ratios of 75% successfully characterize dents in 1/4″ thick pipe in terms of Mode C or P fatigue behavior. For the case of 3/8″ thick pipe, a 30% C-P curve must be used. Evidence was presented suggesting that this thickness effect is related to outer surface residual stresses that influence fatigue life.

Sets of 75% and 30% C-P curves were numerically analyzed. Two master curves were determined for use in distinguishing Mode C and P dents in 1/4″ and 3/8″ thick pipes. These master curves seem to successfully categorize all experimentally observed dent fatigue data in [8] with the exception of the 12″ by 3/8″ situation.

B. Suggested Future Work

There are a number of important open questions in the areas of dent fatigue behavior and the mechanics of dent, or imperfection, stress behavior. Issues in these two areas are, in fact, inter-related because it appears that improved understanding of dent fatigue behavior relies on improved understanding of dent stress behavior.

First, attention needs to be given to the problem of dent width. Experimental evidence in [9] and analytical evidence developed here suggests that relatively wide dents may have stress behavior that differs significantly from that of narrower dents. In fact, extra modes of dent stress behavior may exist for wide dents. One possible direction to take would be to seek to add an extra dimension of dent geometry that accounts for width to the C-P map approach introduced here.

Once the behavior of the full range of dent modes has been established, the problem of estimating actual values for dent stress associated with a given set of dent geometry measurements might be more easily approached. Mode specific models predicting dent stress could be developed. These models could be empirically derived from parametric studies. On the other hand, the two-dimensional semi-analytical model developed here might be adapted to predict Mode C long dent stress concentration behavior.

The fatigue behavior of dents is not only a function of stress concentration features but also of residual stress. A great deal remains to be learned about the residual stress features associated with dents. The relative importance of various dent and pipe parameters on residual stress needs to be established. It would be useful, given complications of accurately modelling residual stress, to develop empirical models that estimate dent residual stress in terms of dent geometry values.

Only when dent stress behavior is better understood can dent fatigue behavior

be thoroughly understood and predicted. It was shown here that an improved understanding of of the mechanics of bounds on dent stress modes can lead directly to a practical dent fatigue assessment tool. It is believed that continued advancement in the area of dent stress mechanics can contribute in meaningful ways to better techniques for evaluating damaged pipelines. In fact, such knowledge could likely have much wider application in other areas of damaged shell structures.

REFERENCES

[1]   United States Department of Transportation Office of Pipeline Safety, 2003,
        "Pipeline Statistics," http://ops.dot.gov/stats.htm.

[2]   Hart, J.D., Powell, G.H., Maple, J.A., Stevick, G.R., and Norton, J.D., 1998,
        "Fatigue Damage Calculations for a Dented and Ovalled Section of the
        TransAlaska Pipeline System at a Thompson Pass," Proc. of the 1998
        International Pipeline Conference, Calgary, Canada, ASME, pp. 263–272.

[3]   Smith, R.B. and Gideon, D.N., 1979, "Statistical Analysis of DOT-OPSO Data,"
        Proc. 6th Symposium On Line Pipe Research, American Gas Association, Oct.
        29–Nov. 1, 1979, Houston, TX, pp. D1–D9.

[4]   McClure, G.M., 1965, "Field Failure Investigations," in Symposium On Line Pipe
        Research, American Gas Association, November 17–18, 1965, Dallas, TX, pp.
        127–138.

[5]   Smith, R.B. and Eiber, R.J., 1969, "Field Failure Survey and Investigations," in
        Fourth Symposium On Line Pipe Research, American Gas Association,
        November 18–19, 1969, Dallas, TX, pp. D1–D18.

[6]   Fearnehough, G.D., 1977, "An Approach to Defect Tolerance in Pipelines,"
        Tolerance of Flaws in Pressurized Components, IMechE Conference Publications
        1978-10, , Institution of Mechanical Engineers, pp. 179–192.

[7]   Alexander, C.R., 1995, "Review of Experimental and Analytical Investigations of
        Dented Pipelines," Operations, Applications and Components, **PVP-Vol 395**,
        ASME, pp.197–205.

[8] Keating, P.B. and Hoffmann, R.L., 1997, "Fatigue Behavior of Dented Petroleum Pipelines," Final report, Texas Transportation Institute, Texas A&M University, for Office of Pipeline Safety, U.S. Dept. of Transportation, College Station, TX.

[9] Fowler, J.R., Alexander, C.R., Kovach, P.J, and Connelly, L.M., 1995, "Fatigue Life of Pipelines with Dents and Gouges Subjected to Cyclic Internal Pressure," in Petroleum Division (Publication) PD69, ASME, pp. 17–35.

[10] Hagiwara, N. and Oguchi, N., 1998, "Fatigue Behavior of Line Pipes Subjected to Severe Mechanical Damage," in Proceedings of the International Pipeline Conference, Calgary, Canada, ASME, pp. 291–298.

[11] American Society of Mechanical Engineers, Liquid Transportation System for Hydrocarbons, Liquid Petroleum Gas, Anhydrous Ammonia and Alchohols, ASME B31.4, 1992.

[12] American Society of Mechanical Engineers, Gas Transmission and Distribution Piping Systems, ASME B31.8, 1995.

[13] Osage, D.A., Krishnaswamy, P., Stephens, D.R., Scott, P., Janelle, J., Mo-han, R., and Wilkowski, G.M.,2001, "Welding Research Council Bulletin 465–September 2001: Technologies for the Evaluation of Non–crack–like Flaws in Pressurized Components–Erosion/Corrosion, Pitting, Blisters, Shell Out–Of–Roundness, Weld Misalignment, Bulges, and Dents," pp. 100-111.

[14] Beller, M., Mattheck, C., and Zimmermann, J.,1991, "Stress Concentrations in Pipelines Due to Presence of Dents," Proc. of the First (1991) International Off-shore and Polar Engineering Conference, Edinburgh, U.K. 11-16, August, ASME, pp. 421–424.

[15]   Rinehart, A.J. and Keating, P.B., 2002, "Rebound Behavior of Dents in Petroleum
        Pipelines," Proc., Texas Section ASCE Spring Meeting, San Antonio,
        TX. ASCE, pp. 195–204.

[16]   Rinehart, A.J. and Keating, P.B., 2002, "Length Effects on Fatigue Behavior of
        Longitudinal Pipeline Dents," Proc. of the 2002 International Pipeline
        Conference, Calgary, Canada, ASME, pp. 1849–1858.

[17]   Calladine, C.R., 1972, "Structural Consequences of Small Imperfections in Elastic
        Thin Shells of Revolution," International Journal of Solids and Structures, **8**, pp.
        679–697.

[18]   Croll, J.G.A., Kaleli, F., and Kemp, K.O., 1979, "Meridionally Imperfect Cooling
        Towers," Journal of the Engineering Mechanics Division, ASCE, **105** (EM5), pp.
        761–777.

[19]   Ellinas, C.P., Croll, J.G.A., and Kemp, K.O., 1980, "Cooling Towers with
        Circumferential Imperfections," Journal of the Structural Division, ASCE, **106**
        (ST12), pp. 2405–2415.

[20]   Godoy, L.A., 1996, Thin–Walled Structures with Structural Imperfections,
        Pergamon, Tarrytown, NY.

[21]   Rinehart, A.J. and Keating, P.B., 2002, "Predicting the Fatigue Life of Long
        Dents in Petroleum Pipelines," Proc. of 21st International Conference on Offshore
        Mechanics and Arctic Engineering, Oslo, Norway, ASME, pp. 1-9.

[22]   Rinehart, A.J. and Keating, P.B., 2002, "Fatigue Life Prediction for Short Dents
        in Petroleum Pipelines," Design and Analysis of Piping, Vessels, and
        Components, ASME, **PVP-Vol. 440**, pp. 103-111.

[23]   Dinovitzer, R.B., Lazor, R.B, Walker, R., and Bayley, C., 1999, "A Pipeline Dent

        Assessment Model," Proc. of OMAE99,18th International Conference on

        Offshore Mechanics and Arctic Engineering, July 11-16, St. Johns, Newfound-

        land, Canada. pp. 83–90, ASME.

[24]   Rosenfeld, M.J., 1998, "Investigations of Dent Rerounding Behavior," Proc. of

        the 1998 International Pipeline Conference, Calgary, Canada, ASME, pp. 299–

        307.

[25]   Lancaster, E.R. and Palmer, S.C., 1993, "Assessment of Mechanically Damaged

        Pipes Containing Dents and Gouges," in PVP-Vol. 261, Service Experience and

        Life Management: Nuclear, Fossil, and Petrochemical Plants. ASME, pp. 61–

        68.

[26]   Dinovitzer, A., Lazor, R., Carroll, L.B., Zhou, J., McCarver, F., Ironside, S.,

        Raghu, D., and. Keith, K, 2002, "Geometric Dent Characterization," ,Proc.

        of IPC'02, 4th International Pipeline Conference, September 29–October 3,

        2002, Calgary, Alberta, Canada, pp. 1589–1598, Institution of Mechanical

        Engineers.

[27]   Suresh, S., 1998, Fatigue of Materials, Cambridge University Press, Cambridge,

        England.

[28]   Hagiwara, N., Meziere, Y., Oguchi, N., Zarea, M., and Champavere, R., 1999,

        "Fatigue Behavior of Steel Pipes Containing Idealized Flaws Under Fluctuating

        Pressure," Japanese Society of Mechanical Engineers International Journal, Series

        A, **42** (4), pp. 610–617.

[29]   Frost, N.E., Marsh, K.J., and Pook, L.P., 1974, Metal Fatigue, Dover Publications, Mineola, NY.

[30]   Barsom, M. and Rolfe, S.T., 1999, Fracture and Fatigue Control in Structures, ASTM, West Conshohocken, PA.

[31]   Dinovitzer, R.B., Bhatia, A., Walker, R., and Lazor, R., 2000, "A Pipeline Dent Assessment Model Considering Localised Effects," International Pipeline Conference, ASME, pp. 735–742.

[32]   Isida, M., Noguchi, H., and Yoshida, T., 1984, "Tension and Bending of Finite Thickness Plates with a Semi-Elliptical Surface Crack," International Journal of Fracture, **26**, pp. 157–188.

[33]   Dowling, N., 1982, "A Discussion of Methods for Estimating Fatigue Life," SAE Technical Paper Series, Paper No. 820691.

[34]   Bloom, J.M.,1194, "An Approach to Account for Negative R-Ratio Effects in Fatigue Crack Growth Calculations for Pressure Vessels Based on Crack Closure Concepts," Journal of Pressure Vessel Technology, **11** (6), pp. 30–35..

[35]   Rinehart, A.J., 2000, "Determination of Thru-Thickness Residual Bending Stresses," M.S. thesis, Texas A&M University, College Station, TX.

[36]   Pal, B. and Salpekar, V.Y., 1999, "Stress Analysis of Damaged Submarine Pipeline Using Finite Element Method, "Proc. of the 9th International Offshore and Polar Engineering Conference, Brest, France, May 30–June 4, 1999, International Society of Offshore and Polar Engineers, pp. 153–159.

[37]   Hibbet, Karlsson, & Sorenson Inc., 1998, *ABAQUS/Standard Users Manuals*, Hibbet, Karlsson, & Sorenson Inc., Pawtucket, RI.

[38]   Croll, J.G.A., Kaleli, F., and Kemp, K.O., 1979, "A Simplified Approach to the Analysis of Geometrically Imperfect Cooling Tower Shells," Engineering Structures, **1**(1), pp. 92–98.

[39]   Croll, J.G.A.and. Kemp, K.O, 1979, "Specifying Tolerance Limits for Meridional Imperfections in Cooling Towers," ACI Journal, **76** (1), pp. 139–159.

[40]   Kato, S. and Yokoo ,Y., 1980, "Effects of Geometric Imperfections on Stress Distributions in Cooling Towers," Engineering Structures, **2**, pp. 150–156.

[41]   Gupta, A.K. and Al-Dabbagh, A., 1982, "Meridional Imperfection in Cooling Tower Design: Update," Journal of the Structural Division, ASCE, **108** (ST8), pp. 1697–1709.

[42]   Moy, S.S.J. and Niku, S.M., 1983, "Finite Element Analysis Techniques for the Analysis of Cooling Tower Shells with Geometric Imperfections," Thin Walled Structures, **1**, pp. 239–263.

[43]   Han, K.J. and Tong, G.S., 1985, "Analysis of Hyperbolic Cooling Towers with Local Imperfections," Engineering Structures, **7**, pp. 273–279.

[44]   Godoy, L.A., 1987, "A Simplified Bending Analysis of Imperfect Spherical Pressure Vessels," International Journal of Pressure Vessels, **27**, pp. 385–399, 1987.

[45]   Tam, C.K. and. Croll, J.G.A, 1988, "Elastic Stress Concentrations in Circular Tubular Members Containing Local Damage," Proc. of the 7th Annual Conference on Offshore Mechanics and Arctic Engineering, Houston, TX February 7–12, 1988, ASME, pp. 375–382.

[46]   Tam, C.K. and Croll, J.G.A., 1988, "Elastic Stress Concentrations in Cylindrical Shells Containing Local Damage," in Applied Solid Mechanics, A.S. Tooth and J. Spence, Eds., Elsevier Applied Science, **2**, pp. 155–177.

[47]   Godoy, L.A., 1993, "On Loads Equivalent to Geometrical Imperfections in Shells," Journal of Engineering Mechanics, **119** (1), pp. 186–187.

[48]   Flugge, W., 1960, Stresses in Shells, Springer-Verlag, Berlin, Germany.

[49]   Novozhilov, V.V., 1964, Thin Shell Theory, 2nd edition, P. Noordhoff Ltd., Groningen, The Netherlands.

[50]   Godoy, L.A. and Flores, F.G., 1987, "Stresses in Thin Spherical Shells with Imperfections Part I: Influence of Axisymmetric Imperfections," Thin Walled Structures, **5**, pp. 5–19.

[51]   Godoy, L.A. and Flores, F. G., 1987, "Stresses in Thin Spherical Shells with Imperfections Part II: Influence of Local Imperfections," Thin Walled Structures, **5**, pp. 145–155.

APPENDIX A

FORTRAN 77 CODE FOR GIVING TWO-DIMENSIONAL DENT SOLUTION

```
** PROGRAM 2DSIMPLENORMAL

        INTEGER NUMMODES,NUMPOINTS
        REAL PI,ANGLE
        PARAMETER(NUMMODES=75,NUMPOINTS=1440)
        PARAMETER(PI=3.14159265)

        INTEGER I,J,M,MODE,POINT
        REAL XI,A,T
        REAL XIBYA,ABYT,PHINOT
        REAL ANGLE,MTERM
        REAL INOT, IM(NUMMODES)
        REAL OUTERSCF(NUMPOINTS),INNERSCF(NUMPOINTS)

        XI = 0.18
        A = 9.
        T = 0.25
        PHINOT = PI/18.
        XIBYA=XI/A
        ABYT=A/T
        k=12*(A/T)**2

        OPEN(UNIT=1,FILE='2datapiby18',STATUS='UNKNOWN')

***FIND INOT AND IM TERMS
        DO 100,MODE=0,NUMMODES-1
                IM(MODE+1)=0.
                DO 50, POINT=1,NUMPOINTS
                ANGLE=((POINT-1)*2.0*PI)/(NUMPOINTS) -PI
                IM(MODE+1)=IM(MODE+1)
   $  +(1-(ANGLE/PHINOT)**2)*EXP(-0.5*(ANGLE/PHINOT)**2)
   $  *COS(MODE*ANGLE)*(2.*PI/(NUMPOINTS))
50              CONTINUE

        IM(MODE+1)=IM(MODE+1)*(1/PI)
        WRITE(1,*)MODE,IM(MODE+1)
100     CONTINUE

**FIND SCFS

        WRITE(*,*)XIBYA,ABYT,PHINOT

        DO 200, POINT=1,NUMPOINTS
                ANGLE=((POINT-1)*2.0*PI)/(NUMPOINTS) -PI
                OUTERSCF(POINT) = 1+(XIBYA/PHINOT**2)
   $            *(1-6*ABYT)*((1+2*k)/(1+k))*IM(1)
                INNERSCF(POINT) = 1+(XIBYA/PHINOT**2)
   $            *(1+6*ABYT)*((1+2*k)/(1+k))*IM(1)

                DO 150, M=1,NUMMODES-1
                        MTERM=(1-(M**2))/((M**4)+2.0*(M**2)+1.)

                        OUTERSCF(POINT)=OUTERSCF(POINT)
   $                    +(XIBYA/(PHINOT**2))*(1-6*ABYT)*IM(M+1)
```

Fig. 85. Page 1 of Fortran 77 code used to implement Eqs. 4.26 and 4.27.

```
$                         *MTERM*COS(M*ANGLE)

                          INNERSCF(POINT)=INNERSCF(POINT)+
$                         (XIBYA/(PHINOT**2))*(1+6*ABYT)*IM(M+1)
$                         *MTERM*COS(M*ANGLE)

150           CONTINUE
200           CONTINUE
        WRITE(1,*)
        WRITE(1,*)'ANGLE,  OUTERSCF,  INNERSCF'
        DO 300, POINT=(NUMPOINTS/2)+1,NUMPOINTS
              ANGLE=((POINT-1)*2.0*PI)/(NUMPOINTS) -PI
              WRITE(1,*)ANGLE,OUTERSCF(POINT),INNERSCF(POINT)
300     CONTINUE



        CLOSE(UNIT=1,STATUS='KEEP')

        END
****************************************************
        SUBROUTINE ZEROMATRIX1(MATRIX,DIM)

        INTEGER DIM,I
        REAL MATRIX(DIM)

        DO 5100, I=1,DIM
              MATRIX(I)=0.
5100    CONTINUE

        END
****************************************************
```

Fig. 86. Page 2 of Fortran 77 code used to implement Eqs. 4.26 and 4.27.

VITA

Adam Rinehart was born in Socorro, New Mexico and grew up primarily in Albuquerque, New Mexico. He attended Grinnell College in Grinnell, Iowa where he studied the liberal arts and received a B.A. in physics in 1998. He then came to Texas A&M University in College Station where he received an M.S. in civil engineering with an emphasis in structural engineering in August of 2000. He remained at Texas A&M for his doctoral work where his emphasis became the fatigue fracture and stress behavior of steel components. He received his Ph.D. in August of 2003. He joined ExxonMobil's Upstream Research Company in the Fall of 2003 where he continued to work on problems of fatigue fracture, failure analysis, and stress analysis in offshore petroleum platforms and pipelines. His permanent address is: 2607 Woodstream Blvd., Sugar Land, TX 77479. He may also be contacted through his parents Eric and Leslie Rinehart at: 340 Chula Vista NE, Albuquerque, NM 87108.